ELECTRICAL CHARACTERIZATION OF METAL-DNA-METAL DEVICE UNDER THE INFLUENCE OF MAGNETIC FIELD

NADIA MAHMOUDI KHATIR

FACULTY OF SCIENCE
UNIVERSITY OF MALAYA
KUALA LUMPUR

2013

ELECTRICAL CHARACTERIZATION OF METAL-DNA-METAL DEVICE UNDER THE INFLUENCE OF MAGNETIC FIELD

NADIA MAHMOUDI KHATIR

THESIS SUBMITED IN FULFILMENT
OF THE REQUIREMENTS
FOR THE DEGREE OF DOCTOR OF PHILOSOPHY

FACULTY OF SCIENCE
UNIVERSITY OF MALAYA
KUALA LUMPUR

2013

To the blessed memory of my father,

To all of those whom I love.

Acknowledgements

Boundless appreciation goes to GOD who gave me the ability to complete this project. I am grateful to my supervisors, Dr. Vengadesh Periasamy and Prof. Dr. Wan Haliza Abdul Majid, who helped me and encouraged me in this research. I believe without them, this piece of thesis would be impossible to complete. I would also like to thank everyone else who might have remotely contributed to my research. I would like to express my indescribable thanks to the staff members of the Faculty of Science and the Department of Physics. I also thank my relatives who have shared my joy and suffering together during my study. Not to forget, the financial assistance provided by University of Malaya for this research is greatly appreciated. I would like to extend my gratitude to Dr. Mitra Damghanian for his assistance in the fabrication laboratory. Special thanks are also due to Hooman Fatoorehchi and Dr. Ehsan Najafi for their valuable guidance. It is my pleasure to express my sincere appreciation to S. Maryam Banihashemian and Dr. Abolghasem Akbari for their valuable help and companionship.

Lastly, I would like to thank S. Belin Tavakoli for everything. I do greatly appreciate my family; beloved brother Taher, my nice sister Aida, my mom and my merciful dad (who passed away during the course of the study) for their unconditional love and support. I am also thankful to everyone else who might have touched my life during the struggle to accomplish my PhD.

List of Publications

Journal Papers

1. Khatir, N.M., Banihashemian, S.M., Periasamy, V., Abd Majid, W.H., Rahman, S.A. and Shahhosseini, F. (2011). DNA Strand Patterns on Aluminium Thin Films.Sensors, 11(7), 6719-6727.

2. Khatir, N.M., Banihashemian, S.M., Periasamy, V., Abd Majid, W.H. and Rahman, S.A. (2012). Electrical Characterization of Gold-DNA-Gold Structures in Presence of an External Magnetic Field by Means of *I-V* Curve Analysis.Sensors, 12(3), 3578-3586.

3. Mahmoudi Khatir, Nadia, Banihashemian, Seyedeh Maryam, Periasamy, Vengadesh, Abd Majid, Wan Haliza and Abdul Rahman, Saadah. (2012). Current-Voltage Characterization on Au-DNA-Au Junctions under the Influence of Magnetic Field.Advanced Materials Research, 535, 1350-1353.

Conferences

Absorption in Terahertz Frequency of Electromagnetic Wave for Tissues Cancer The 5th Mathematics and Physical Sciences Graduate Congress (5th MPSGC), 7-9 December 2009, Chulalongkorn University, Thailand (Regional) - Best Poster.

Designing DNA sensor based on Contact Metal-Biomaterial, 1st Nanotechnology Conference (NTC), 2-3 June 2009, Payam e Noor University, Iran (International).

The investigation of diffusion barrier layer's effect on nanostructure of Platinum Silicide infrared detectors made on Silicon, Inform Connect 2010 Seminar, 13-15 January 2010, University Malaya, Malaysia (International).

A New Method of Forming Nano Cracks Using DNA Strands, National Physics Conference (PERFIK 2010) DamaiLaut, 27-30 October 2010, University Kebangsaan Malaysia, Perak, Malaysia (National).

Novel Method of Fabricating Nano-Gaps using DNA Strands, The 6th Mathematics and Physical Science Graduate Congress 2010 (6th MPSGC), 13-15 December 2010, University of Malaya, Malaysia (Regional).

Investigation of magnetic field affect on DNA chain by current-voltage characterization, 26th Regional Conference on Solid State Science and Technology (RCSSST) 2011, 22-23 November 2011, University Kebangsaan Malaysia, Malaysia (Regional).

Nano scale pattern of DNA strands of Aluminium thin film, 4th international congress on Nanoscience and Nanotechnology (ICNN) 2012, 8-10 September 2012, University of Kashan, Iran (International).

Patent

A New Method of Fabricating Nano-Gaps on Aluminium/Silicon Structures using DNA Strands (2010), Patent Number 2010700067.

Award

Silver Medal-Novel Method of Fabricating Nano-Gaps Using DNA strands, Persidangan dan Ekspo Ciptaan Institusi Pengajian Tinggi Antarabangsa (PECIPTA), Pusat Konvensyen Kuala Lumpur (KLCC), 13-15 September 2011 (International).

Abstract

Recently, Deoxyribonucleic Acid (DNA) has become an interesting candidate for conduction of electrical current. The outcome could be useful in nanotechnology and nanoelectronics for the design of electrical circuits, which could in turn help to overcome the limitations that classical silicon (Si)-based electronics would be facing in coming years. In this work, DNA strands from *Bosenbergia rotunda* were used as the fundamental element.

The aim of this study was based on electrical characterization of gold (Au)-DNA-Au and Aluminium (Al)-DNA-Al structures under the presence and absence of external magnetic fields. The present work was investigated in two parts. First part involved using DNA as a material to create nano-gaps (NGs); DNA strands mixed in buffer solutions were applied onto thin films of Al on Si enabling chemical interactions between the strands and metal. This creates nanometer scale arbitrary patterning when directly transferring the DNA strands onto the Al substrate. This simple and cost-effective method may in future be utilized in the fabrication of various components in electronic chips for Nanoelectromechanical (NEM) and Microelectromechanical (MEM) systems application in general.

The second type of work utilized DNA as a semiconducting material in Metal-DNA-Metal (MDM) structures. Au thin film evaporated using thermal evaporation technique was employed for fabricating the MDM structure (Au-DNA-Au structures). Its electrical behavior without and when subjected to an external magnetic field (up to 1200 mT) was studied through its current-voltage (*I-V*) curves. Acquisition of the *I-V* curves demonstrated that DNA as a semiconductor exhibits diode behavior in the MDM

structure. The current versus magnetic field strength followed a decreasing trend because of a diminished mobility in the presence of a low magnetic field. This made clear that an externally imposed magnetic field would boost resistance of the MDM structure up to 1000 mT. For higher magnetic field strengths, an increase in potential barrier was observed in the MDM junctions. The magnetic sensitivity achieved in this work indicates the promise of using MDM structures as potential magnetic sensors.

Abstrak

Dalam beberapa tahun kebelakangan ini, Deoxyribonukleik Asid (DNA) telah menjadi calon yang menarik untuk pengaliran arus elektrik. Ia mungkin berguna dalam nanoteknologi dan nanoelektronik bagi rekaan bentuk litar elektrik yang boleh membantu untuk mengatasi kekangan yang dihadapi elektronik klasik berasaskan silicon (Si) dalam tahun-tahun akan datang. Untaian DNA daripada *Bosenbergia rotunda* telah digunakan sebagai elemen asas dalam kajian ini.

Tujuan kajian ini berdasarkan pencirian elektrik struktur emas (Au)-DNA-Au dan Aluminium (Al)-DNA-Al dalam dan tanpa kehadiran medan magnetik luaran. Penyiasatan kajian ini merangkumi dua bahagian. Pertama, penggunaaan DNA sebagai bahan untuk mewujudkan jurang nano; untaian DNAdicampur ke dalam larutan buffer telah digunakan dalam penerapan ke atas filem nipis Al pada Si menyebabkan interaksi kimia antara lembar DNA dan logam. Ini mewujudkan corak rambang berskala nanometer berikutan pemindahan langsung untaian DNA ke atas substrat Al. Kaedah ringkas dan menjimatkan kos ini boleh digunakan pada masa hadapan dalam fabrikasi pelbagai komponen dalam cip elektronik untuk applikasi system Nanoelektromekanikal (NEM) dan Mikroelektromekanikal (MEM) secara amnya.

Penyiasatan kajian yang kedua ialah penggunaan DNA sebagai semikonduktor dalam struktur Logam-DNA-Logam (MDM). Filem nipis Au yang tersejat dengan teknik penyejatan terma digunakan untuk struktur MDM (struktur Au-DNA-Au). Sifat elektriknya di dalam dan tanpa medan magnet luaran (sehingga 1200 mT) telah dikaji melalui lengkok arus-voltan *(I-V)*. Lengkungan *I-V* yang dijanakan menunjukkan DNA itu mempamerkan sifat semikonduktor diod dalam struktur MDM. Kekuatan arus aliran

elektrik berbanding kekuatan medan magnet mengikut trend yang menurun kerana mobiliti berkurang dengan kehadiran medan magnet yang rendah. Ini jelas menunjukkan bahawa medan magnet luaran yang dikenakan akan meningkatkan ketahanan struktur MDM sehingga 1000 mT. Untuk kekuatan medan magnet yang lebih tinggi, kita boleh melihat peningkatan dalam potensi halangan di cantuman MDM. Sensitiviti magnet yang tercapai di dalam kerja ini menunjukkan kemungkinan penggunaan struktur MDM sebagai sensor magnetik.

Table of Contents

List of Tables

List of Figures

List of Abbreviations

AFM	Atomic Force Microscopy
SFM	Scanning Force Microscopy
SEM	Scanning Electron Microscopy
STM	Scanning Tunneling Microscopy
DNA	Deoxyribonucleic Acid
UV	Ultraviolet
FESEM	Field Emission Scanning Electron Microscopy
NGs	Nano Gaps
A	Adenine
G	Guanine
C	Cytosine
T	Thymine
dsDNA	Double Stranded DNA
ssDNA	Single Stranded DNA
LUMO	Lowest Unoccupied Molecular Orbital
HOMO	Highest Occupied Molecular Orbital
E_F	Fermi Level
PE	Photoelectric Effects
CMOS	Complementary Metal–Oxide–Semiconductor
DC	Direct Current
RF	Radio Frequency
I–V	Current-Voltage
PECVD	Plasma Enhanced Chemical Vapor Deposition
CPD	Critical Point Dryer
DOF	Depth Of Focus
PGMEA	Propylene Glycol Monomethyl Ether Acetate
MEMS	Micro Electro Mechanical Systems
EGA	Ethylene Glycol Acetate
PVD	Physical Vapor Deposition
MDM	Metal-DNA-Metal
CVD	Chemical Vapor Deposition
SWCNT	Single-Walled Carbon Nanotube
LEEPS	The Low-Energy Electron Point Source

IINESC MN	INESC Microsistemas e Nanotecnologias
PCR	Polymerase Chain Reaction
CNTs	Carbon Nanotubes

List of Symbols

Activation energy (eV)	E_a
Average cross-section $(cm)^2$	A
Boltzmann's constant (j/K)	K
concentration of DNA (ng/nL)	C
Current (A)	I
Diode ideal factors (nm)	N
Distance between the electrodes (nm)	d
Effective mass (gr)	m^*
Electron affinity (eV)	$q\chi$
Electron charge (C)	q
Fermi Level (eV)	E_F
Hopping distance (nm)	a
Intrinsic resistance (Ω)	R
Length of the DNA (nm)	L
Length of the primer (nm)	N
Number of junctions along a percolated path	M
Planck's constants (j.s)	H
Potential barrier height (eV)	Φ_{bi}
Richardson constant ($ACm^{-2}K^{-2}$)	A^*
Schottky barrier height (eV)	φ_B
Sequence length (nm)	L_{DNA}
Thermal voltage(eV)	V_T
Tunneling decay length (nm)	β
Work function (eV)	φ_m

Chapter I: General Introduction

1.0 Introduction

Current advancement in biology, genetics and medicine are greatly influenced by the breakthrough discovery of the DNA structure by Watson and Crick (Watson, Crick F, 1953). They successfully postulated the famous double helix arrangement for DNA molecules. DNA as a biological molecule has shown promising results in the fabrication of nanostructures and nanoelectronic devices. In this pioneering work, we have utilized these structures for nano-patterning using the principles of the chemical etching mechanism. Chemical interactions between the Al and DNA strands cause etching of the deposited Al thin film leaving imprints of the strands on the surface. The patterning achieved using the DNA strands as shown in this work proved to be a simple low-cost trajectory process.

DNA molecules could also be used as or in assembly of nano devices and computational elements. Inspired by developments in science and technology, molecular electronics has become an important emerging research field. It mainly consists of two inter-related research pathways. One is the investigation of electron transport within single molecules in the hope for discovery of new physical effects on molecular scales. The other is to pursue new materials and approaches for assembling molecular electronic devices as described by Braun & Keren (E. Braun, Keren, 2004). Another part of this work, involves investigating the magnetic sensitivity of Au-DNA-Au structure (DNA based devices) as a suitable candidate for magnetic field detectors/sensors. The MDM structure may provide a good option in the fabrication of magnetic diodes and sensors.

1.1 Background and Scope

The DNA molecule, famous for its carrying of genetic codes in all living species, has recently been the center of attention for chemist and physicist. A major reason for such an increasing interest lies in the DNA's potential for application in nanoelectronic devices, either as a template for assembling nanocircuits or as a piece of such circuits. Undoubtedly, a practical conducting variant of DNA would vastly impact developments in nanotechnology (Endres, Cox, Singh, 2004).

Two most unique and eye-catching characteristics of DNA for molecular electronics are a particular structuring which enables its use for self-assembly and double-strand recognition. Molecular recognition relates to the ability of a molecule to construct selective bonds with other molecules or substrates, dependent upon the information saved in the structural features of the interacting partners. Molecular recognition processes might play a decisive role in molecular devices through steering the fabrication of devices or the integrated circuits from basic building blocks, uniting them into supramolecular arrays, enabling selective operations upon given species potentially serving as dopants and finally conducting the feedback to external perturbations stemmed from interacting partners/applied fields (Porath, Cuniberti, Di Felice, 2004).

Self-assembly is the ability of molecules to be automatically organized to supramolecular aggregates in appropriate experimental circumstances (Lehn, 1990) and might guide the design of well-structured systems. Researchers are amazed by the idea that DNA may have practical uses in nanoelectronics. Accordingly, research plans started all over the world to investigate DNA conductivity (E. Braun, Eichen, Sivan et al., 1998; De Pablo, Moreno-Herrero, Colchero et al., 2000; Fink, Schönenberger, 1999; Kasumov, Kociak, Gueron et al., 2001; Porath, Bezryadin, De Vries et al., 2000b;

Rakitin, Aich, Papadopoulos et al., 2001; Storm, Van Noort, De Vries et al., 2001; Watanabe, Manabe, Shigematsu et al., 2001). On a less favorable scenario, if DNA molecules do not tolerate measurable currents, yet another interesting alternative scheme arises. This is to prepare hybrid objects (metal nanoparticles/wires, proteins/antibodies) in which electrons transfer and carry current flows, templated by DNA helices at fixed locations (E. Braun, Eichen, Sivan et al., 1998; Richter, Mertig, Pompe et al., 2001). This approach also makes it possible to embed conducting objects into some hybrid architectures, such as a carbon nanotube DNA-templated nanotransistor by Karen et al (Keren, Berman, Buchstab et al., 2003). Either of these routes can pave the road towards DNA-based molecular electronics (R. Felice, Porath, 2008). The first direct electrical transport measurement on a single, 16 μm long λ-DNA, was reported by E. Braun and co-workers (E. Braun, Eichen, Sivan et al., 1998). A year later in 1999, Fink and colleagues (Fink, Schönenberger, 1999) observed ohmic behavior in λ-DNA molecules with resistance in the MΩ range.

In another brilliant experiment published by Porath et al. (Porath, Bezryadin, De Vries et al., 2000b), electrical transport was measured through 10.4 nm long (30 base-pairs) homogeneous poly (dG)-poly(dC) molecules while being electrostatically trapped between two Pt electrodes (Bezryadin, Dekker, 1997; Bezryadin, Dekker, Schmid, 1997). A year later, Kasumov and co-workers (Kasumov, Kociak, Gueron et al., 2001) reported on ohmic behavior in the resistance of λ-DNA molecules settled on a mica surface and stretched between rhenium carbon electrodes. Through another effort made to resolve the riddle about the DNA conduction properties, de Pablo and his team members (De Pablo, Moreno-Herrero, Colchero et al., 2000) exploited a different method to measure single λ-DNA molecules on the substrate in ambient conditions (Porath, Cuniberti, Di Felice, 2004). As depicted in Table 1.1, the number of scientific

paper publications on magnetic resistance of DNA or metal-DNA-metal or *I-V* DNA has undergone an increasing trend during the last 20 years.

Table 1.1: Some scientific paper publications on magnetic resistance of DNA

Year	Title and Summary
1997	Metal clusters - new perspectives in future nanoelectronics. The physical properties of these 'nanomaterials' lie somewhere between those of the bulk phase, which can be explained by classical physics and those of the respective atoms or molecules, which can be explained by quantum mechanics (Schmid, Hornyak, 1997).
2002	Nanotechnology approaches to self-organized bio-molecular devices. They briefly describe new strategies to exploit self-assembled solid-state biomolecular materials as active elements of electronic devices. The transport characteristics of different devices such as diodes, photodetectors and metal–semiconductor–metal structures were described (Cingolani, Rinaldi, Maruccio et al., 2002).
2005	Electrical detection of biomolecular interactions with metal–insulator–semiconductor diodes. They reported the label-free detection of DNA hybridization using a metal–insulator–semiconductor (MIS) diode or capacitor (Estrela, Migliorato, Takiguchi et al., 2005).
2005	Field effect detection of biomolecular interactions. They reported detection of biomolecular interactions using field effect devices such as metal-oxide-semiconductor (MOS) capacitor structures and polycrystalline silicon thin film transistors. DNA interactions occurring at the metal gate of the devices lead to an increase of negative charges attached to

	the gate (Estrela, Stewart, Yan et al., 2005) .
2008	Time-resolved Förster-resonance-energy-transfer DNA assay on an active CMOS microarray. The functionality of their system by measuring a DNA target concentration series using TR-FRET with semiconductor quantum dot donors (Schwartz, Gong, Shepard, 2008).
2010	Ultrahigh (100%) barrier modification of n-InPSchottky diode by DNA biopolymer nanofilms. DNA increases an effective barrier height as high as 0.87 eV by influencing the space charge region of n-InP device with a good rectifying behavior (Ömer Güllü, 2010).
2011	Electronic properties of Al/DNA/p-Si MIS diode: Application as temperature sensor. The Schottky diode shows non-ideal *I–V* behaviour with ideality factors *n* equal to 1.34 ± 0.02 and 1.70 ± 0.02 at 300 K and 200 K, respectively, and is thought to have a metal-interface layer-semiconductor (MIS) configuration (Ö Güllü, Türüt, 2011).
2011	Synthesis of nano ground nutshell-like polyindole by supramolecular assembled salts of ss-DNA assisted chloroauric acid. The effect of DNA on the electronic property of polyindole is studied by fabricating Schottky junctions with Al metal (A. Kumar, Prakash, 2011).

1.2 Aims and Objectives

The main aim of this research is to investigate the electrical properties of metal-DNA-metal device under the influence of an external magnetic field. In order to achieve this main aim, several specific objectives have been identified as follows;

I) Investigating the DNA effect on Al metal surface.

II) Investigating the current-voltage (*I-V*) of Au-DNA-Au device at different temperature with and without the influence of magnetic field.

III) Investigating the potential barrier and assessing the saturation current, I_s behavior under different magnetic field strength.

IV) Evaluating the resistance behavior under different magnetic field strengths.

1.3 Thesis Outline

The thesis is organized into 7 chapters. Chapter I provide an introduction to the subject and objectives of the research and an outline to the thesis. Chapter II meanwhile highlights major literature review regarding different aspects of the research. Some basic theories and previous studies related to this research are discussed in detail.

Chapter III explains fabrication methodology of the DNA chip. Fabrication sample includes mask design, lithography and deposition techniques. Chapter IV describes the materials used for this research. Results and discussion are presented in Chapter V. Here the formations of NGs using the DNA strands are explained thoroughly.

Results and discussions in Chapter VI meanwhile investigate the behavior of the chip in the presence and absence of magnetic field. The main outcomes of this research and future works are finally outlined in Chapter VII.

Chapter II: Literature Review

2.0 Introduction

Recently, there has been a great deal of focus on electrical properties of biological materials. DNA is definitely referred to as the most eminent molecule in nature and as a significant material for applications in molecular electronics (Petty, 2007).

2.1 Discovery of DNA

The knowledge over the structure of DNA is due to works reported by James Watson and Francis Crick in 1953 (Watson, Crick F, 1953). Their discovery was the outcome of a sequence of scholarly research works carried out by Oswald T. Avery, Colin MacLeod and Maclyn McCarty's postulation (McCarty, 1986). In 1944, Avery et al. published an article that reported DNA as being hereditary molecules and not just simple proteins. According to today's records on history of DNA, it is often regarded as if it started with these basic discoveries. However, the very initial description of DNA actually goes back to 135 years ago to the efforts of Friedrich Miescher in 1869, an unsung scientist who isolated the hereditary material (Dahm, 2005).

2.1.1 DNA Structure

Deoxyribonucleic acid, or more famously known as DNA, is the hereditary element in literary all living creatures. Being a biopolymer, it consists of monomer units called nucleotides; each nucleotide in turn is comprised of a 5-carbon sugar ring (deoxyribose), a nitrogen-holder base connected to the sugar and a phosphate backbone. The polymer is known as a "polynucleotide". DNA is formulated into structures in cells called chromosomes (Ohayon, 2011) and is made up of four different types of nucleotides, which includes derivatives of two compounds including pyrimidine and purine. According to Manohar (Manohar, 2010), DNA contains two primary purine

bases, adenine (A) and guanine (G) and two principal pyrimidine bases, cytosine (C) and thymine (T). A schematic view of general and chemical structure of DNA is presented in Figure 2.1.

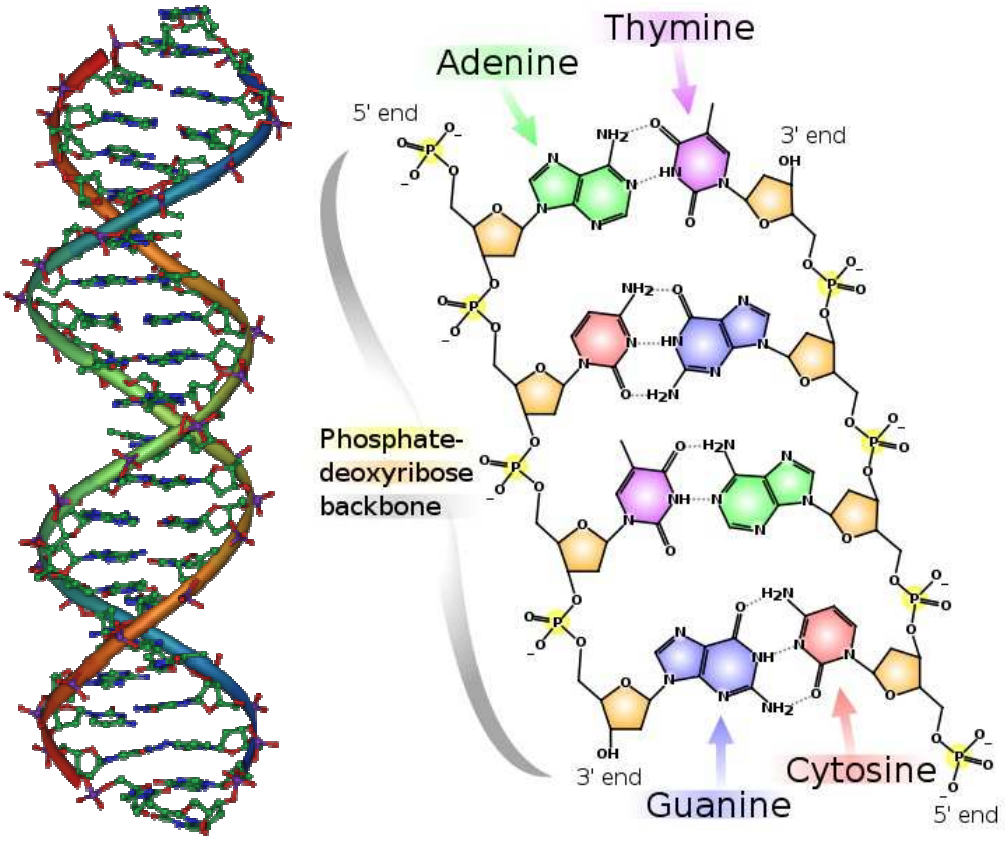

(a) (b)

Figure 2.1: (a) Schematic view of DNA double-helix structure and (b) Chemical structure of DNA (Saenger, 1984).

Base pairing is complementary since there are specific geometry requirements for formation of hydrogen bonds between the heterocyclic amines. A possible application of this (hydrogen bonding principle) is the heterocyclic amine base pairing. In Figure 2.1 (a), note the T-A pair interactions via two hydrogen bonds denoted as (T=A) and that the C-G pair interacts through three hydrogen bonds abbreviated by (C≡G). This property is illustrated in Figure 2.2.

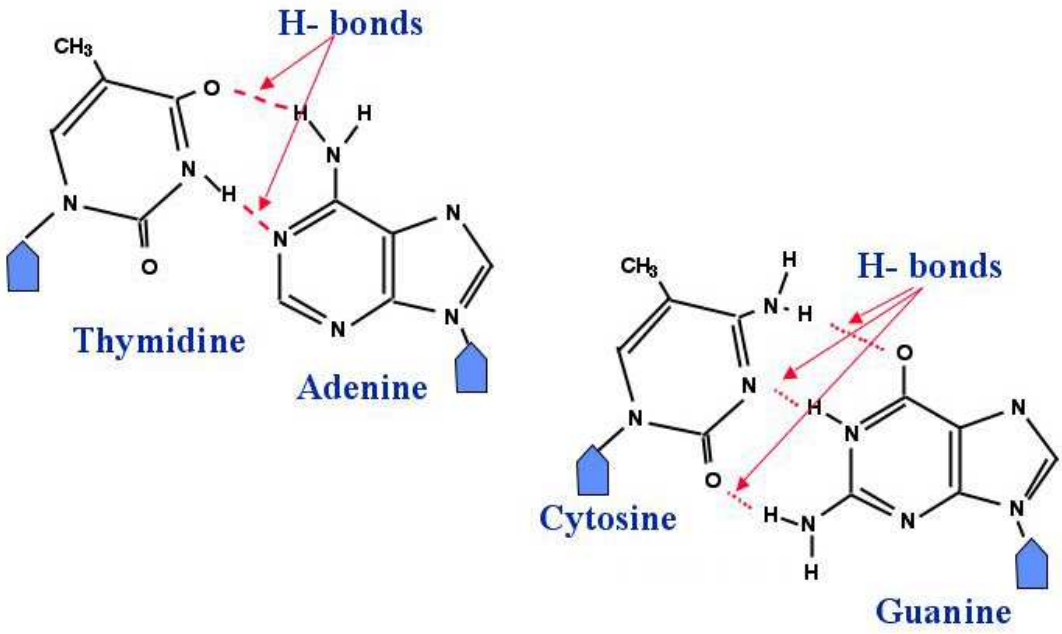

Figure 2.2: Illustration of complementary base pairs, two strands are held together by hydrogen bonds between complementary bases adenine hydrogen bonds (base pairs) to thymine guanine hydrogen bonds to cytosine (van der Wijst, Guerra, Swart et al., 2006).

As shown in the figure, A and G preferentially binds with T and C respectively. Double helical DNA has nanometric dimensions. As revealed in Figure 2.3, one full turn of DNA double helix span 0.34 nm and the width of a duplex DNA is about 2 nm. On nanometer scale, double stranded DNA (dsDNA) exhibits inflexibility with persistence length of about 50 nm (Bustamante, Smith, Liphardt et al., 2000). Single stranded DNA (ssDNA) meanwhile is relatively flexible, with persistence length of less than 1 nm (Chhabra, 2009).

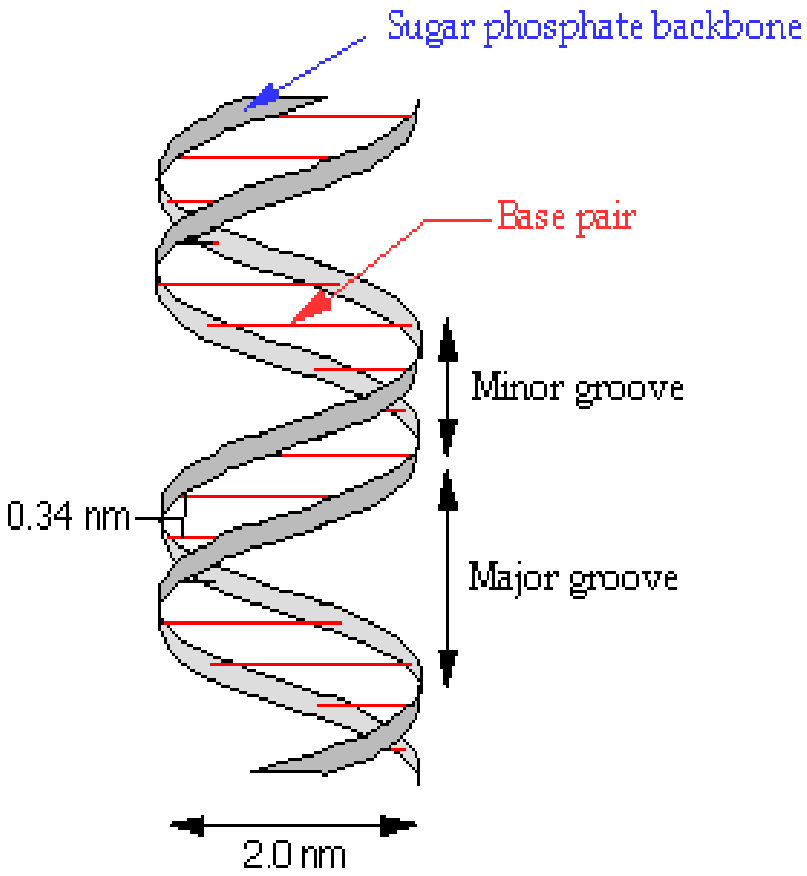

Figure 2.3: DNA double helix dimensions. The helix diameter is 2.0 nm and the base pairs are 0.34 nm (Chhabra, 2009).

2.1.2 Conductivity of DNA

Whether DNA is intrinsically conducting or not is open to criticism. The experimental results are somewhat inconclusive revealing many possible deductions (Endres, Cox, Singh, 2004). According to Saenger (Saenger, 1984), DNA has several structural configurations depending on concentration, base sequence and type of counter ions together with relative humidity. It did not take long to notice the semiconducting property of DNA double helix structure subsequent to its early discovery (Eley, Spivey, 1962). More recently, a great deal of interest has been focused on the conductivity of DNA and many efforts have been carried-out in this respect. The results are sometimes contradictory; DNA is shown to be a possible insulator (Dunlap, García, Schabtach et al., 1993),

It is consequently assumed that the electron transport phenomenon of DNA differs with the base sequence, counter ion type (buffer type) and relative humidity (measurement environment; whether in the vacuum or atmosphere). As shown in Figure 2.4, the electron transport characteristics also hinges on the sample shape and measurement methodology.

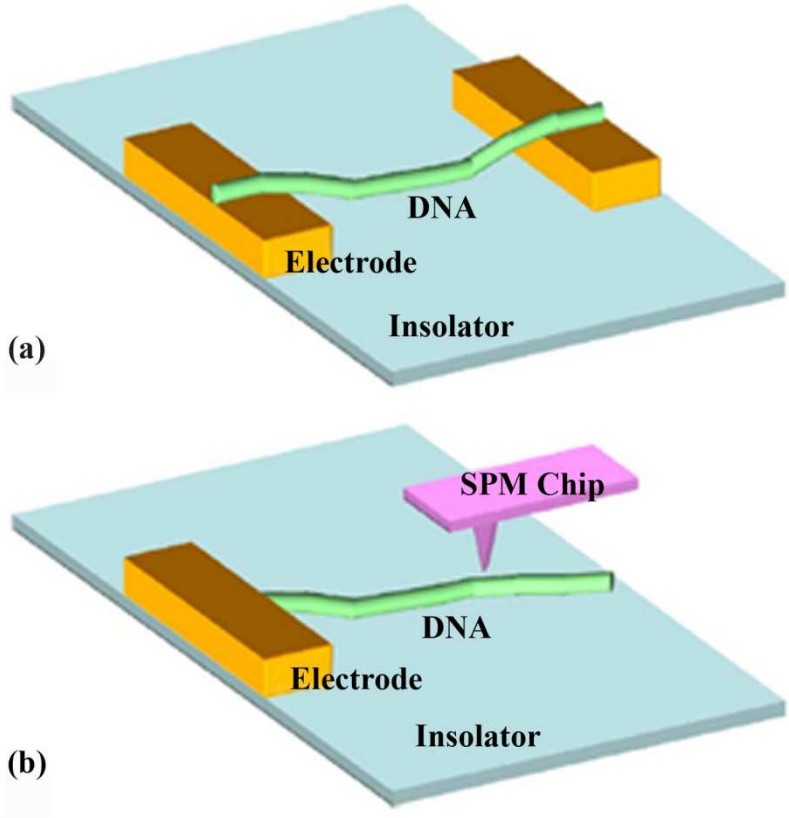

Figure 2.4: Schematic diagram of typical measuring methods of electrical conductivity. (a) Micro- and nano-gap electrode method. In this method DNA molecules are trapped between two metal electrodes. These electrodes are prepared using photolithography or electron-beam lithography. (b) Scanning probe method (Taniguchi, 2006).

DNA molecules were placed onto an insulating substrate and the electrode was produced on one end of the DNA molecule. A scanning probe tip was used as the other electrode (Taniguchi, 2006). The gap length between the electrodes becomes a key factor particularly when settled electrodes on an insulating substrate were utilized. Some of the experiments reported to date can be classified into three categories; insulators,

semiconductors and conductors. Each category is summarized in terms of base sequence, buffer (counter cation), sample shape and measurement environment and method. A summary is provided in Appendix A (Taniguchi, 2006).

2.2 Basic Theory

2.2.1 Schottky Barrier

Metal-semiconductor junction has an old history and is a fundamental topic in semiconductor theory. When a metal slab is pushed against the surface of a semiconductor, the applied current is observed to be one-directional. A metal-semiconductor combination with such a rectifying contact is referred to as a Schottky diode. Braun (F. Braun, 1874) is credited for discovery of the metal-semiconductor contact, in 1874 is regarded as the basis of one of the oldest semiconductor devices. The oldest model of potential barrier formation and rectification across the metal-semiconductor interface is based on parallel observations by Walter Schottky and Mott (Mott, 1938) in 1938. Bethe (Bethe, Laboratory, 1942) in 1942 later demonstrated the formulation of the thermionic-emission theory. It was refined much later by Crowell and Szein 1966 (Crowell, Sze, 1966). This was followed by Bardeen in 1947 who developed the theory of surface states for better understanding the experimental results (Bardeen, 1947). In the following work, Lepselter and co-workers used silicide (in place of metal) on silicon substrate. In order to study the *I-V* characteristics of a metal-semiconductor barrier, three kinds of structures were fabricated on a single wafer (Lepselter, Sze, 1968). A good discussion of the history of metal-semiconductor devices is given by Henisch in 1957 (Henisch, 1957) with a more recent review by Tung in 2001 (R. T. Tung, 2001). DNA exhibited semiconductor behavior upon contact with metal (Ö Güllü, Çankaya, Barış et al., 2008; Kalofonou, Toumazou, 2013; Kamioka, Suzuki, Tamiya et al., 1989). According to De Yu and Grote (De Yu, Grote, 2007),

schematic diagrams of energy bands in a metal (gold) and an n-type semiconductor (n-type DNA) at ideal conditions before and after contacting can be shown as in Figure 2.5. Prior to contacting, thermal equilibrium is not achieved in the system. Once contacted, the charges will flow from semiconductor to metal and electronic equilibrium is reached. Here, LUMO or Lowest Unoccupied Molecular Orbital, Fermi Level E_F and Highest Occupied Molecular Orbital (HOMO) are the conduction, Fermi and valence energy levels respectively. q is the electron charge, φ_m is the gold work function (which is about 5.1 eV for gold), φ_B is the Schottky barrier height and $q\chi$ is the electron affinity measured from the conduction band to the vacuum level. If the DNA is a p-type semiconductor, the energy band diagrams after metal-DNA contacting is shown as in Figure 2.5(c).

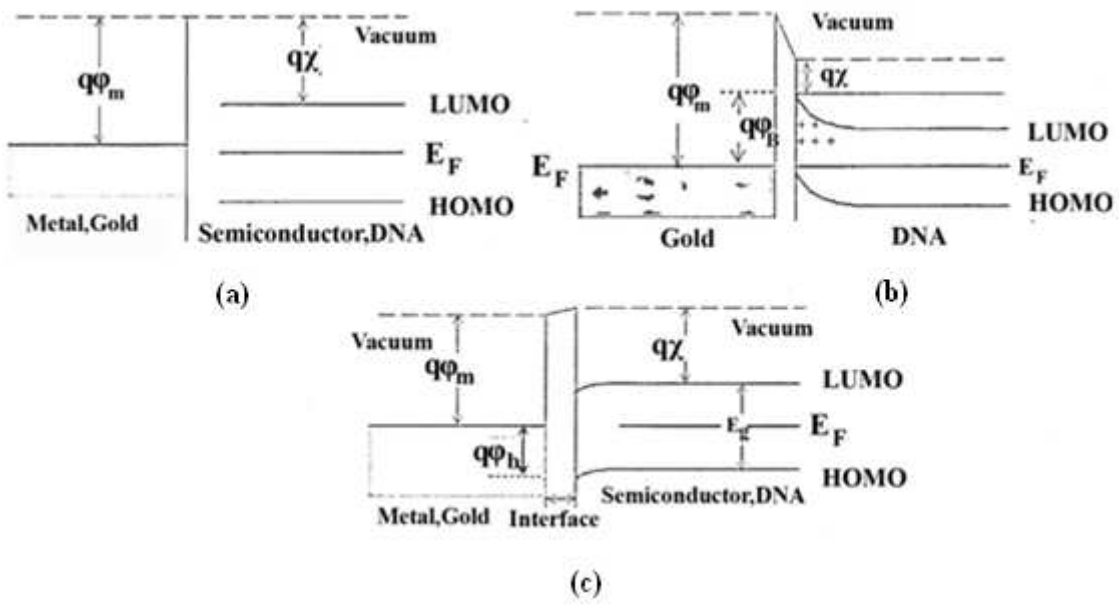

Figure 2.5: Energy band diagrams of metal (gold)-semiconductor (DNA) contacts. Before contacting (a); after contacting: n-type semiconductor (b); and p-type semiconductor (c) (De Yu, Grote, 2007).

2.3 Theoretical Model for Charge Transfer

Roche conducted theoretical studies on some types of artificial and genomic DNA. Model of hole transport through the guanine bases have been developed for transport

mechanisms. An effective 1-dimensional tight-binding Hamiltonian (H) that is described by Eq. 2.1 explains this model;

$$H = \Sigma_n - t_{DNA}\, cos\left(\theta_{n,n+1}\right)\left(c_n^{\dagger}c_{n+1} + h.c.\right) + \varepsilon_n c_n^{\dagger}c_n \qquad \text{Eq. 2.1}$$

where $c_n^{\dagger}c_n$ is the operator for charge generation (annihilation) in the location of n, t_{DNA}introduces the amplitude for $\pi - \pi$ coupling among closest neighbor orbitals, ε_n refers to energies of the hole site and $cos\left(\theta_{n,n+1}\right)$ depends on temperature and is a measure to show the decrease of coupling among base pairs because of thermal changes (Roche, 2003).

In order to evaluate system conductivity, consider the electron transmission calculated by Landauer formulation to obtain the energy-dependent transmission coefficient *T(E)*. While the DNA sequence is attached to metallic leads and the electrode Fermi levels are increased up to the G-HOMO, energy dependence of *T* is essential for explanation of properties of charge transfer. Landauer Eq. describes an electronic wave packet that has energy of *E* and wave vector of *k* is injected from a metallic contact inside a DNA sequence as seen in Figure 2.6. The coefficients *R* and *T* identify the amplitudes, which are respectively reflected by the DNA sequence and transmitted to another one or to the other metallic contact. Current conservation rule leads to $R + T = 1$.

The inverse transmission rate *R/T* is related to the dimensionless resistance (ρ) and for weak transmission, the DNA resistivity is proportional to $[(1 - T_{av})/T_{av}]\, S_{DNA}/L_{DNA}$. T_{av} is the average of the transmission coefficient for energies close to the HOMO-G ionization energy, S_{DNA} equals to 3×10^{-18} m^2 which is the average DNA cross section and L_{DNA} is defined as the sequence length (Roche, 2003).

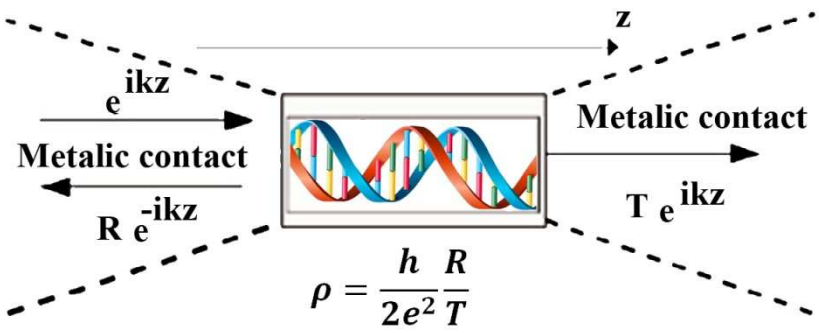

Figure 2.6: Demonstration of the transmission during a DNA sequence which was connected to two metallic contacts (Roche, 2003).

2.4 Nanostructures of DNA

Seeman and Kallenbach (Seeman, Kallenbach, 1983) were the first to take advantage of the DNA's molecular recognition characteristics to fabricate complex mesoscopic structures merely based on DNA. Branched DNA was utilized in their studies to shape stick figures by selecting the sequence of the complementary strands. Macrocycles, DNA quadrilateral, DNA knots, Holliday junctions and other structures were designed. Figure 2.7 illustrates a four-armed stable branched DNA junction created by DNA molecules and the application of the branched junctions to shape periodic crystals (Seeman, 1999). The research team also successfully designed two-dimensional crystalline forms of DNA double crossover molecules that are programmed to self-assemble by the complementary binding of the sticky ends of the DNA molecules (Winfree, Liu, Wenzler et al., 1998). These lattices can possibly play the role of a scaffolding material, in turn, for other biological materials. An elaborate review on this subject was provided by Seeman (Seeman, 1998). Other researchers have also made efforts on utilizing DNA to shape complex architectures. Bergstrom et al. in 1997 (Shi, Bergstrom, 1997) have designed rigid tetrahedral connectors with arylethynylaryl spacers to guide the assembly of attached oligonucleotide connector arms into new DNA macrocycles. It is worth noting that Bergstrom's approach utilizes rigid tetrahedral organic vertices, where the attached oligonucleotides serve as the connectors

for the design of more complex architectures. This is in opposite to Seeman's approach where the DNA serves as both the vertices and the edges of the assembled architectures. Basically, a variable number of oligonucleotide arms could be attached to the core tetrahedral organic linkers to allow for the construction of different kinds of DNA structures (J. Chen, Seeman, 1991; Nalwa, 2005; Seeman, 1982).

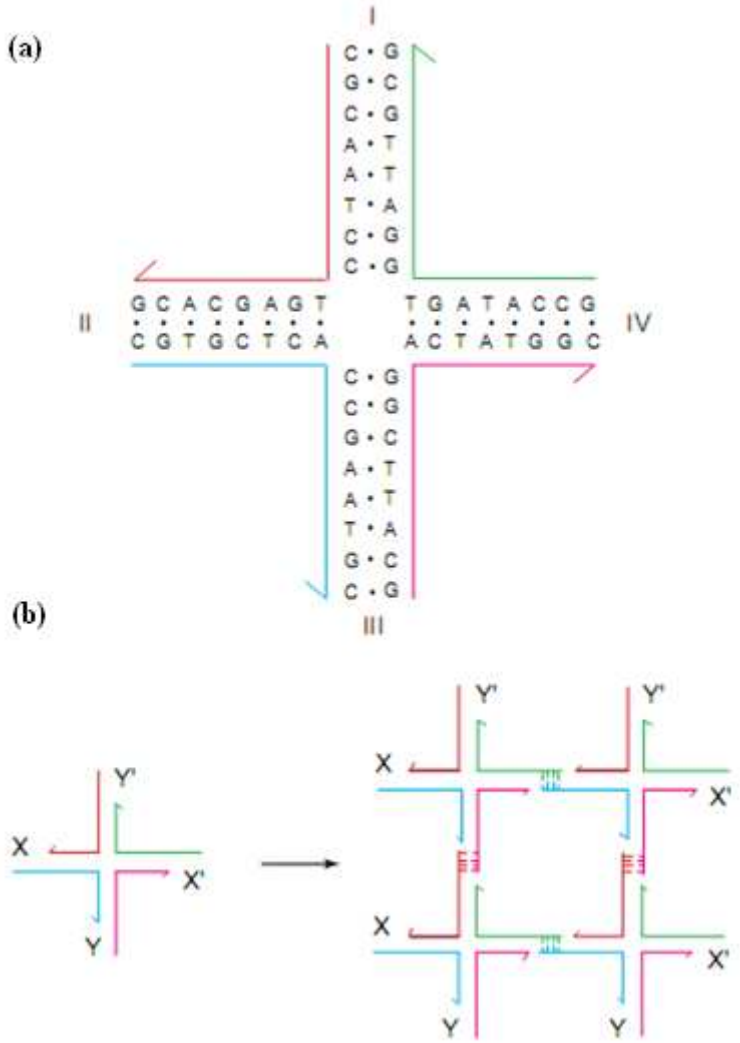

Figure 2.7: Four-armed constant branched DNA junction made by DNA molecules. (a) Stable branched DNA molecule. (b) Sticky ends of the DNA molecules and assembly of four sticky-ended DNA molecules into a square-shaped pattern (Seeman, 1999).

2.5 Electrical Properties

2.5.1 Charge Transport in DNA

Charge transport in DNA is being intensely studied by scientists in context of its biological implications in repair, protein bonding and conceptualized integration in future bioelectronics or DNA-based electronic chips. In this work, the charge transport mechanism was investigated in two sections. The electron transport behavior of DNA alters the base sequence, counter ion type (buffer type) and relative humidity (measurement environment, that is whether in a vacuum or the atmosphere). The electron transport property also relies on sample shape and the measurement method. In particular, when fixed electrodes on an insulating substrate are used, the gap length between the electrodes becomes a critical factor (Taniguchi, 2006).

2.5.2 Indirect Measurements of Charge Transport in DNA

Murphy and co-workers (Murphy, Arkin, Jenkins et al., 1993) declared that charge through DNA is transported from an excited donor to an electron acceptor. Henderson and colleagues (Henderson, Jones, Hampikian et al., 1999) covalently attached a 60-base pair DNA oligomer derivative to an anthraquinone derivative. In similar experiments, Brun and Harriman et al. (Brun, Harriman, 1992, 1994; Harriman, 1999) implemented organic donors and acceptors. Also they reported that the charge-transfer rates drop off faster as the length of the DNA increases contradicting the result of Murphy et al. (Murphy, Arkin, Jenkins et al., 1993). Other experiments studied metal complexes and modeled the data (Lincoln, Tuite, Nordén, 1997). The consequences imply that the metal complexes must cooperatively bind onto the DNA, which explains the fast rate of charge transfer and its small “distance dependence” (Lincoln, Tuite, Nordén, 1997; Olson, Hu, Hörmann et al., 1997). Later, further research was carried-out both experimentally and theoretically by Krider et al. (Krider, Meade, 1998; Lewis,

Letsinger, 1998; Netzel, 1998; Priyadarshy, Risser, Beratan, 1998; Turro, Barton, 1998). Additional updated measurements by Boon and Barton (2002) and Giese (2002) (Boon, Barton, 2002; Giese, 2002) were conducted under better controlled circumstances and the sequence dependence of charge transfer has been scientifically underlined. In several of these experimentations, three G-C pairs were the acceptors (G-G-G). DNA transfers charge over long distances of up to hundreds of angstroms (Boon, Barton, 2002). The main findings are that the rate of transfer strongly depends on the base sequence. Rate of charge transfer between a G-C pair and a hole injector, separated by a small number of A-T pairs, drops off exponentially with the number of A-T pairs. However, the rate stays relatively constant with increasing number of A-T pairs when there are more than four A-T pairs. A number of transport readings on DNA films or bundles between electrodes were carried-out by the research team of Tomoji Kawai in 1980 mostly reporting considerable currents with a reliance on sequence and doping (R. D. Felice, 2009). The numbers of scientific paper publications on indirect measurements of *I-V* characteristic are listed in the table below.

Table 2.1: Scientific paper publications on indirect measurements of *I-V* characteristics

Year	Title and Summary
2012	A mechano-electronic DNA switch. They reported a new kind of DNA nanomachine that, fueled by Hg^{2+} binding and sequestration, couples mechanical motion to the multiply reversible switching of through-DNA charge transport (Cingolani, Rinaldi, Maruccio et al., 2002).
2012	Charge transport within a 3-dimensional DNA nanostructure framework. They reported kinetic studies of DNA-mediated charge transport (CT) within a 3D DNA nanostructure framework (Schmid, Hornyak, 1997).

2012	Effects of cytosine methylation on DNA charge transport. They found a measurable difference in the conductance between the two types of molecules, and demonstrated that this difference is statistically significant (Hihath, Guo, Zhang et al., 2012).
2011	Electrical and optical characterization of DNA molecules as a function of concentration in aqueous solution. The results reported here provide a contribution for the possible use of DNA molecules in the field of electro-optical biosensors (Polcari, Romano, Sabatino et al., 2011).
2007	Modeling of the electrical conductivity of DNA. The authors had developed a model of the electrical behavior of DNA molecules for use in nanoelectronic circuit design. This is important because having models of DNA molecules in the form of equivalent electronic circuits would be useful in the design of nanoelectronic circuits and devices (Hodzic, Hodzic, Newcomb, 2007).
2006	Electrical characterization of self-assembled single- and double-stranded DNA monolayers using conductive AFM. They found that the ability of dsDNA to transport electrical current under the appropriate conditions, demonstrate the efficiency of an ssDNA monolayer as an insulating layer and emphasize the crucial role of an efficient charge injection through covalent bonding for electrical transport in single dsDNA molecules (Cohen, Nogues, Ullien et al., 2006).

2.5.3 Direct Measurements of *I-V* Characteristics

Watanabe and colleagues (Watanabe, Manabe, Shigematsu et al., 2001) measured the electric properties of a three-terminal single molecule DNA device with a triple-probe

Atomic Force Microscope (T-AFM). The T-AFM permits them to connect a single DNA molecule with carbon nanotube (CNT) electrodes as source, drain and gate terminals. The later comprised of two multiwalled CNTs as depicted in Figure 2.8(a) where *NT*, P_1 and P_2 indicate gate and the two sources respectively. Contacting two CNT probes of a nanotweezer to a single DNA molecule individually to form the source and drain terminals. A single-walled CNT (SWCNT) was set at the side of the DNA molecule using a T-AFM (gate) to connect with the gate terminal. Figure 2.8(b) demonstrates the *I-V* characteristics of source and drain at a distance of 25 nm under a dry nitrogen atmosphere at room temperature.

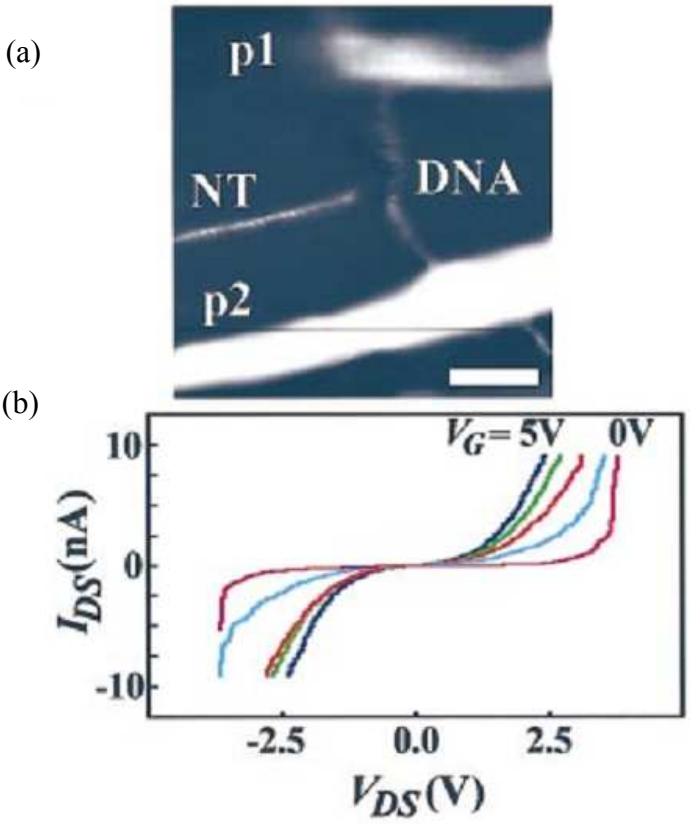

Figure 2.8: (a) AFM image (scale bar, 10 nm) of the experimental setup. P_1 is the source and P_2 the drain of the two-probe nanotweezer. NT is the carbon nanotube used to apply the gate voltage. (b) *I-V* characteristics of biological DNA at different gate voltages, V_G (Watanabe, Manabe, Shigematsu, et al., 2001).

(a)

(b)

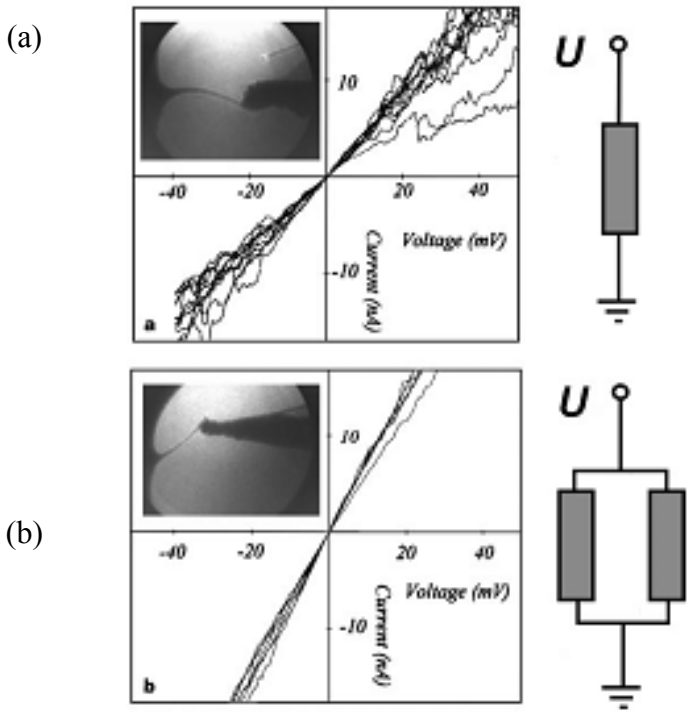

Figure 2.9: *I-V* characteristics of DNA chains. (a) *I-V* curve taken for a 600 nm-long DNA. (b) *I±V* curve when manipulation-tip is attached to both DNA ropes (Fink, Schonenberger, 1999).

De Pablo with his group reported on *I-V* characteristics with a clear gap of about 2 V and resistance of 3 GΩ at 4 V, for 10 nm long free standing poly(G)-poly(C) DNA chains, ρ of about 100 Ω.cm (De Pablo, Moreno-Herrero, Colchero et al., 2000). Fink and Sehtinenherger (Fink, Schönenberger, 1999) discovered a linear *I-V* characteristic, for λ-DNA (random sequence, it's DNA from a particular bacteriophage called lambda) molecules 1 μm long, with resistivities ρ of about 10^{-4} Ω.m. The resulting *I-V* behavior is depicted in Figure 2.9, while the inset shows the low-energy electron point source (LEEPS) picture of DNA attached to a tungsten tip.

Kasumov et al. (Kasumov, Kociak, Gueron et al., 2001) discovered ohmic behavior of the resistance of λ-DNA molecules deposited on a mica surface and stretched between rhenium carbon (Re/C) electrodes (Figure 2.10). In order to investigate the behavior, room temperature was varied from ambient temperature to 1 K. Below 1 K, an unusual

result was noticed; proximity-induced superconductivity in DNA. The resistance was measured directly with a lock-in technique and no *I-V* curves were presented. This amazing proximity-induced superconductivity is in opposition to available published data and with theory. No similar results were observed after that by any group (Kasumov, Kociak, Gueron et al., 2001).

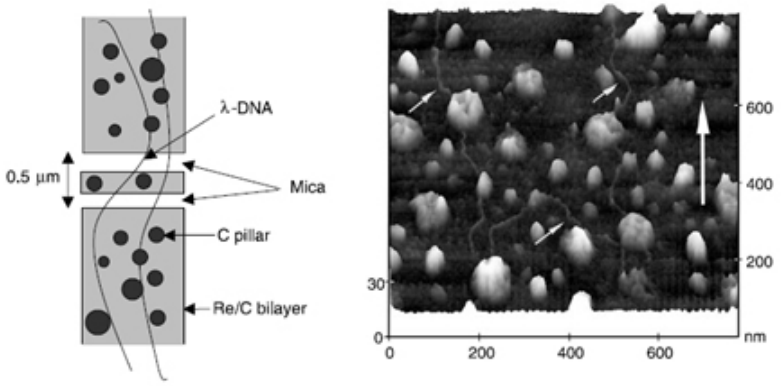

(a) (b)

Figure 2.10: (a) Schematic drawing of the measured sample, with DNA molecules combed between Re/C electrodes on a mica substrate. (b) Atomic force microscopy image showing DNA molecules combed on the Re/C bilayer (Kasumov, Kociak, Gueron, et al., 2001).

Porath and his coworkers' measured *I-V* curves at room temperature on a DNA molecule trapped between two metal nanoelectrodes. The DNA molecule (30 base pairs, double stranded poly(G)-poly(C)) is 10.4 nm long and the nanoelectrodes are separated by 8 nm. Subsequent *I-V* curves (different colours) show similar behaviour but with a variation of the width of the voltage gap. Note that the conductance in these measurements is limited by a 2 GΩ series resistor and air humidity is 50% (Porath, Bezryadin, De Vries et al., 2000a). Deposition of a DNA molecule between the electrodes was achieved with electrostatic trapping (Bezryadin, Dekker, 1997; Bezryadin, Dekker, Schmid, 1997). As shown in Figure 2.11, it is evident that the DNA oligomer does not conduct charge for biases below 1 V at room temperature, which

shows that the poly(dG)-poly(dC) DNA with a large band-gap behaves like a semiconductor.

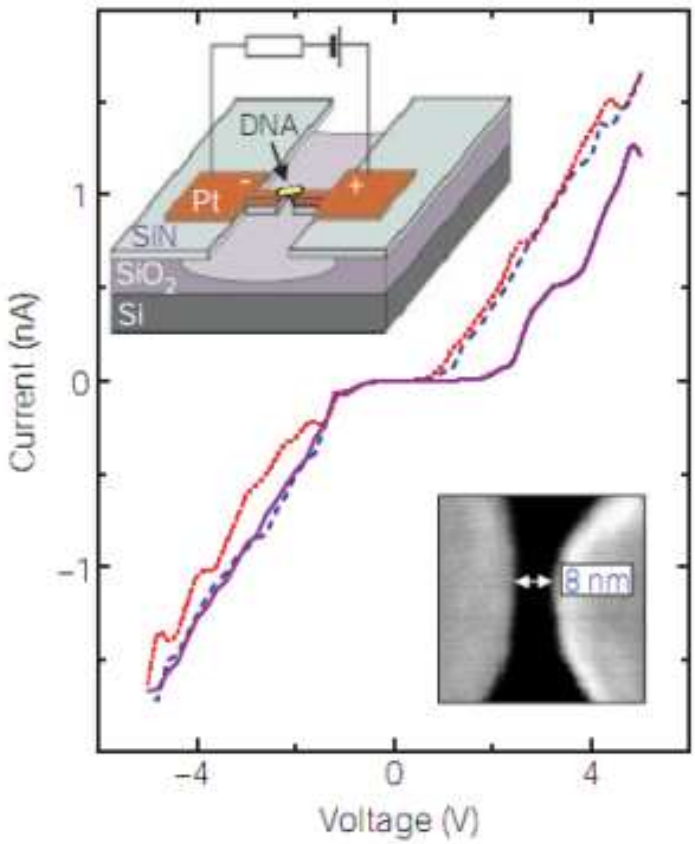

Figure 2.11: Current-voltage curves on a DNA molecule (D. Porath, A. Bezrvadin, S. De Vries, et al., 2000).

Xu and co-workers (B. Xu, Zhang, Li et al., 2004) developed a STM-based method to measure the *I-V* curves of DNA molecules in a wet environment by capturing directly from solution. They studied both uniform poly(GC)-poly(CG) sequences of length varying from 8 to 14 base pairs and similar sequences intercalated by A-T pairs in the middle (total length changing from 8 to 12 base pairs) and A-T (length changing from 0 to 4 base pairs). The molecules were terminated by $(CH_2)_3$-SH thiol groups at the 3′ ends to form stable S-Au bonds with the gold substrate. Technique to create molecular junctions first involves an STM tip brought into contact with a flat gold surface covered by the DNA solution. The tip is then retracted under the control of a feedback loop to

break the direct tip-electrode contact. During this step, the DNA molecules will bridge the tip and the substrate as shown in Figure 2.12 (R. D. Felice, 2009).

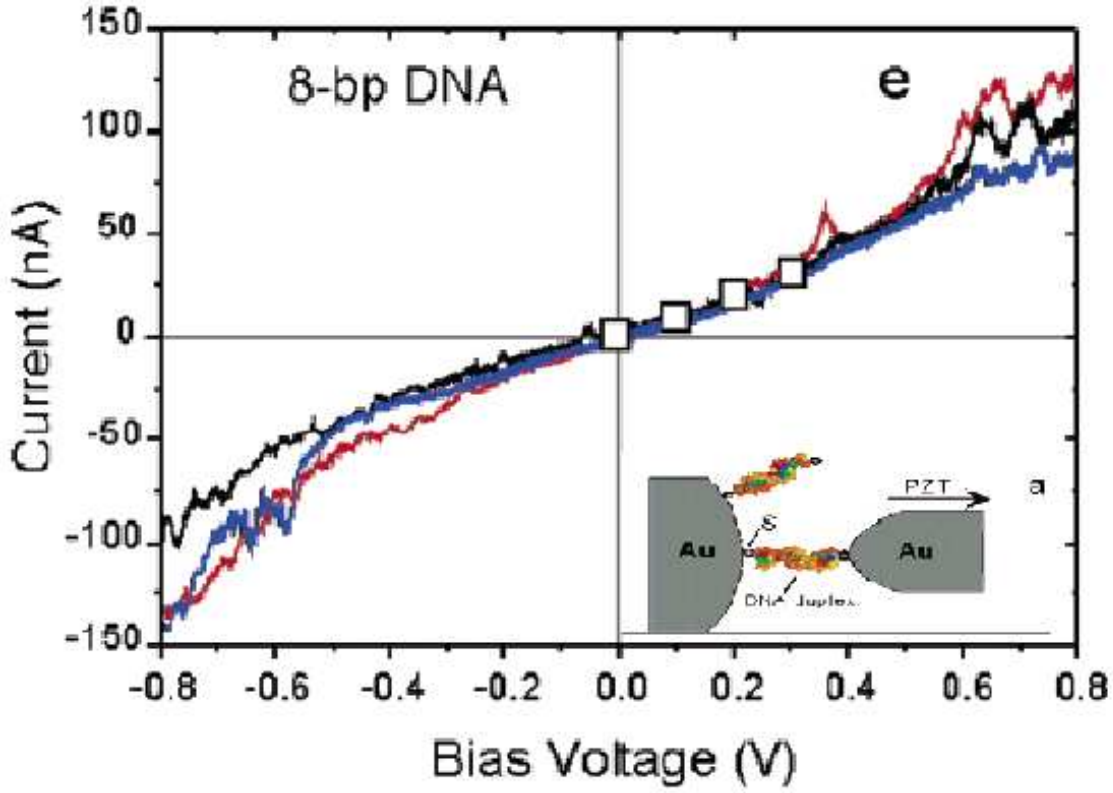

Figure 2.12: *I-V* curves of three different junctions formed by the same kind of 8-base pair DNA molecules of sequence (GC) 4 (B. Xu, Zhang, Li et al., 2004).

De Yu and his colleagues (De Yu, Grote, 2007) reported the first observation of unanticipated photoelectric effect (PE) under visible and near-infrared illuminations and diode-type rectifying *I-V* characteristics in DNA-metal contact devices. These devices are constructed with DNA film sandwiched between gold (or some other metal) and transparent conductive ITO electrodes. Since the gold work function and the band gaps of ITO and DNA are greater than 4 eV, in order to release an electron in these materials, the photon energy must be greater than 4 eV. This indicates the need for an ultraviolet light source. To explain these phenomena, they hypothesize that a Schottky barrier was formed at the DNA-gold interface when the gold layer was deposited on the soft DNA film during the sputtering process (De Yu, Grote, 2007). Storm et al. (Storm, Van

Noort, De Vries et al., 2001) reported electrical transport measurements for double-stranded DNA molecules located between nanofabricated electrodes. They observed the absence of any electrical conduction through these DNA-based devices, both at the single-molecular level as well as for small bundles of DNA. They also find a lower bound of 10 TΩ for the resistance of a DNA molecule at length scales larger than 40 nm. It is concluded that DNA is insulating. This conclusion was based on an extensive set of experiments in which they varied key parameters such as the base-pair sequence, length between contacts 40-500 nm, substrate SiO_2 or mica, electrode material (gold or platinum) and electrostatic doping fields. Hwang et al. (Wang, Kawde, 2002) performed direct measurements with the aid of gold electrodes on a SiO_2 substrate. They reported the details of the electrical transport through 60 base pairs of poly(G)-poly(C) DNA molecules between two electrodes with nanometer spacing. An almost monotonic increase in the current is observed from the sample with the gap of 30 mm and with a DNA solution droplet. *I-V* graph measured from various samples with the electrode gap ranging from 20 to 100 nm at different conditions show reproducible clear staircases. Cai et al investigated direct measurements of the intrinsic electrical characteristics of polynucleotides using a conducting-probe AFM under vacuum. Poly(dA).poly(dT) self-assemble a cross-interlaced network on mica, but poly(dG).poly(dC) self-organize a uniform 2-dimensional reticulated structure where poly(dA).poly(dT) and poly(dG).poly(dC) are kind of DNA which one strand contains adenine (A) bases, and the other only thymine (T) bases and one strand contains adenine (G) bases, and the other only thymine (C) bases, respectively. Transport studies demonstrate that poly(dG).poly(dC) can act as a semiconducting nanowire and show a better conductance than that in poly(dA).poly(dT) (Figure 2.13) (Cai, Tabata, Kawai, 2000).

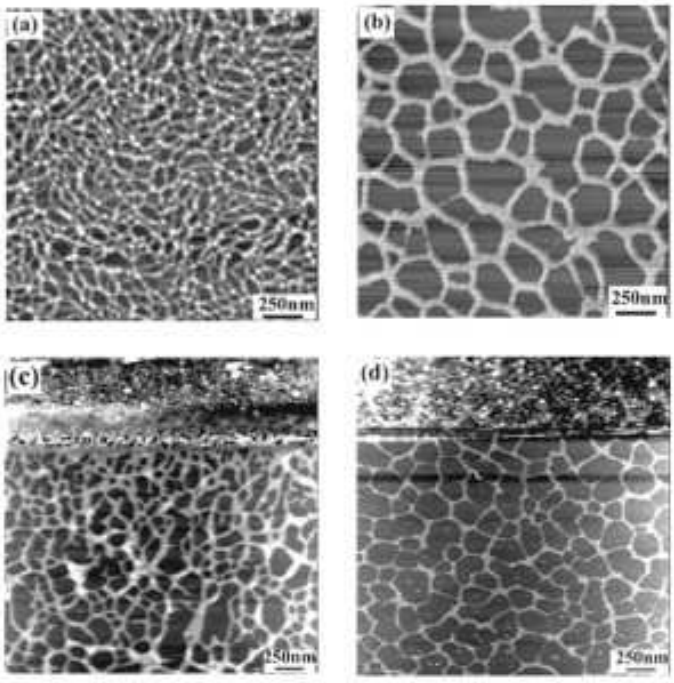

Figure 2.13**:** Self-assembled DNA networks of (a) poly(*dA*).poly(*dT*)/5*U* and (b) poly(*dG*).poly(*dC*)/5*U* on mica. A gold electrode is evaporated on the DNA networks of (c) poly(*dA*).poly(*dT*)/4*U* and (d) poly(*dG*).poly(*dC*)/5*U*. (1*U*550 μg/ml) (Cai, Tabata, Kawai, 2000)**.**

Details of these structures can also be controlled (Kanno, Tanaka, Miyoshi, Fukuda et al., 2000; Kanno, Tanaka, Miyoshi, Kawai, 2000a, 2000b). As shown in Figure 2.13(c) and (d), a gold electrode was evaporated to form a contact to the DNA network. A conducting probe AFM in Figure 2.14(a) is performed to explore the local electrical characteristics of DNA bundles and single molecules. Figures 2.14(c) and 2.14(d) show the typical I(V) curves of poly(dG).poly(dC) (Cai, Tabata, Kawai, 2000).

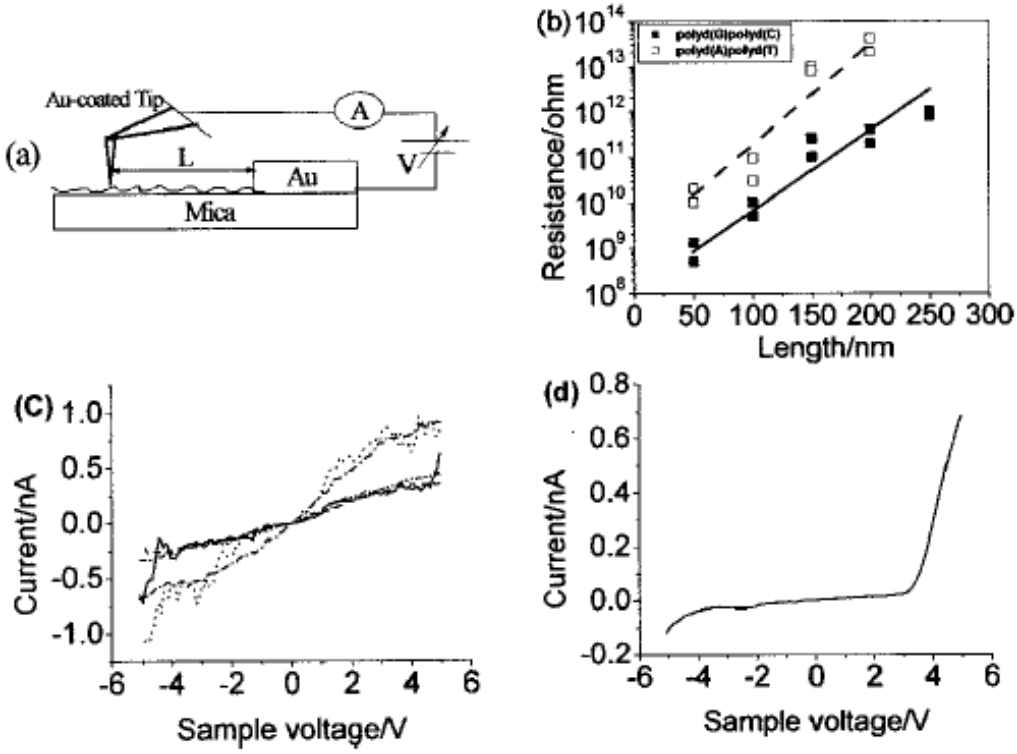

Figure 2.14: (a) Schematic illustration of the measurement with the conducting probe AFM. (b) Relationship between resistance and DNA length. (c) Typical *I-V* curves of poly(dG).poly(dC). (d) rectifying curves of poly(dG).poly(dC) (Cai, Tabata, Kawai, 2000).

Yoo et al. reported direct measurements of electrical transport through poly(dA)-poly(dT) and poly(dG)-poly(dC) DNA molecules containing identical base pairs. They have also investigated the effect of gate voltage on the *I-V* curve. It demonstrates the possibility of a DNA field-effect transistor operating at room temperature. Furthermore, the gate-voltage dependent transport measurements show that poly(dA)-poly(dT) behaves as an n-type semiconductor, whereas poly(dG)-poly(dC) behaves as a p-type semiconductor. They also studied temperature dependence of the current (Yoo, Ha, Lee et al., 2001). Measurements were repeated under both vacuum and ambient conditions, the results indicate no significant difference (Bezryadin, Dekker, Schmid, 1997). The *I-V* characteristic curve for DNA revealed a considerable band-gap at below 161 K. This can be accounted for by a small polaron hopping model (Böttger, Bryksin, 1985), where the current is given by Eq. 2.2;

$$I \propto \sinh bV e^{-E_a/k_B T} \quad \text{Eq. 2.2}$$

where E_a is the activation energy, $b = \frac{ea}{2K_B T} d$, a is the hopping distance, T is the background temperature, d is the distance between the electrodes and e is the electron charge.

2.6 Charge Transport Mechanisms

Charge transport in DNA is intensively investigated in view of its biological implications in damage and repair, protein bonding and envisioned integration in future bio-electronics or DNA-based chips. The previous section outlined the major experiments on the transport characteristics of DNA, suggesting that in several examples these experimental works afforded contradictory results, even on apparently similar system configurations. This section presents an interpretation of the experiments according to physical models. Many transport mechanisms have been suggested to explain different experimental results. These versatile results happen due to the difference in conducting properties of DNA. Among the well-known mechanisms for interpreting results, three well-known transports are mostly referred to. These mechanisms are sequential tunneling, thermal hopping and coherent tunneling (Figure 2.15). Other methods are polaron and soliton formation and will be discussed at the end of this section. However, in some rare conditions, these well known mechanisms are ignored due to DNA configuration or test conditions. For instance in fluorescence experiments; charges can jump between bases because of thermal fluctuations (Figure 2.15A). Nonetheless, this process requires quite large amount of thermal energy. Therefore, this case is very unlikely to happen. Charges may tunnel from one site to the next sequentially (Figure 2.15B). After each tunneling process, the coherence of the charge wave function is lost through dephasing processes, such as scattering with

molecular vibrations. It is worth noting that none of the mentioned mechanisms depend on DNA length. Finally, charge can tunnel through the whole length of DNA as shown in Figure 2.15C. In this case, the charge wave function does not lose phase coherence. So, the process is called coherent or unistep tunneling. This mechanism is strongly based on distances (Di Ventra M., 2004). The vertical axis represents energy, *E*, and the horizontal axis represents the spatial position, *x*.

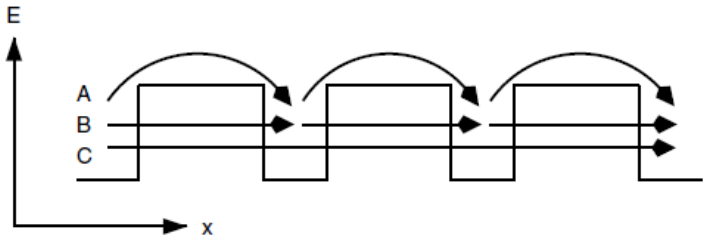

Figure 2.15: Representation of three possible mechanisms for charge transfer in DNA, depicted as a series of energy barriers, (A) Thermal hopping (B) Sequential tunneling (C) Coherent or unistep tunneling (Di Ventra M., 2004).

Several researchers believe that charge coherently tunnels through the whole length of DNA with a rate of charge transfer *R*;

$$R \propto e^{\beta L} \qquad \text{Eq. 2.3}$$

where β is the tunneling decay length and *L* is the length of the DNA. As the value of β increases, the rate of tunneling decreases rapidly with increasing distance (Krider, Meade, 1998; Lewis, Letsinger, 1998; Netzel, 1998; Priyadarshy, Risser, Beratan, 1998; Turro, Barton, 1998). Long-range charge transfer has also been examined through a scattering matrix formalism and Büttiker's dephasing model (X. Q. Li, Yan, 2001; Y. Yan, Zhang, 2002). This mechanism has been successfully used to interpret the experimental consequences of Porath and co-workers (Porath, Bezryadin, De Vries et al., 2000b), Lee, et al. (Lee, Tanaka, Otsuka et al., 2002) and Li and Yan (S. H. Li, Chow, 2001) on a DNA molecule having 30 GC pairs between two electrodes. A

convenient agreement between experiment and theory has been obtained by supposing partial dephasing.

Schuster et al. and Henderson and co-workers proposed a phonon-assisted, polaron-like hopping mechanism for charge transfer (Henderson, Jones, Hampikian et al., 1999; Schuster, 2000). Since structural fluctuations of DNA are relatively fast (Brauns, Madaras, Coleman et al., 1999; Liang, Freed, Keyes et al., 2000), the local structure around a charged base is likely to rearrange. The distance and angle in between base pairs would thus decrease.

Berlin and co-workers (Berlin, Burin, Ratner, 2002) investigated the competition between hopping transport and coherent using a 1-dimensional tight-binding model. In this case, the DNA sequence was selected to be of the form $(AT)_m$-GC-$(AT)_n$-GC-$(AT)_m$ where n is the number of AT pairs and m is to simulate exposed or buried donor and acceptor groups. The rate for tunneling is calculated with Eq. 2.4;

$$v_{tun}e^{-\beta L} \qquad \text{Eq. 2.4}$$

where $L = (n + 1)a$ is the distance between the two GC pairs, a is the distance between base pairs, β is the tunneling decay length derived from the tight-binding model and v_{tun} is a fitting parameter. The rate for thermal transport is assumed to be;

$$v_{therm}e^{\left(-\frac{g_G}{k_BT}\right)} \qquad \text{Eq. 2.5}$$

where g_G is the energy separation between the hole state on the G-C pair and the bottom of the A-T band, which is derived from the tight-binding model. There is a critical value

of n when these two rates are equal, at which the main mechanism will switch from tunneling to thermal hopping. Using this model, it is estimated to be between three and five, depending on the value of the transfer integral between adjacent base pairs. This is in agreement with the experimental work of Giese (Giese, 2002), where the transfer rate has been found to drop exponentially up to a bridge length of three A-T pairs. This also agrees with experimental evidence that suggests some charge is localized on the A-T bridge (Sartor, Boone, Schuster, 2001; Williams, Odom, Barton, 2000). In this context, the property of structural distortions and fluctuations have also been measured (Berlin, Burin, Ratner, 2001; Grozema, Siebbeles, Berlin et al., 2002; Wan, Fiebig, Kelley et al., 1999; Zhang, Austin, Kraeft et al., 2002).

At last, we need to reiterate that besides the three main transport mechanisms discussed herein, polaron (Breslin, Coury, Anderson et al., 1997; Gasper, Schuster, 1997; Henderson, Jones, Hampikian et al., 1999; Yoo, Ha, Lee et al., 2001) and soliton (Hermon, Caspi, Ben-Jacob, 1998; Lakhno, 2000) formation in DNA have also been investigated. The former concerns the coupling of the vibrational and electronic mode degrees of freedom while the latter pertains to the formation of domain walls in dimerized bonds of DNA.

2.7 Magnetic Properties

Currently, the magnetic field biosensors and magnetoresistive biochips particularly is being pursued by a number of research laboratories around the globe (Anguelouch, Reich, Chien et al., 2004; Ejsing, Hansen, Menon et al., 2004; Freitas, Ferreira, Graham et al., 2004; Rife, Miller, Sheehan et al., 2003; Shen, Liu, Mazumdar et al., 2005). Even though this kind of devices promise a specific biosystem that gives great sensitivity, low delay time and high throughput, some obstacles still must be removed before

possible commercialization. Ferreira with his group described the responsibility to various magnetic label concentrations. The fabricated at Microsistemas and Nanotecnologias (INESC MN) is used for disease diagnostics (H. A. Ferreira, Graham, Feliciano et al., 2005). This kind of device was established on the influence of magnetically labeled biomolecules with *AC* field according to focusing method (H. Ferreira, Feliciano, Graham et al., 2005).

Modern findings of electromagnetic (EM) signal transduction in the membrane Na, K-ATPase are well described by direct interaction between magnetic and electric fields with mobile charges inside the enzyme. Interaction with moving charges is a mechanism that also happens in other biopolymers. New findings on DNA illustrate that large electron flows can happen inside the stacked base pairs of the double helix. So, gene activation by magnetic fields might be decided owing to direct interaction with moving electrons inside DNA. Electric and magnetic fields stimulate transcription and both fields could interact with the DNA directly. The mechanism of EM field stimulated transcription may be related to the process in striated muscles, where endogenous electrical activity induces the synthesis of new proteins (Blank, Goodman, 1997).

Electric fields, in a similar manner to magnetic fields, have been proved to stimulate transcription. Comparison of the effects of both fields have revealed the same transcripts with analogous patterns of frequency, amplitude and time dependence (Blank, Soo, Lin et al., 1992). A study was dedicated to the sensitivity of magnetoresistance of DNA-chip proposed for diagnostic test. The microchip, involved of several parts such as an array of (2.5×80) μm^2 with U-shape, spin sensors combined within current line systems for magnetic analysis. Enabling detection at 30 Hz with magnetic nanoparticles size of 250 nm, it was shown that the sensor sensitivity

increased linearly with concentration. A thermal noise of 10^{-17} V^2/Hz with a $1/f$ knee at 50 kHz at a 1 mA obtained from these sensors also allows low detection limits that are feasible for this kind of thermal noise (H. Ferreira, Cardoso, Ferreira et al., 2006). In direct confrontation to the common opinion that exposure to magnetic field of low frequency simulates mutations in organisms, it has been postulated that a magnetic field can actually favor the efficiency of DNA repair (Chow, Tung, 2000).

Henbest and Maeda et al. encountered a magnetic-field effect on the photochemical yield of a flavin–tryptophan radical pair in *Escherichia coli* photolyase. This result provides an evidence of principle that photolyases, and most likely by extension also cryptochromes, have the fundamental necessities required to form the basis of a magnetic compass (Henbest, Maeda, Hore et al., 2008). The effect of an external magnetic field on the elastic inter-electrode tunneling intervened by a molecular wire is investigated theoretically (the case with the wire containing paramagnetic ions) (Petrov, Tolokh, May, 1998).

2.8 Connection of DNA to Surfaces

The basic step towards DNA-based nanotechnology is to link DNA molecules to surfaces. The most commonly used attachment routine so far exploits the covalent bond between gold and sulfur (Bain, Troughton, Tao et al., 1989; Dubois, Nuzzo, 1992; Herne, Tarlov, 1997; Hickman, Laibinis, Auerbach et al., 1992; Nuzzo, Allara, 1983; Yang, Yau, Chan, 1998). Nuzzo and Allara were the first reporting the formation of long chain ω-substituted dialkyldisulfide molecules upon gold substrates (Nuzzo, Allara, 1983). Bain and co-workers (Bain, Troughton, Tao et al., 1989) explained a simulated system made up of long-chain thiols to be adsorbed from solution onto gold to build compressed and packed, oriented monolayers. Sulfur bonding head group to the

gold substrate is in form of a metal thiolate, which is a very strong connection (~44 kcal/mol) and yet the resulting films are extremely stable and very suitable for surface attachment of functional groups. The DNA molecule can be functionalized with a thiol (S-H) or a disulfide (S-S) group at the 3' or 5' end, For example. Hickman and Colleague also explained the selective and orthogonal self-assembly of disulfide with isocyanide and gold with platinum (Hickman, Laibinis, Auerbach et al., 1992). Biotinylated oligonucleotides adsorption on a surface of particle coated with avidin have also been studied (Alivisatos, Johnsson, Peng et al., 1996; Niemeyer, Bürger, Peplies, 1998). It is worthwhile mentioning other techniques to adhere DNA to surfaces, for example the covalent binding of DNA oligonucleotides to a preactivated particle surface (Pathak, Choi, Arnheim et al., 2001).

2.9 Nanoelectronics-DNA Applications in Nanoscale Electronics

2.9.1 DNA: Molecular Electronics

In the mid 1990s, a short time after Barton's molecular wire hypothesis, Warman and co-worker (1996) gauged the radiation-induced conductivity of arranged DNA films. Although hydrous DNA exhibited mobile charge carriers, the lack of anisotropy in the connection argued against a quasi-1-dimensional metal. New experiment was performed for the last few years on DNA's conductance, revealing diversity results of ranging from wide-gap insulating behavior to proximity-induced superconductivity. This is of intense significance to determine these issues, particularly since conducting DNA could breed a variety of applications in biotechnology as well as molecular electronics. Just to mention some of these potentials, think of the DNA chip, which is employed for DNA sequencing, detection of disease and expression of gene analysis. Provided that DNA can conduct adequately well, a sequence could be electronically deciphered instead of visualized (using fluorescent dyes) as performed at the current stage of art. The essence

of the innovation is that the single strands hanging of DNA are insulating while well-stacked double stranded DNA, once undergone satisfactory hybridization, could be conducting, thus enabling an electronic re-read. It's scheme may have the advantage of a higher density of single-strand DNA samples on the chip (the density of single-strand area on present optically read chips is resolution-limited) with the prospective of quicker and more efficient sequence analysis (Endres, Cox, Singh, 2004).

2.9.2 Self Assembly

DNA is a crucial biological polymer which carries genetic data. It is extremely interesting as a functional nano-scaled material, and that's because of its salient characteristic which cannot be found in other polymers. DNA owns complementarity; self-assembling ability that can always forms hydrogen-bonded base pairs of A and T and of G and C, where the base pairs line up 1-dimensionally at 0.34–0.36 nm intervals. For this reason of self-assembling ability, DNA can be highly integrated without any error with no need for microfabrication technologies (Taniguchi, 2006). Controlling the on-chip organization and conformation of DNA is important for a number of interrelated nanotechnological disciplines (Reisner, Larsen, Flyvbjerg et al., 2009). Numerous researchers have shown that the diverse properties of DNA make it especially flexible in a broad range of applications from computation to fueling nanomechanical devices (Liu, Sha, Seeman, 1999; Lo, Karam, Aldaye et al., 2010; Lukatsky, Frenkel, 2005; Mao, LaBean, Reif et al., 2000; Mao, Sun, Seeman, 1999; Niemeyer, Adler, 2002; Nulf, Corey, 2002; Winfree, Liu, Wenzler et al., 1998; Yurke, Turberfield, Mills Jr et al., 2000).

Ordering and arrangement of nanoparticles is the key to materialize storage media and electronic devices. Nonetheless, this is a tough task, for example, to arrange hexagonal

closed-packed structures (Brust, Bethell, Kiely et al., 1998; Fendler, 1996; Henrichs, Collier, Saykally et al., 2000; Sastry, 2000; Whetten, Khoury, Alvarez et al., 1996). A DNA template, from another viewpoint, is flexible enough to be shaped in many different ways. For instance, a number of geometrical structures of DNA, such as cubes and knots have already been fabricated (Seeman, 1998). Periodic arrays are presently being analyzed as the chief components in nano-scaled memory devices and other electronic applications. One likely drawback of using DNA in these applications lies in it that the yielded structures are not rigid (Seeman, 1998).

2.9.3 DNA as a Nanowire

Recently, progress in electrochemical biosensors for DNA analysis has become quite prominent. Two current major concerns confronting DNA analysis are selectivity and sensitivity. The former can be attained by using peptide nucleic acids as probes or by relying on the DNA-mediated electron transfer. Particular emphasis has been addressed to the efforts for high sensitivity, entailing combination with Polymerase Chain Reaction (PCR) techniques, enzyme-labeled schemes, direct label-free detection and nano-based approaches (Ju, Zhao, 2005). DNA's self-assembly and electronic properties have been the center of much research during the past few years. Both properties hold immense importance in understanding the functionalities of DNA in living cells and points that DNA could be of application in nanoscience. On the other hand, the transport characteristics of DNA are of benefit in several areas of science and technology due to their relevance to damage and mutation in DNA (Breslin, Coury, Anderson et al., 1997; W. Chen, Turro, Friedman et al., 1997; Daniel, Barton, 1997; Guallar, Douhal, Moreno et al., 1999; Heller, 2000; Loft, Poulsen, 1996; Olson, Hu, Hörmann et al., 1997; Steenken, 1989, 1997). The use of molecules and nanomaterials to devise new schemes of detection, manipulation and sequencing of DNA is also currently being investigated

(Aziz, Golovchenko, Branton et al., 2001; Kasianowicz, Brandin, Branton et al., 1996; C. V. Kumar, Punzalan, Tan, 2000; Marziali, Akeson, 2001; Meldrum, Holl, 2002; Meller, Nivon, Branton, 2001; Taton, Mirkin, Letsinger, 2000; Terbrueggen, Johann, Barton, 1998; Vercoutere, Winters-Hilt, Olsen et al., 2001; D. Wemmer, 1998; D. E. Wemmer, 2000). The properties of DNA charge transport are essential to such progressions. For example, alterations of electrochemical detection of structural owing to protein binding or base mismatches is being examined at the moment (Boon, Barton, Pradeepkumar et al., 2002; Erdem, Ozsoz, 2002; Fahlman, Sen, 2002; Gooding, 2002; Kelley, Boon, Barton et al., 1999; Lisdat, Ge, Krause et al., 2001; Marshall, Hodgson, 1998; Niemeyer, 2010).

More recently, Dutch researchers have shown that a 10.4 nm-long (30-base-pair) poly(G)-poly(C) sequence has electrical characteristics similar to that of a semiconducting diode that allows current to flow in one direction only (Porath et al., 2000). The researchers measured *I-V* curves in the range of –4 to +4 V and observed that the measured current did not drop more than 1 pA below a certain threshold. Within the mentioned voltage range, DNA acted as an insulator. Beyond the threshold voltage, the current picked up sharply, making DNA conduct charge and hence behave similarity to silicon-based semiconductors used in the electronic industries. The basic combination arrangement for constructing an Ag nanowire attached to two gold electrodes can be seen in Figure 2.16. Two gold electrodes apart from each other by a defined distance (12 to 16 μm) were placed onto a glass slide using photolithography. Transforming the DNA bridge into a conductive wire was achieved by specific metal coating using the DNA molecule as a template (Figure 2.17).

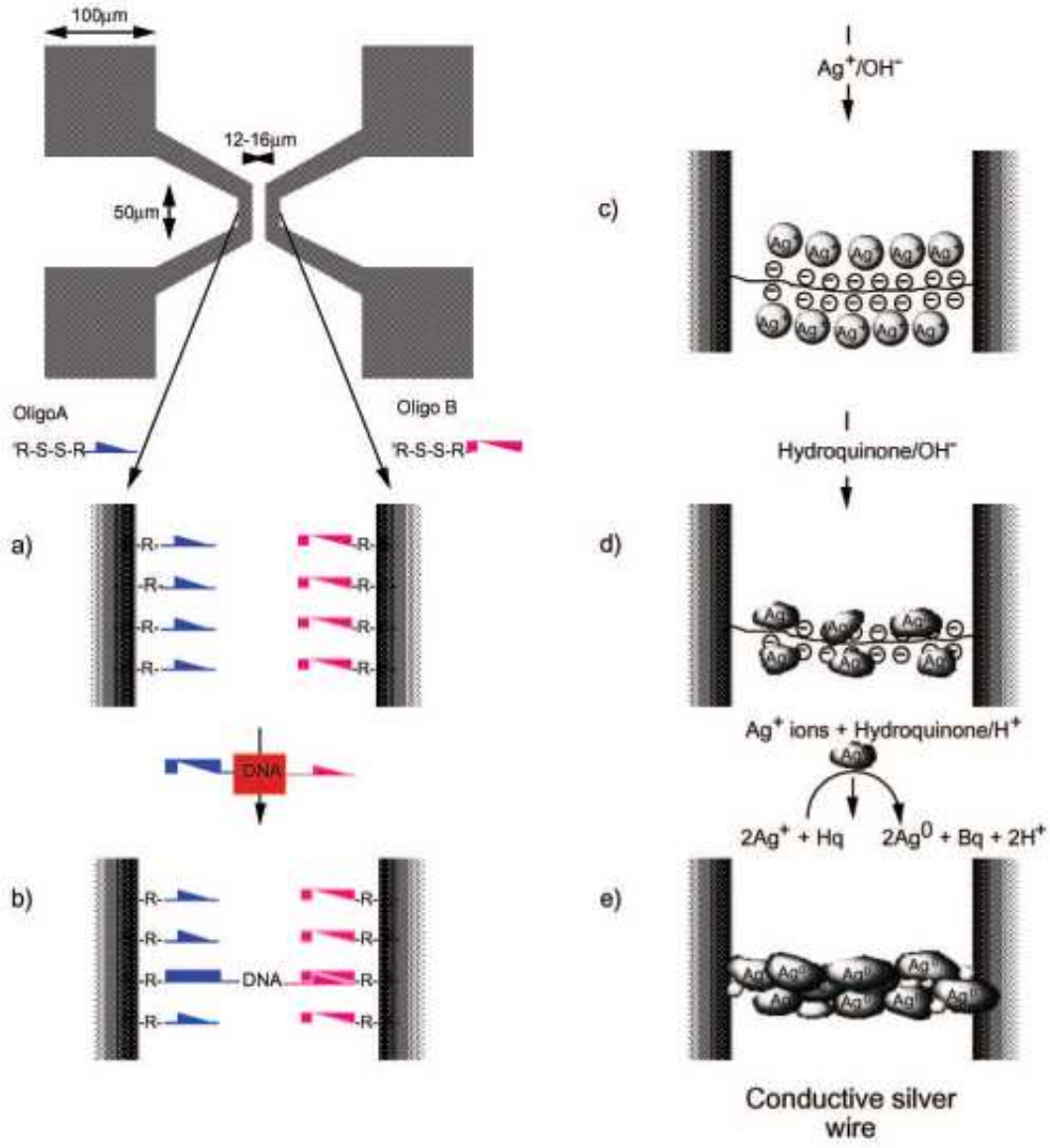

Figure 2.16: Construction of a silver wire connecting two gold electrodes. The top left image shows the electrode pattern (0.53×0.5 mm) used in the experiments. The two 50 µm long, parallel electrodes are connected to four (100×100 mm) bonding pads. (a) Oligonucleotides with two different sequences attached to the electrodes. (b) λ-DNA bridge connecting the two electrodes. (c) Silver-ion-loaded DNA bridge. (d) Metallic silver aggregates bound to the DNA. (e) Fully developed silver wire. A full description of the preparation steps can be found in the Methods section (E. Braun, Eichen, Sivan,et al., 1998).

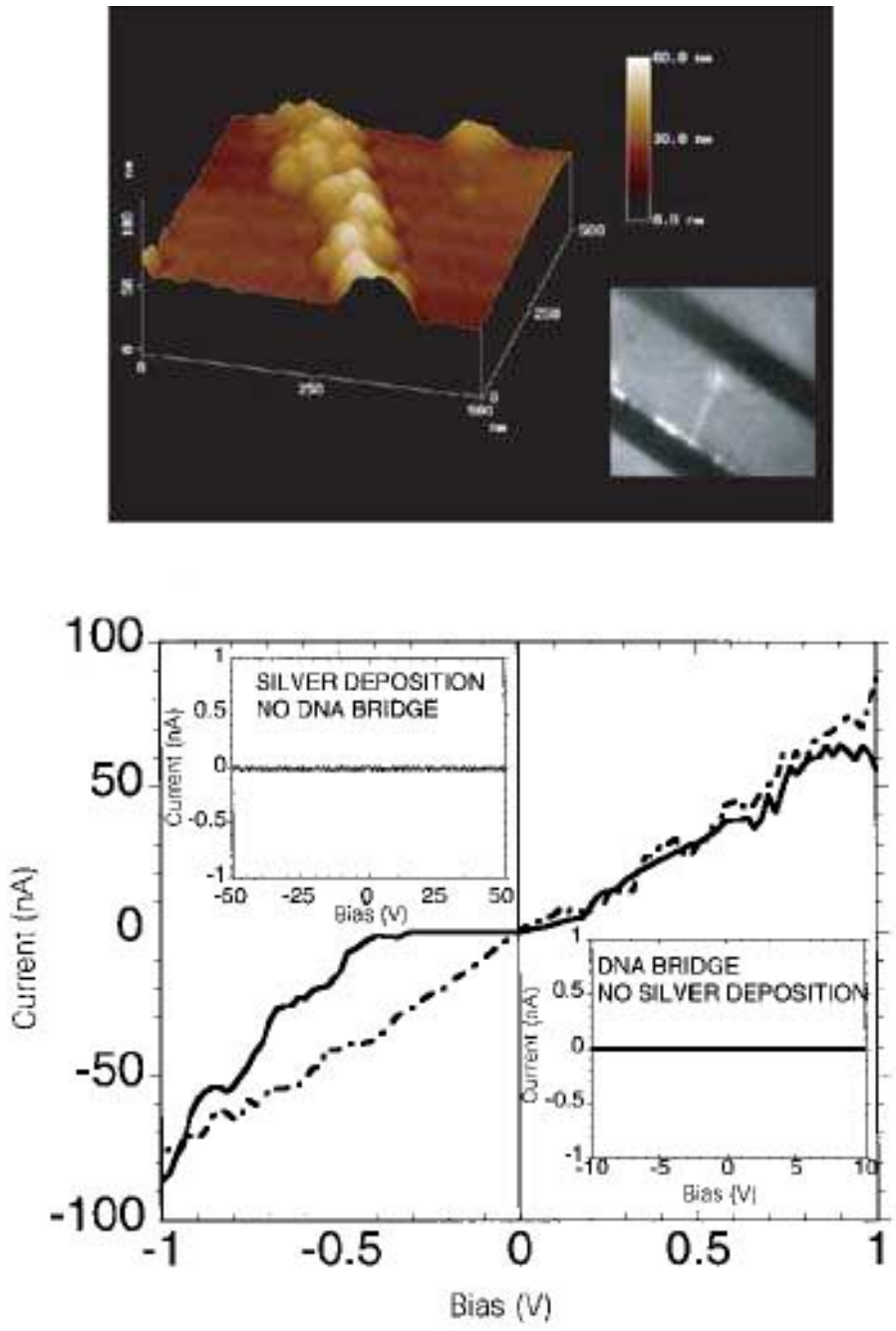

Figure 2.17: AFM image of a silver wire connecting two gold electrodes 12 μm apart and 0.5 μm field size. Inset: Fluorescently labeled λ-DNA molecule stretched between two gold electrodes (dark strips), 16 μm apart (E. Braun, Eichen, Sivan et al., 1998).

The electrodes are connected to large bonding pads 0.25 mm away (see Figure 2.17). The image on the bottom show two-terminal *I-V* curves of the silver wire. Note the current plateau (dashed dotted line), on the order of 0.5 V. Applying 50 V to the wire, permanently eliminated the plateau to give an ohmic behavior (solid line) over the

whole measurement range. *I-V* curves of a DNA bridge without and with silver deposition in the absence of DNA bridge are depicted at the bottom and top insets respectively. Clearly, the sample is insulating in both cases. As the fabrication process synthesizes many wires, it was necessary to measure each wire's resistance by systematically cutting them. The yielded wires exhibited ohmic behavior as shown in Figure 2.18. The measured resistance was found to correspond approximately to 700 Ω, which translates to a specific conductivity of 2×10^4 Scm^{-1} which is about one order of magnitude less than bulk palladium.

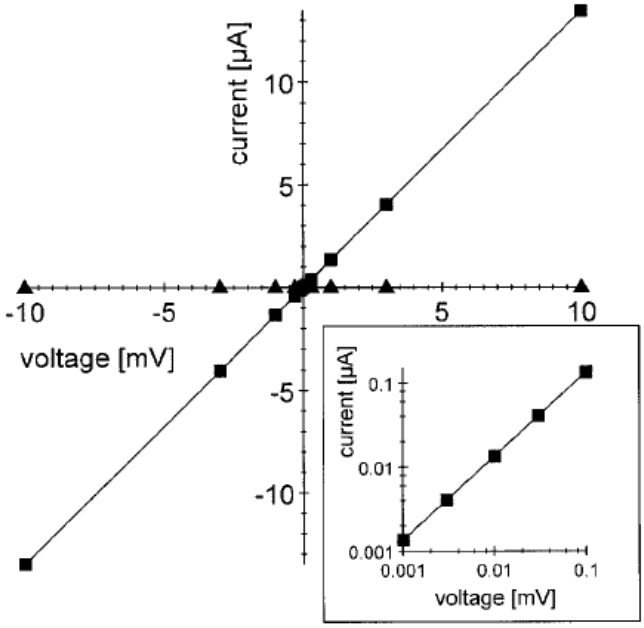

Figure 2.18: Two-terminal *I-V* curves of the single, pinned nanowire shown in Figure 2.19 before (■) and after (▲) cutting, taken with a patch-clamp amplifier (EPC9, Heka, Germany). The wire resistance is 743 Ω corresponding to a minimum estimated specific conductivity of $\boldsymbol{\sigma}$ of about 2×104 Scm^{-1}. The inset shows the ohmic *I-V* characteristic of the nanowire down to 1 µV. After cutting, the sample was found to be insulating (Richter, Mertig, Pompe et al., 2001)

Richter and her colleagues presented measurements of the electrical conductivities of metallic nanowires, which were fabricated by chemical deposition of a thin continuous palladium film onto single DNA molecules to install electrical functionality. The DNA molecules have been positioned between macroscopic Au electrodes and were

metallized afterwards. Low-resistance electrical interfacing was obtained by pinning the nanowires at the electrodes with electron-beam-induced carbon lines. The investigated nanowires exhibited ohmic transport behavior at room temperature (Richter, Mertig, Pompe et al., 2001). A single palladium wire is shown in Figure 2.19.

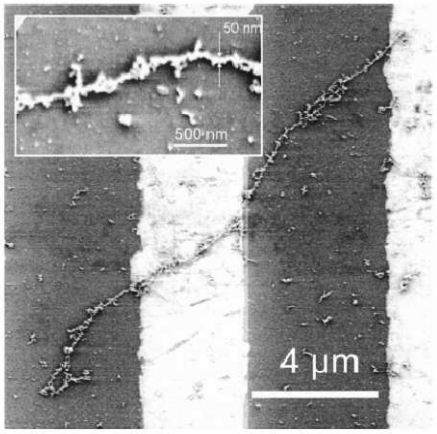

Figure 2.19: Palladium wire made from metallization of λ-DNA (Richter, Mertig, Pompe et al., 2001).

Martin and his colleagues reported on the preparation of Ag and Au wires with using the DNA as a main or template (Martin, Dermody, Reiss et al., 1999). The fundamental intention of this work was to synthesize platinum or gold metal wires, functionalize them with complexes formation between the DNA and gold bases. *I-V* characteristics were recorded to appraise the possible use of these nanowires. Researchers also declared that the formation of luminous self-assembled poly (p-phenylenevinylene) wires with liable applications in optics (T. S. Mayer, 1999).The work seems so promising with avenue for further research to control the wire width, the contact resistances between the silver wires and the gold electrode and implementation of other metals/materials.

Richter and his colleagues in 2002 also presented low-temperature measurements of the electrical conductivity of metallic nanowires assembled on single DNA molecules by chemical deposition of a thin continuous palladium film. Just like their earlier work

(Richter, Mertig, Pompe et al., 2001), nanowires exhibit ohmic transport behaviour at room temperature. At low temperature, they observed an increase of resistance with decreasing temperature following a logarithmic dependence. This behaviour can be described with quantum effects in a disordered metallic film (Reichert, Ochs, Beckmann et al., 2002).

Yan and co-workers (H. Yan, Park, Finkelstein et al., 2003) offered the design and fabrication of a DNA nanostructure that possesses a square aspect ratio and easily self-assembles into two separate lattice forms namely 2-dimensional nanogrids and nanoribbons. The 4 by 4 tile contains four four-arm DNA branched junctions, pointing in four directions. Such nanogrids have large cavity size, which may serve as tethering or binding sites for other molecular components. The loops for example, at the center of each tile can be adapted with appropriate functional groups and used as a scaffold, directing periodic assembly of desired molecules. Periodic protein arrays achieved by templated self-assembly of streptavidin onto the DNA nanogrids. The founders also used the 4 by 4 tile assemblies as templates to build a highly conductive and uniform-width silver nanowire. A double terminal *I-V* measurement of resulting silver nanowire was achieved at room temperature. The *I-V* curve is linear, presenting ohmic behavior in the range of -0.2 to 0.2 V. This nanowire is easily reproducible and has remarkably higher conductivity than previously reported double-helix DNA-templated silver nanowires (E. Braun, Eichen, Sivan et al., 1998). Besides applying DNA, some reports on using other biomolecules to synthesize nanowires were also reported. Djalali et al. (Djalali, Chen, Matsui, 2003) developed a new biological approach to synthesize Au nanowires exploiting sequenced peptide nanotubes as templates. Other research teams have also succeeded in synthesizing DNA based nanowires (Ford, Harnack, Yasuda et al., 2001; Harnack, Ford, Yasuda et al., 2002; Patolsky, Weizmann, Lioubashevski et

al., 2002). For the sake of reference, Harnack et al. fabricated a gold wire network upon a DNA template. In their work, Au nanoparticles of 1 to 2 mm topped with tris (hydroxymethyl) phosphine were bound to DNA. Nanowires with dimensions of 30 to 40 nm and resistivities around 1000 times larger than bulk gold were synthesized (Harnack, Ford, Yasuda et al., 2002). Ford and his co-workers (Ford, Harnack, Yasuda et al., 2001) meanwhile assembled DNA with 1 nm size platinum grains as a precursor to a larger wire. In their work, the platinum was attached directly to the bases, instead of benefiting from the ionic interaction with the backbone. The intention is to yield smaller wires with the preferred *I-V* characteristics (Ford, Harnack, Yasuda et al., 2001; Mertig, Ciacchi, Seidel et al., 2002).

2.9.4 DNA as a Sensor

Another application of the DNA's recognition mechanism is in its ability as a sensor material. The basic mechanism of a chemical sensor is a reaction between the sensor itself and the target. If the chemical to be detected is a single strand DNA, then nature already gave what the sensor has to use to complete the reaction; the complementary strand. Although the principle is very simple, the implementation of this reaction in a sensor that gives an output requires some talent. Single strands are attached to an AFM cantilever (Figure 2.20), and they are all dipped in the solution under test. If their corresponding complementary strands are present, they will bind to the attached ones, thus producing some stress and a deflection of the cantilever.

A different kind of DNA sensor, due to complementary binding, is the one where the signal comes out as a fluorescent signal or its cancellation. Commercially available, some companies have already begun selling the so-called DNA chips (Dewarrat, 2002).

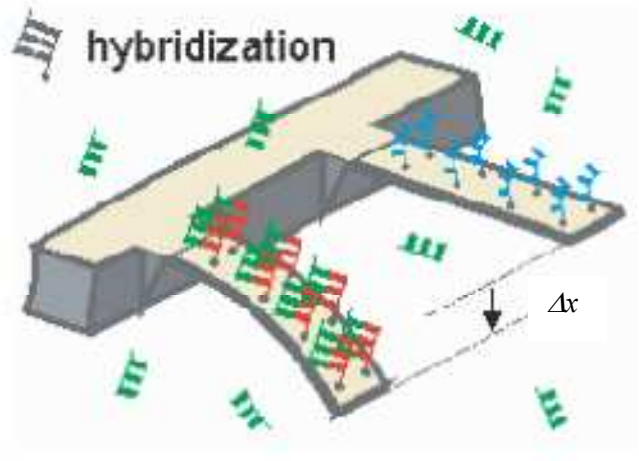

Figure 2.20: Detection system of AFM cantilevers. Hybridization occurs on the cantilever, provides matching sequence (red) to the nucleotide in solution (green), giving a unlike signal Δx (Fritz, Baller, Lang et al., 2000).

2.10 Al-DNA-Al Interaction and Creation of Nanogaps

In this work, NGs were created on the surfaces of thin Al films by chemical etching between DNA strands and Al. The RCA (Reaction Chemical Agents) process involving 10 min of boiling the p-type Si wafer in solutions of NH_3, H_2O_2 and H_2O (ratio 1:1:6) followed by boiling for 10 min in HCl, H_2O_2 and H_2O (ratio 1:1:6) was performed to prepare the substrate. The native oxide on the frontal surface of the substrate was removed using HF and H_2O solutions in the ratio of 1 to 10. Finally, it was rinsed in de-ionized water for 30 s (Figure 2.21(a)), followed by deposition of 100 nm of Al using thermal evaporation method (Figure 2.21(b)). The resulting thin film of Al thin film was then annealed for 30 min at 200°C.

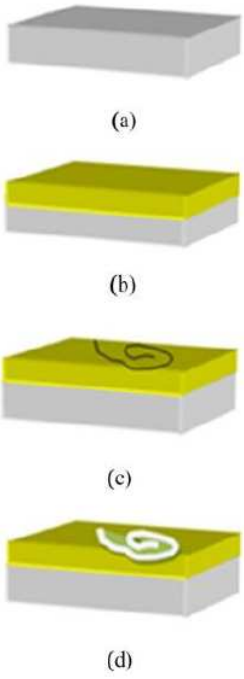

Figure 2.21: Schematic diagram showing the sample (a) cleaning silicon surface with standard method. (b) Al deposition with thermal evaporation method. (c) DNA strands transfer on Al surface. (d) Removal of DNA strands off the surface reveals imprint of strands on surface.

The DNA solution was first diluted to a suitable concentration of 0.01 (μg/nL) and allowed to flow along the Al surface using a micro syringe (Hamilton micro syringe) (Figure 2.21(c)). The prepared chip was then left exposed to the dry gas to let the liquid gradually and completely evaporate away. We control the duration of the interaction between DNA and Al thin film. This means that after 10, 20, 30, and 40 min of exposure of the DNA solution with the Al surface, the DNA strands are removed off the surface (Figure 2.21(d)). The NGs were later investigated using AFM technique (N. M. Khatir, S. M. Banihashemian, V. Periasamy et al., 2010). The proposed technique provides a simple and easy method for producing NGs with a diameter of about 63 nm and a depth of less than 100 nm. This kind of interaction between DNA and Al is important for design and fabrication of electronic chips as well as synthesis of NGs for investigation of electrical characteristics of biomaterials, particularly DNA strands. NGs are usually used as nano-electrodes in sensors to detect low dimensional structures such

as nano-particles and nano-wires. They are also used to characterize electrical transport in organic molecules (BioMath, 2011; Borneman, Schwarz, Stickler, 1955). The edges are not interdigitated but rather closely spaced nano-scaled gaps or distance between the edge which are maintained as small as possible (less than 1 to 100 nm) to enable trapping of nano scale molecules and have been widely utilized as NGs (Madelung, 1996; Malaquin, Vieu, Genevieve et al., 2004).

There are several techniques to fabricate NGs and can be found in various sources (Choo, Devereux, 1975; Chu, Wada, Inoue et al., 2006; McCarty, 1986; N. M. Khatir, S. M. Banihashemian, V. Periasamy et al., 2010). Etching method is a common technique to create nano and micro gaps. For many years, the interaction between metal and DNA strands has been the focus of research among scientists. Al, a metal with a positive charge in ionic form, prefers attaching to sites of DNA possessing a negative charge, J. Anastassopoulou in 2003 (Anastassopoulou, 2003) and Wu, et al. In 2005 (Wu, Du, Zhang et al., 2005) reported research on DNA interaction with metals and identified two kinds of bonding between DNA, based on water molecules and ions in the DNA environment. The mechanism for the interaction of Al ions with DNA is not well understood. Nanolithography based on X-ray exposure through a photo mask on a photosensitive material and ion beam lithography are techniques used for nano and microelectronic device fabrication (Park, Kim, Choi et al., 2010; Tsvetkova, Takahashi, Zayats et al., 2005). Nanotransfer printing or stamping is another method for patterning on the surface of metals and semiconductors (Mayer, 1959; Trimbach, Feldman, Spencer et al., 2003).

Lercel et al. (1964) and Snow et al. (1999) investigated the AFM method of nanopatterning on substrates based on a chemo-mechanical mechanism. Lercel et al.

(1964) and Headrick et al. (Headrick et al., 2005) meanwhile reported that alkyl monolayer-coatings could be used to etch nanoscale patterns on Si substrates. Traditional patterning methods using the AFM technique employ probe tips. Chemical bonds on the surface of the samples are broken by using the AFM tip creating lines with widths down to about 20 nm (Wacaser, Maughan, Mowat et al., 2003) corresponding to the tip radius. Self-assembly (Black, Nealey, Thywissen et al., 2000) is meanwhile a useful nanotechnology tool and is the conventional technique used in molecular biology. DNA is one of the biomaterials capable of self-assembly allowing more capability and flexibility in fabrication resulting in efficient sensing elements (Crespo-Hernández, Arce, Ishikawa et al., 2004). Recently, Becerril and Woolley (Becerril, Woolley, 2007) reported that they utilized a new method of patterning called shadow nanolithography employing immobilized DNA strands. The use of DNA as a building block for nanosized materials has made it possible to extend this application to other branches of science such as nanoelectronics.

This thesis describes a new and simple patterning method using DNA strands involving patterning on thin film surfaces of Al deposited over Si absorbed layers using DNA strands. One important advantage of DNA strands is their capability as a smart etching element for patterning with self-assembly and reorientation in external electric fields. This method relies on chemical interactions between DNA and the Al surface to create nanometer scaled patterns. As a result of this interaction, traces of DNA strands would remain on the Al surface. Using AFM and FESEM techniques, the patterns corresponding to the dimensions of the DNA strands with lengths and diameters in the micron and nanometer scales, respectively were obtained. This type of patterning technique may be further optimized for utilization in microelectronics engineering, particularly for electrical and biosensors fabrication.

Chapter III: Design and Fabrication of Device

3.0 Introduction

In this chapter, the design and fabrication of DNA biosensors are explained in detail. The procedure involved must be of high quality, reproducible and good control abilities comparable to Complementary Metal-Oxide-Semiconductor (CMOS) fabrication technique. Due to the enormously small size (on the order of the width of a human hair), this fabrication technique was conducted in a controlled environment. A piece of dandruff on the inside of a wafer is enough to ruin a device. As such, the experiments were conducted in a class 10K clean room. Usual clean rooms are rated at 100 to 1000K classes, which correspond to 100 to 1000 particles per cubic feet of air respectively. Figure 3.1 presents an overview of this chapter.

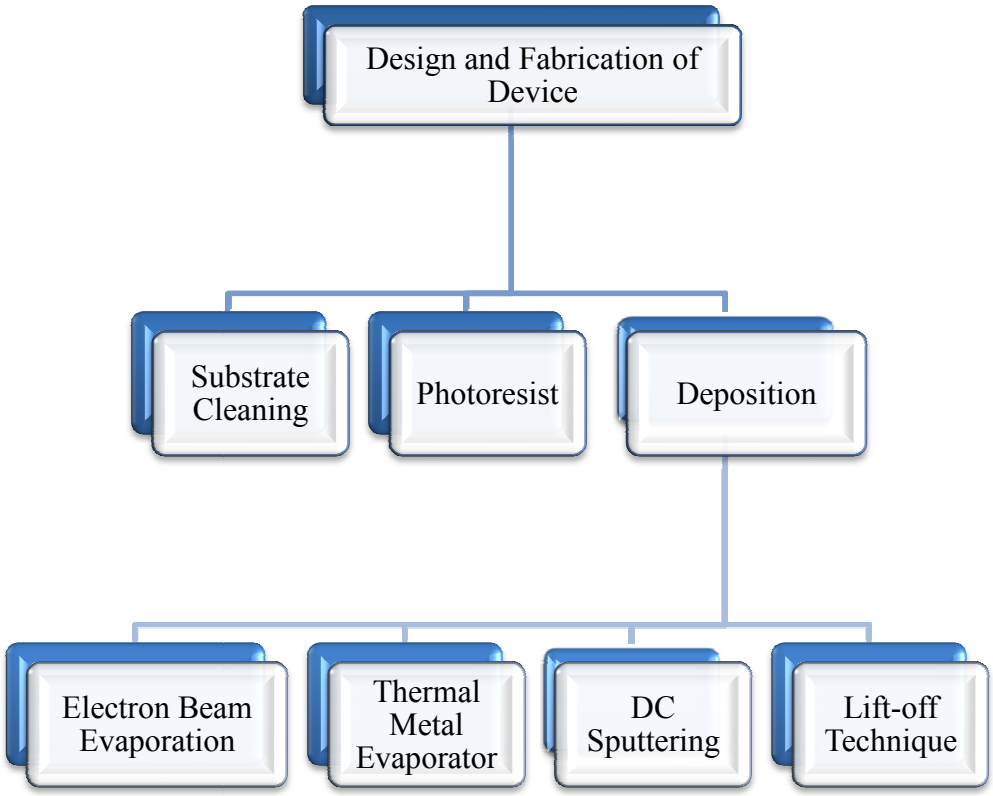

Figure 3.1: Design and Fabrication of Device.

3.1 Design and Fabrication of Device

The fabrication process of the planned sensor involves various materials undergoing diverse processes. Each of the process steps needs to be optimized in order to achieve the most favorable result. For better optimization of fabrication, each process were studied separately while considering that they should be non-destructive to other processes in terms of materials, applied conditions (including indirect effects and temperature, contamination), scratches and others. Optimal method and technique derived from each set of experiments are critical for successful fabrication of the whole structure. The following section will thoroughly explain every crucial process steps towards the final suggested fabrication process.

3.2 Explanation of Terms

Because of various techniques and processes involved in micro-fabrication and micro machining, the most common techniques used in the fabrication of MEMS devices will be outlined below. The process of selectively depositing and removing materials from the surface of a wafer is known as surface micromachining as utilized in realization of the designed sensor (Leondes, 2006; X. Li, Bhushan, 2003; X. Li, Bhushan, Takashima et al., 2003). A list of common terms and techniques, listed under the general categories of patterning, deposition and etching are provided in Section 3.2.1.

3.2.1 Photo-lithographic Patterning

Mask maker - A device, which selectively exposes small apertures onto the surface of photosensitive masking plate.

Photo-mask - patterned layer of material that is opaque to light and is used to pattern photosensitive material on the surface of a wafer. A typical photo-mask consists of a glass plate with a reflective chrome surface and covered with photoresist.

Photo-resist - Depositing on the surface of a wafer that is a light sensitive material. Depending on the polarity of the photoresist, when an area of the photoresist is exposed to UV light, it can either be removed or preserved while the unexposed area are either preserved or removed, respectively, during the developing process. Positive photo-resist involves removal after exposure and negative photo-resist involves retention after exposure.

Image reversal photo-resist - A particular type of negative photoresist that reverses its polarity after a second exposure. This process creates a special profile or lip at the edge of the resist pattern that is advantages for use in lift-off techniques.

Mask aligner - A machine that aligns a mask to an existing pattern on a wafer. After exposing the aligned mask and wafer with UV light, the pattern was transferred from the mask to the photoresist.

Developer - A chemical solution that will selectively remove exposed or unexposed area of photoresist, depending on the polarity of the resist. These developers are often matched to a particular type and variety of photoresist.

Exposure: Process of allowing light to reach light-sensitive material to create latent image: by either (a) opening shutter to expose film or (b) illuminating dark subject with flash of light or energy or (c) both.

Acetone - A strong chemical solvent capable of completely stripping or removing most photoresist materials from a wafer or mask.

Soft bake - Heating step to partially remove solvent from photoresist before aligning and exposing a wafer.

Hard bake - Heating step to solidify photoresist after it has been developed.

3.2.2 Material Deposition

Electron beam evaporator - A machine, which uses high-energy electron beam to evaporate materials from a source crucible. The evaporated materials are ejected from the surface of the crucible and deposited as a thin film on the surface of a wafer. Common source materials include Au, Al, Cr, Ag, Pt, NiCr and Cu. These materials are often deposited in a lift-off process where photoresist protects area of the wafer from direct deposition. The metal deposited on the photoresist is then removed when the photoresist is stripped from the wafer using acetone.

Stutterer - A device, which uses high-energy plasma to etch particles from a source target and after that redeposit the particles on the surface of a wafer. Source particles are ejected from the plasma in random directions, ensuring a conformal coating of a surface. The plasma, a mixture of charged particles and electrons, can be excited using a DC or a radio frequency (RF) source. DC plasmas are often used to deposit metals such as Au, Al, Ti, Cr and Cu. RF plasmas are used to deposit metal and dielectric materials such as Si, Sio_2, SiN, SiCr and TaN.

Metal evaporator - The evaporator uses high current to evaporate metal in high vacuum conditions. A piece of cylindrical target, for example tungsten wire, is placed inside the spiral wire in the chamber.

PECVD (Plasma Enhanced Chemical Vapor Deposition) - This technique uses RF plasma with specific gaseous mixtures to deposit materials on the surface of a wafer. It is often used to deposit dielectric films such as SiO_2 and SiN.

3.2.3 Etching Techniques

Plasma etching - Technique that uses RF plasma and chemical etching to remove materials from surface of wafer. The technique is often used to etch SiO_2 and SiN films.

Wet chemical etching - The use of wet chemical agents to selectively etch a material from the surface of a wafer. The surface, which is not preferred to expose to the chemical wet etchant, is usually covered with a protective layer such as photoresist.

3.2.4 Liberation

Sacrificial layer - A layer of material that separates a deposited layer from underlying layers to create vertical gaps between the layers. The sacrificial layer is then removed to release portions of the top layer from the underlying layers with the aid of proper solvent or highly selective etchants.

CPD (Critical Point Dryer) - A device, which allows the release of MEMS devices from their sacrificial layers without collapse due to surface tension of wet chemical etchants. This device consists of a chamber that fills with liquid CO_2, which mixes with and purges the wet chemicals from around the MEMS devices. The chamber is pressurized and heated to the critical point of CO_2 in which CO_2 exists as liquid and vapor simultaneously. Pressure is then lowered slowly and the liquid is converted directly to vapor eliminating the collapse of the devices due to liquid surface tension.

3.3 Substrate Material

There are a lot of choices to select for the substrate material. Substrate material can be selected with respect to some considerations such as mechanical stability, high electrical resistivity and compatibility with the fabrication process. Silicon and glass have been chosen as the substrate material in this work. Both of these materials have a good mechanical stability but are different in conditions of electrical resistivity. The essential electrical resistivity for silicon at room temperature is 2500 Ωm. Conversely, glass (borosilicate type or Pyrex) can be used as a substrate material without any passivation layer regarding to its outstanding insulation properties with electrical resistivity in the order of 10^{13} Ωm at room temperature (William Jr, 2007).

3.4 Substrate Cleaning

Within the clean room, there are a number of common facilities and procedures for cleaning substrates prior to and during processing. These are normally wet processes, involving liquid solvents (Banks, 2006). After cutting the glass and Si wafers into pieces with automatic cutter (Figure 4-1: Karl Suss automatic wafer scriber) or manually, cleaning was done.

3.4.1 Glass Substrate

The initial step involves rinsing of the substrate using DI water followed by boiling for 10 minutes in solution of H_2O:H_2O_2:HCl at a ratio of 6:1:1. After that, the samples were rinsed again in DI water followed by immersion in H_2O:H_2O_2:NH_4OH (ratio 5:1:1). Following subsequent rinsing of the samples in DI water and immersion in H_2O:HF at ratio 10:1. Finally, the samples were re-rinsed in DI water before usage.

3.4.2 Silicon Substrate

Si substrates were left in a beaker containing soap water and then later immersed into ultrasonic bath for 15 minutes. The substrates were then rinsed in DI water followed by rinsing with acetone. Finally, the substrates were re-rinsed using etanol and DI water, respectively.

Figure 3.2: Karl Suss automatic wafer scriber (Universiti Kebangsaan Malaysia).

3.5 Photoresist

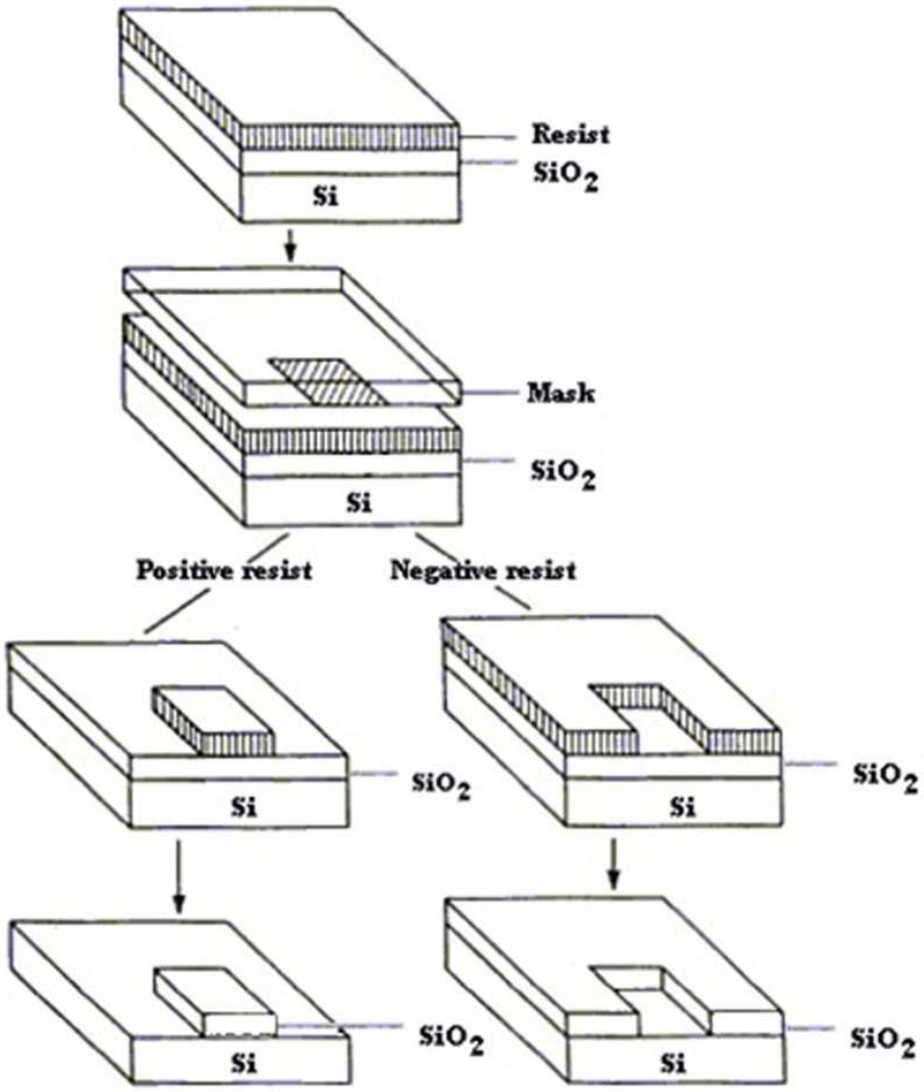

Figure 3.3: Differences in patterns generated from the use of positive and negative resist.

A photoresist is a light sensitive material. Two types of photoresist are available; positive and negative. Positive resists, the resist is exposed with UV light whenever the underlying material is to be removed. In these kinds of resists, upon exposure to the UV light, the chemical structure changes the resist in a way that it becomes more soluble in the developer. Then the resist is washed away by the developer solution, leaving windows of the bare underlying material. In other words, "*whatever shows, goes*." Therefore the mask, contains an exact copy of the pattern which is to remain on the

wafer. Negative resistance behaves completely vice versa. Being in touch or in front of the UV light, causes the negative resist to become polymerized and more difficult to dissolve. The negative resist, therefore, remains on the surface wherever it is exposed, and the developer solution removes only the unexposed portions. So, masks used for negative photoresists, contain the inverse (or photographic "negative") to be transferred pattern. Figure 3.3 shows the pattern differences generated from the use of negative and positive photoresist.

Table 3.1: Some photoresists popular for micro-engineering and MEMS (Banks, 2006).

Resist	Source	+/-	Features
SU-8	MCC (Micro Chem Corp.)	-	Epoxy-based resist, 2–200 μm thickness, very resilient, can be difficult to remove, excellent structural resist, adhesion promoters not normally required, image reversal possible, near-UV 350–400 nm
SJR5740	S (Shipley)	+	High-aspect-ratio positive resist up to >20 μm thickness, broadband resist, good for electroplating
S1800	S (Shipley)	+	Good general-purpose positive resists, 0.5–3 μm thick positive resist, thick positive resist, image-reversible positive resist
AZ4562	AZ (Clariant Corp.)	+	
AZ9260	AZ (Clariant Corp.)	+	
AZ5214	AZ (Clariant Corp.)	+	

For the present work, AZ 1500 series photoresist suitable for semiconductor and microelectronics manufacturing was used. It can be used in both 435 nm (g-line) and broadband exposure. Formulated with the solvent propylene glycol monomethyl ether acetate (PGMEA), the photoresist is safer compared to the one with ethylene glycol acetate (EGA). Some outstanding features offered by AZ1500 include; excellent pattern profile in sub-micron lithography, wide exposure latitude and DOF (depth of focus) margin, no scum and peeling during the developing process and good thermal stability and dry etching stability. Other types of photoresist are shown in Table 3.1.

AZ 1500 series photoresist are photo definable, therefore all processes should be performed in standard clean room conditions under yellow light. Obtaining a high quality coating and patterning of a good layer includes special considerations on the coating, baking temperature and exposure time followed by the precise timing of the exposure, develop and final cure of the surface.

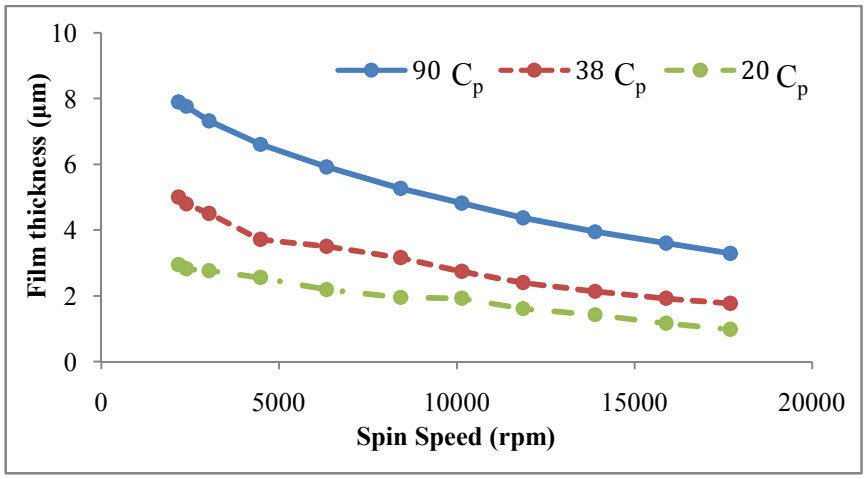

Figure 3.4: Film thickness versus spin speed (Manual book for photoresist, UKM).

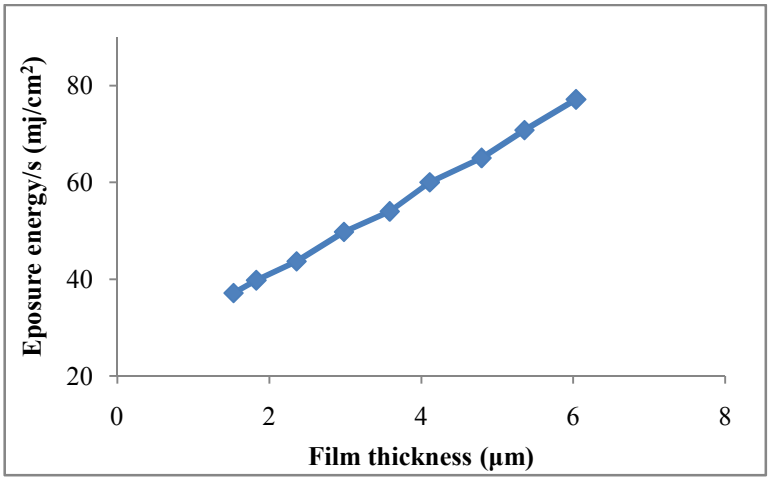

Figure 3.5: Film thickness versus exposure energy (Manual book for photoresist, UKM).

Figure 3.4 shows the spin curve describes the relation of film thickness with respect to spin speed for several photoresist viscosities, where Cp is the unit for viscosities of photoresist (centipoises). A decrease in the film thickness was observed with increasing rpm in several photoresist viscosities. Based on the observations, it can be concluded that exposure energy increases with film thickness (Figure 3.5) and decreases with developing time (Figure 3.6).

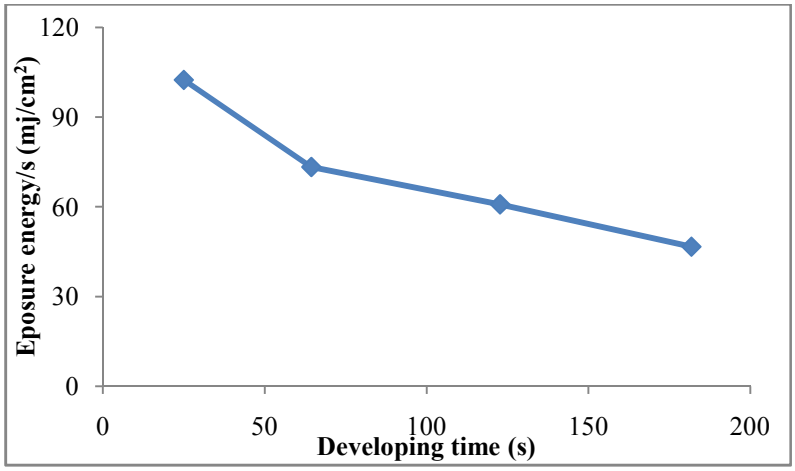

Figure 3.6: Exposure energy versus developing time (Manual book for photoresist, UKM).

3.6 Manufacturing Process

3.6.1 Deposition on Metal Layers

Deposition of metal layers can be applied by PVD techniques such as evaporation and sputtering. There are some parameters in each of these processes to control the thickness of the final deposited layer. Some of the common parameters for this purpose are target size in the thermal evaporation technique, time and electron beam intensity in e-beam evaporation technique or time and current intensity in the sputtering techniques. Comparing evaporation and sputtering techniques in terms of thickness controllability of the process indicates that in evaporation technique, thickness is generally not easy to control where sputtering allows some possible controls. Moreover, continuous

deposition in sputtering is achievable while only one deposition per charge is possible for the resistive evaporation technique. In this single charge, the size of the target material is limited to the size of the tungsten filament. As such, size of the filament limits the thickness of the deposited film.

To get a metal layer in the range of l or 2 μm, a series of successive deposition steps should be applied. Due to limitations of available facilities, a maximum 900 s time period and a maximum 40 mA current were used to achieve stable plasma (BALTEC SCD-005 mini sputter system). These specifications limit the maximum thickness of metal layer achievable in each interval of 900 s. According to the measured deposition rates for 30 mA and 40 mA currents, the appropriate timing to achieve desirable Cu thickness can be set.

Another set of experiments was also conducted using the evaporation technique to generate thick metal layers. E-beam evaporation and thermal evaporation are the two methods utilized in this set of experiments. This time, Al was selected as the target material. The only control parameter for the thickness of the deposited layer in thermal evaporation technique seemed to be the target size, which is, however, not an accurate choice. Here for an Al layer of 2μm thickness, five successive deposition steps were conducted. Poor thickness controllability of this process is a more significant issue in thin layer depositions. Total obtained thickness of the deposited layer was 2.23±0.01 μm. In each attempt, Al bars with l cm length and 2 mm thickness were used as deposition targets. The average deposition rate for each step was obtained at 3.20±0.01 μm per shot. Opening the evaporator chamber for each charge of the target material caused a thin Al oxide layer between each of the two deposited layers.

This undesirable oxide layer may affect the mechanical and chemical properties (for example wet etch characteristics) of the deposited thick metal layer, which should be considered in the successive fabrication process steps. Using e-beam evaporator technique for deposition of Al layer gave a deposition rate of 8.00±0.01 nm/min with 4.5 kV of voltage and 50 mA of current. It was observed that long evaporation times would affect temperature sensitive materials that might exist on the specimen such as the different resists. This makes e-beam evaporation as an improper choice in deposition of thick metals for lift off process in cases where photo resist layer exist under the metal structure. The thicknesses of the deposited layers were all measured step by step using TENCOR Pl2 surface profiler. A sharp step on each sample was created either by masking tape or etching in order to measure the thickness of the deposit.

The step coverage in each of the utilized deposition techniques was also another significant parameter under investigation. Experiments show that e-beam evaporation provides the minimum step coverage among these three PVD techniques. This fact along with the lower deposition rate makes e-beam evaporator suitable for being utilized in modified lift-off technique for submicron deposition steps. On the other hand, both thermal evaporation and DC sputter techniques provided good quality step coverage. Lower temperature in the chamber during the process was another difference between the two recent deposition techniques and the former e-beam evaporation technique. Long evaporation time in e-beam evaporation may cause high temperatures, which cannot be utilized in some cases such as, where a low temperature process is ideal or there is a temperature sensitive material included. In contrast, thermal evaporation has a very short process time (a few seconds), which does not generate high temperatures in the chamber for long time periods.

In this section some of the preliminary processes which will be utilized in the fabrication process are described. There are two kinds of methods of deposition as described; first is CVD and second is PVD. The famous chemical process is CVD, which produces high-purity and high-performance solid materials. This process is often used in the semiconductor industry to produce thin films of Al and gold. PVD meanwhile involves vacuum assisted deposition and is a general term used to describe any of a variety of methods to deposit thin films by the condensation of a vaporized form of the material onto various surfaces.

3.6.2 Electron Beam Evaporation Technique

Figure 3.7: E-beam evaporation is a form of physical vapour deposition in which a target anode is bombarded with an electron beam given off by a charged tungsten filament under high vacuum (Low Dimensional Material Research Centre (LDMRC), Department of Physics, University of Malaya).

In this method, the material to be deposited (generally metals) by high-vacuumed electron bombardment is evaporated at high temperatures provided by the imposed collision energies of electrons. The system has also provision for standard thermal

evaporation. The e-beam evaporator is more common for depositing thin layers of metals such as Ni, Al or Cr (Figure 3.7).

3.6.3 Thermal Metal Evaporator

The thermal metal evaporator is preferred for thicker layers; however, it has the demerit of poorer controllability over the thickness of the deposited layer. Average thickness of the deposited layer is about 0.3 μm and to achieve higher thicknesses, the procedure must be repeated. In each attempt, the target material, which is a cylindrical metal wire, was recharged into the spring filament (tungsten wire) and the device vacuumed to reach the desired chamber pressure of 2.5×10^{-5} mbar only. Then, the required current was applied to generate heat and evaporate the target material (Figure 3.8).

Figure 3.8: Thermal metal evaporator (LDMRC, Department of Physics, University of Malaya).

3.6.4 DC Sputtering

DC Magnetron Sputtering (Figure 3.9) was utilized for Cr deposition. With the aid of this sputter coater, a time delay of 10 minutes, deposits Cr of thickness 4000-4300 Å. For coating Cr the regulations necessary are air pressure of 0.4-0.6 kg/cm^2, power condition at +/-10 V and +/-0.5 A and pressure of 1.1×10^{-3}Torr.

Figure 3.9: DC Magnetron Sputter.

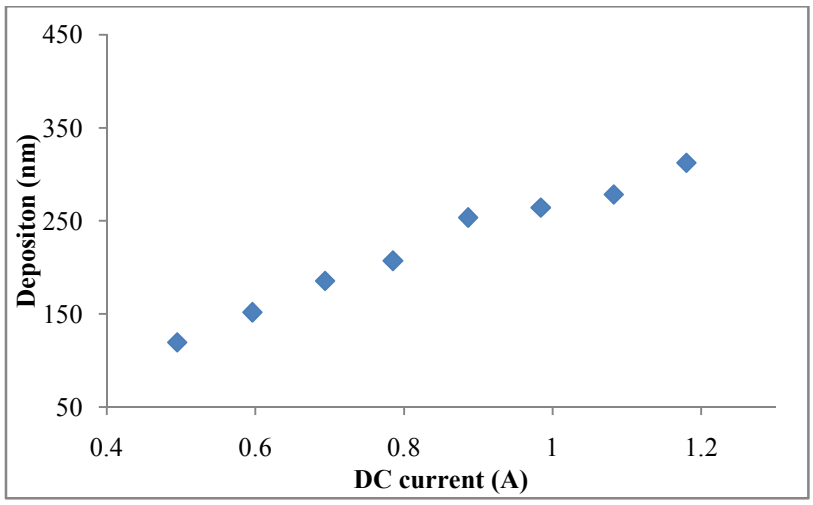

Figure 3.10: Rate of Cr deposition using the DC Magnetron Sputter.

Rate of Cr deposition in DC Magnetron Sputter system is plotted in Figure 3.10.

3.6.5 Lift-off Technique

There are a number of techniques for patterning a layer but they mostly involve lithography. The result is usually a patterned layer that is mounted on top of other layers. Compared to other lithography-based methods, lift-off approach is a well-known method particularly in cases that patterning directly a layer is difficult. In preliminary lift-off process series, a solvent dissolves the photoresist that is below the deposited metal. It starts from the edge of the resist and finally lifts off the metal (Zaouk, Park, Madou, 2006). In order to remove the photoresist easily, the thickness of photoresist is considered approximately twice of the deposited metal thickness. This consideration decreases the probability of connection among deposited metal in the remaining and removed parts. Therefore, the release of photoresist leads to a successful lift off (Damghanian, Majlis, 2008).

Chapter IV: Characterization of Fabrication Process

4.0 Introduction

The concept of a minimum feature size is important in mask design. Minimum feature size is the width of the smallest line or gap that appears in the design. The present chapter presents the process by which such masks are designed.

4.1 Design and Fabrication Masks

The mask design produced using CorelDraw X5 is shown below;

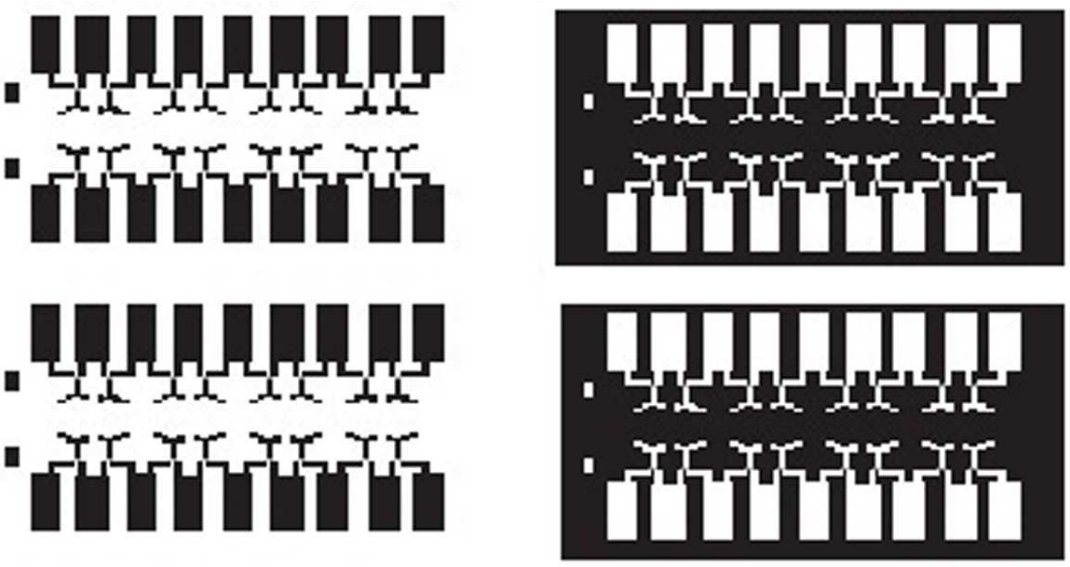

Figure 4.1: Mask designed with CorelDraw X5 software.

In this process of fabrication, masks were utilized to prepare the chips. The defined fabrication process flow requires two different photo masks. Each of these photo masks were printed on transparent films. Size of the sensor cells considered is (50×50) μm in the masks. The spacing between the cells was chosen in a range that was applicable to be used in the fabrication process. In real implementation of the device, high-resolution masks on quartz wafers were produced. The lithography process was accomplished by precise aligners, which help to keep the minimum spacing between cells and so achieve

the desired resolution of the image at 500 dpi. Masks are prepared for single cell as well as 1-dimensional and 2-dimensional arrays. Figure 4.2 shows the mask layouts used in the fabrication process of a 2 by 3 sensor array.

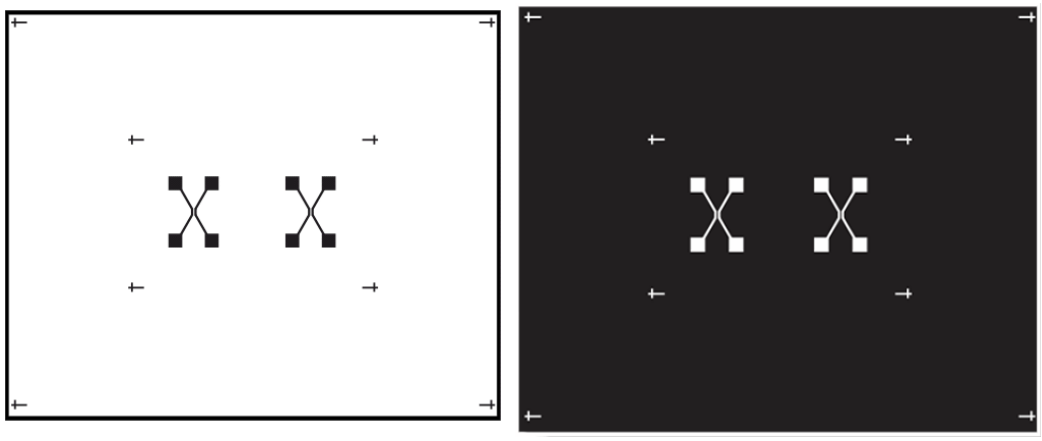

Mask 1 Mask 2

Figure 4.2: Mask layouts for implementation of an area sensor.

Mask 1 implements negative photoresist and bias lines as well as contact pads in rnodified lift-off process. Mask 2 meanwhile was designed as a positive photoresist.

4.2 Printed masks on transparent films

Since the size of each sensor cells is desired to be (50 × 50) μm, mask layouts shown in Figure 4.2 have more precise feature sizes including lines and spacing in the range of l0 to 90 μm. This high accuracy masks should be prepared precisely using laser writers or very high definition printers. Quartz is the material preferred for the masks because it offers long life and several hundreds of contacts and exposure cycles. However, quartz masks are very costly for use in laboratory scale experiments. It is common in these kind of experiments to have mask layouts printed out on transparent films which can be used as a low quality contact mask enabling only a few lithography cycles. Therefore, the lower cost of the mask and flexibility in mask design and ordering, results in lower accuracy and poorer quality of the masks.

Usually, it is claimed that some modern printers can offer print resolution up to 5000 dpi, which means potentially they can print even 5 μm feature sizes. However, inaccuracies in the range of l0 to 20 μm were widely observed in the 2 mask layouts ordered for the designed fabrication process flow. In each of the masks, features were designed if some of the mask layouts have been printed several times to get a better quality of the mask, yet even the final ones could not satisfy the minimum accuracies required in this precise structure.

In spite of all described inaccuracies in the transparent masks, they have been chosen as the contact masks for realization of the designed fabrication process. Short time preparation and the possibility to be easily changed are needed to modify samples quality in laboratory scale fabrication processes. It should be pointed out that mask inaccuracies would become less significant in the bigger feature sizes. For example, if the feature size were 100 μm, the tolerances of the final printed feature would be between 80 to 120 μm. In a feature size of only l0 μm, this would result in the connection of neighbor patterns or sometimes the elimination of the entire pattern.

4.3 Fabrication of Chip

After designing masks suitable for achieving the desired resolution, the first step involves cutting substrates and cleaning as mentioned in Chapter III. After cleaning the substrates, the photoresist layer was deposited on the top region of substrates using a spin coater (Figure 4.3). A single layer of AZ1500 photoresist of 2 μm thickness on a glass wafer of 1000 pm thickness was deposited.

Figure 4.3: Spin coater used in the experiment (Physics Department UM).

4.4 Lithography technique

Photoresist AZl512 was used in the lithography process, as this type of photoresist is positive. For each lithography step that is targeted to pattern a photosensitive material, a mask is designed to define the areas, which is either exposed or protected to or from the UV light respectively. The positive or negative resist means that the exposed area will be either removed or maintained in the developing stage respectively. Mask alignment process was performed using Karl-SUSS MIB 3 Mask Aligner system as shown in Figure 4.4: This exposure system is an optical contact aligner, which transfers a pattern from a glass mask to a photoresist-coated wafer by exposing it to UV light. Mercury lamp produces diverse wavelengths of UV light, particularly at 365 nm (*i*-line), 405 nm (*h*-line) and 435 nm (*g*-line). The aligner used utilized UV light with wavelengths of 365 nm (*i*-line).

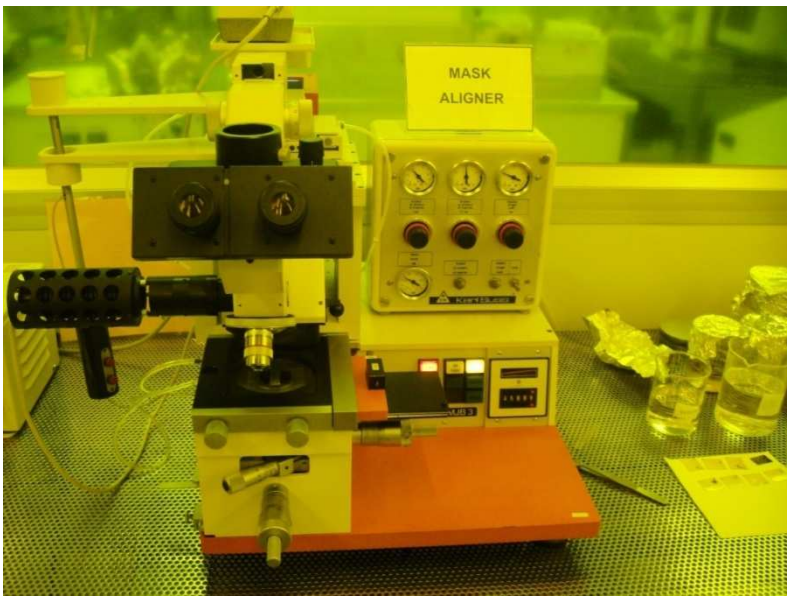

Figure 4.4: Karl-SUSS MIB 3 Mask Aligner System (IMEN UKM MEMS Fabrication Laboratory).

Essential experiments in lithography were conducted to obtain patterned photoresist film with sharp edge lines and good uniformity. According to results of current work, thickness of photoresist was obtained at 2 μm. Tables 4.1 and 4.2 show the details.

Table 4.1: Procedure used to get a single layer of AZ1500 photoresist with final film thickness of 2 μm on glass wafer with 1000 pm thickness.

Process	Parameter	Condition
Spin coat	Spin speed Spin time	2500 rpm 20 s
Pre-bake	Method Temperature Time	Direct hotplate 100°C 2 minutes
Exposure	UV source Intensity time	365 nm 10 mW/cm^2 (average) 25 s
Development	Developer Time	AZ300K 10 Sec-3 times
Post-bake	Method Temperature Time	Direct hotplate 125°C 5 minutes

Table 4.2: Procedures to get a single layer of AZ1500 photoresist with final film thickness of 2.2 µm on silicon wafer with 675 pm thicknesses.

Process	Parameter	Condition
Spin coat	Spin speed Spin time	3500 rpm 20 s
Pre-bake	Method Temperature Time	Direct hotplate 90°C 80 minutes
Exposure	UV source Intensity Time	365 nm 10 mW/cm^2(average) 50 sec
Development	Developer Time	AZ300K 30 s
Post-bake	Method Temperature Time	Direct hotplate 125°C 4 minutes

4.5 DC Sputtering

The mini sputter system was also used for deposition of metals especially Au, Cu, Ni and Cr layers (Figure 4.5). The deposition rates achieved for some metallic targets and the suitable current setting of the sputtering system are listed in Table 4.3.

Figure 4.5: BALTEC SCD-005, mini sputter system (LDMRC, Physics Department, UM).

Table 4.3: Deposition rates achieved for the mini sputter system.

Target	Current (mA)	Deposition Rate (nm/min)
Cu	45	30
Au	35	42
Ni	30	44
Cr	30	46

4.6 Lift-off Technique

Lift-off is another process to prepare samples. A pattern is defined on a substrate using photoresist. A film, usually metallic, is blanket-deposited all over the substrate covering the photoresist and areas in which the photoresist has been cleared. During the lifting-off, the photoresist under the film is removed with solvent (acetone), taking the film with it, and leaving only the film that was deposited directly on the substrate. There are a number of techniques for patterning a layer. It usually results in a patterned layer stacked on top of the other layers. Lift-off, among several lithography-based layer-patterning techniques, is an established method especially when a layer could not be directly and easily patterned. In the fundamental lift-off process series, a solvent dissolves the photoresist under the deposited metal starting at the edge of the resist and lifts off the metal (Madou, Kellogg, 1998). It is suggested that for easy removal of the photoresist, consider the thickness at least two times of the deposited metal. This will decrease the chance of connection between the deposited metal in the remaining and removing parts and it will guarantee a better release of successful lift-off process of resist leading (Figure 4.6).

Photoresist spin coat and bake

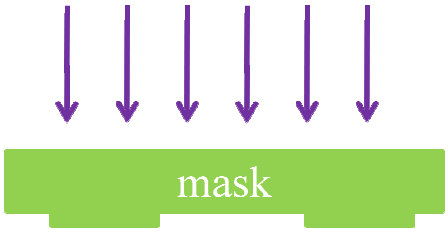

Photoresist patterning

Develop

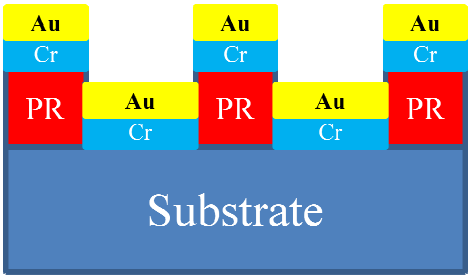

Sputtering

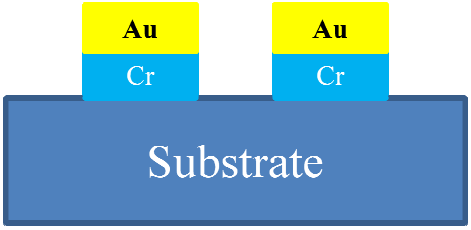

Lift-off

Figure 4.6: Lift-off processing flow creates a flat surface.

Photographs showing the successful and unsuccessful lift-off during chip preparation are presented in Figure 4.7.

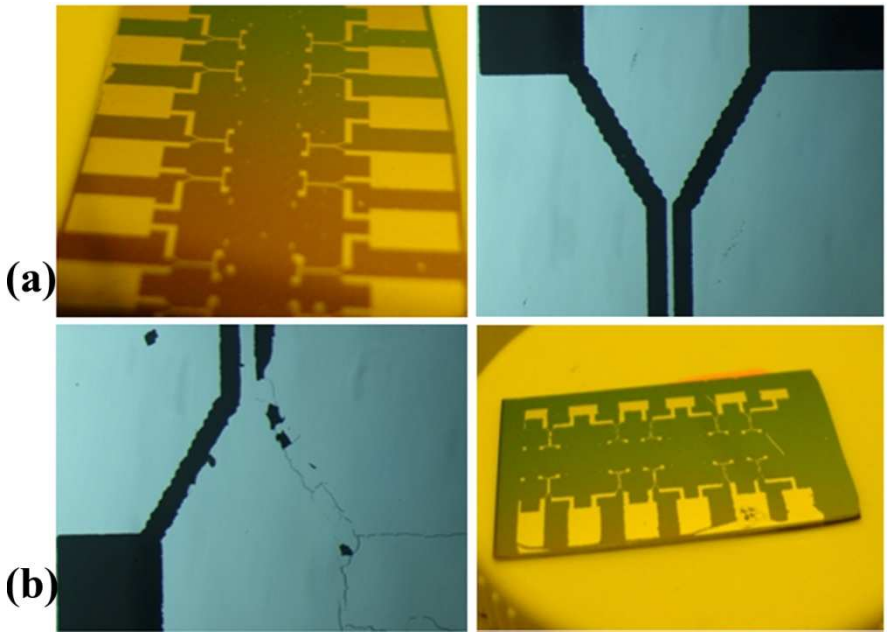

Figure 4.7: Lift-off results for preparation of chip (a) Successful lift-off and useful for next step of work and (b) Unsuccessful lift-off process.

4.7 Materials

DNA molecules from the plant *Boesenbergia rotunda* belonging to the ginger family were extracted in the Institute of Biological Science, University of Malaya. DNA sequence exported from the ginger is shown below.

GGAGAATAACAAGGGTGCACGTGTGATGGTGGTGTGCTCCGAGCTCAACGTGATGTTCT
TCCGTGGGCCTGACGACCACCACTTTGAGAACCTTATCGCACAAGCCCTCTTCGGCGACG
GTGCTGCGGTGGTGATTGTCGGTGCAGGCCCAAAGGAGACAGAGAGACCGATCTACGAAG
TGGCCTCGGCAGCACAGGTGATGCTGCCAGAGAGCGAGGAGATGGTTGCAGGGCACCTGA
GGGAGATCGGGTTGACATTCCACTTAGCGAGTAAACTGCCGGCTGTTGTTGGCGCGAACA
TCCAACGGTGCCTGGAGGTGTCTTTCGCGCCAATGGGGGTTTCAAACTGGAACGAGCTAT
TCTGGATTGTGCACCCAGGCGGGAGAGCCATTGTGGACCAAGTTGAAATGAGTGCCGGGC
TGGAGGCAGGGAAGCTAGCCGCGACTAGGCATGTGCTGAGGGAGTATGACAACATGCAGA
GTGCTTCAGTGCTATTCATCATGGACGAGATGAGGAAGCGGTCGGTGGCAGAGGGATGCA
CCACCACCGGCGACGGCTTCGACTGGGG

Figure 4.8: DNA sequence exported from the ginger.

Sequence analysis indicated that the order of base pairs as follows; A (22%), T (20%), G (35%) and C (23%). Substrate used for etching was a p-type Si wafer (orientation <100>) of diameter (150.0 ± 0.1) mm, thickness (675 ± 25) μm and a resistivity of 1 to 10 Ω-cm (MEMC Electronic Materials). High purity chemicals (NH_3, H_2O_2, HF, HCl and acetone) were supplied by Sigma Aldrich and used directly. DI water was obtained using a Barnstead Company (Nanopure) water system. Al wire (99.999% purity) used in thermal evaporation meanwhile was bought from the Kurt J. Lesker Company. Cr (99.999% purity) and gold (99.999% purity) used in sputtering meanwhile were bought from the same company and had a diameter of 6 and 0.125 inch of thickness respectively.

4.8 Preparation and Measurement Set-up

4.8.1 Preparation

After cleaning the p-type Si wafer sample with Reaction Chemical Agents (RCA) process involving 10 minutes of boiling in solution of NH_3, H_2O_2, H_2O (ratio 1:1:6) followed by 10 minutes of boiling in HCl, H_2O_2, H_2O (ratio 1:1:6), 100 nm Au was deposited over the substrate. A drop of DNA solution was then applied on the sample. The electric field generated by voltage amount 12 V, with frequency of 200 KHz within 30 seconds on the DNA solution on the Au thin film meanwhile allowed parallel arrangements of the strands along the field direction (Figure 4.9). The concentration of DNA is 0.1 ng/nL. It was found that the number of strands oriented increased with the applied external field. Prior to application of electric field, the DNA strands are randomly and irregularly placed on the sample. However, after applying the electric field, DNA strands became regular and parallel to the field (to be discussed further in Chapter 5).

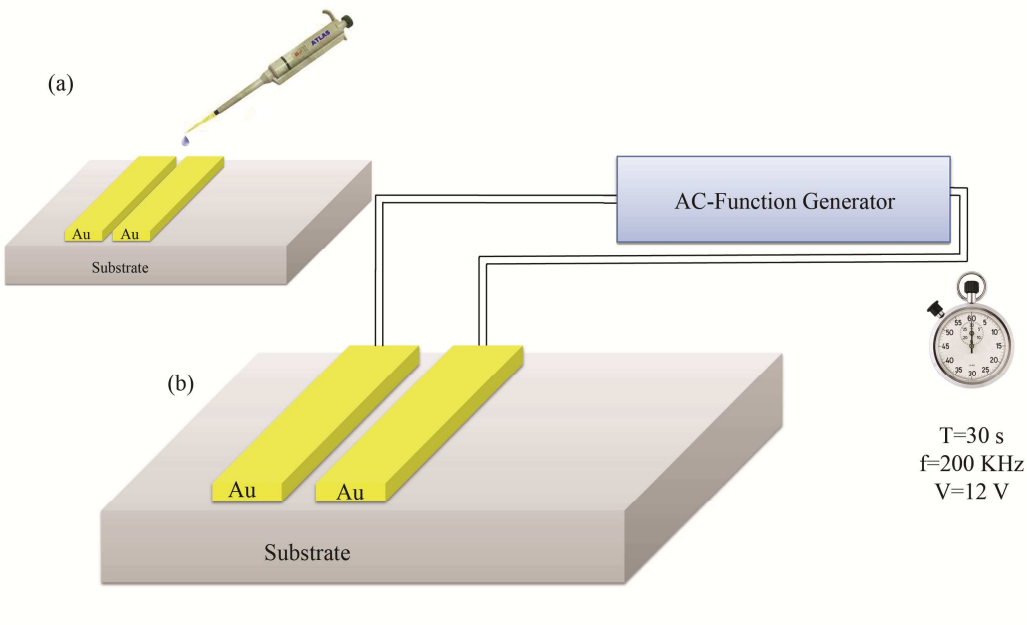

Figure 4.9: Preparation process of the sample (a) Gold layer deposition and a drop of DNA solution was applied on the sample and (b) applying electric field on the sample.

4.8.2 Measuring

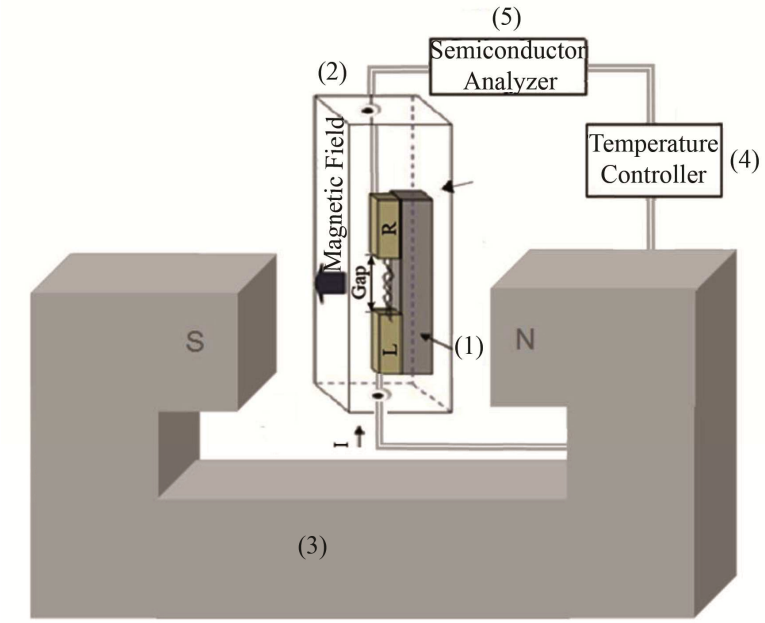

Figure 4.10: Illustration showing the chip holder specifications, (1) chip holder and connection in dewar, (2) cryostat system: The cryostat is a large, stainless steel structure surrounding the vacuum holder and superconducting magnets, providing a super-cool, vacuum environment, (3) Magnetic field generator and detector: a 1000 turn coil makes the generator. The coil is placed near the edge of the large nail, (4) Thermal controlling device: A device for decrease and decrease and monitoring temperature, (5) *I-V* measurement units: Semiconductor analyzer for measuring current via voltage.

I-V characterization of MDM structure in the presence and absence of magnetic field (Electromagnet 3472-50) in dark condition (inside Dewar cryostat) was achieved using a semiconductor analyzer (SMU 236, Keithley) at different temperatures using a Lakeshore-331 temperature controller (Figure 4.10).

Chapter V: Investigation of NGs on Al/Si Structures using DNA Strands

5.0 Introduction

A new method of fabricating NGs on Al thin films using DNA strands is reported and proposed. 100 nm thick Al films were utilized to deposit DNA strands on p-type Si surface. The interaction between Al and the DNA strands causes helical imprints of the DNA strands on the Al thin film surface in absence of external field. NGs with diameter of 63 nm were formed through wet chemical etching process between DNA and Al. This method does not require lithographic patterning and could be utilized in electronic and bio-electronic devices. Figure 5.1 shows the AFM images of the NGs formed.

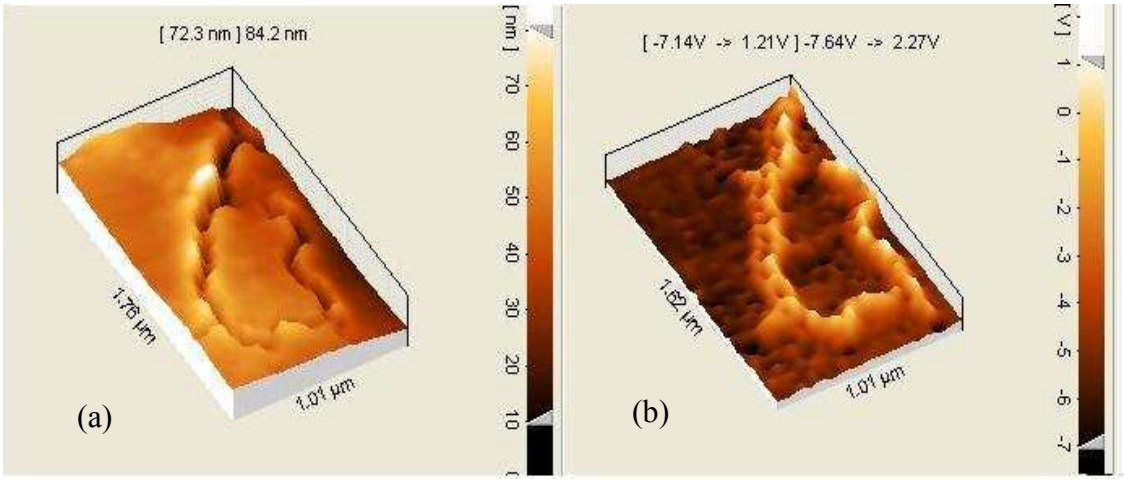

Figure 5.1: AFM imaging of bundled DNA strands shown in (a) phase and (b) dimension traces.

Figure 5.1(a) is a topographic image of the surface and Figure 5.1(b) is the phase image of surface to detect variations in composition on the surface. Both images illustrate the formation of NGs and nano-patterns corresponding to the dimensions of the strands used in the experiment.

5.1 Results and Discussion

For many years, the interaction between metal and DNA strands has been the focus of research among scientists. Al, a metal with a positive charge in ionic form, prefers to attach to sites of DNA possessing a negative charge. J. Anastassopoulou (Anastassopoulou, 2003) reported his research on DNA interaction with metals and indentified two kinds of bonding between DNA and metal; direct and indirect, based on water molecules and ions in the DNA environment. The mechanism for the interaction of Al ions with DNA is however not well understood.

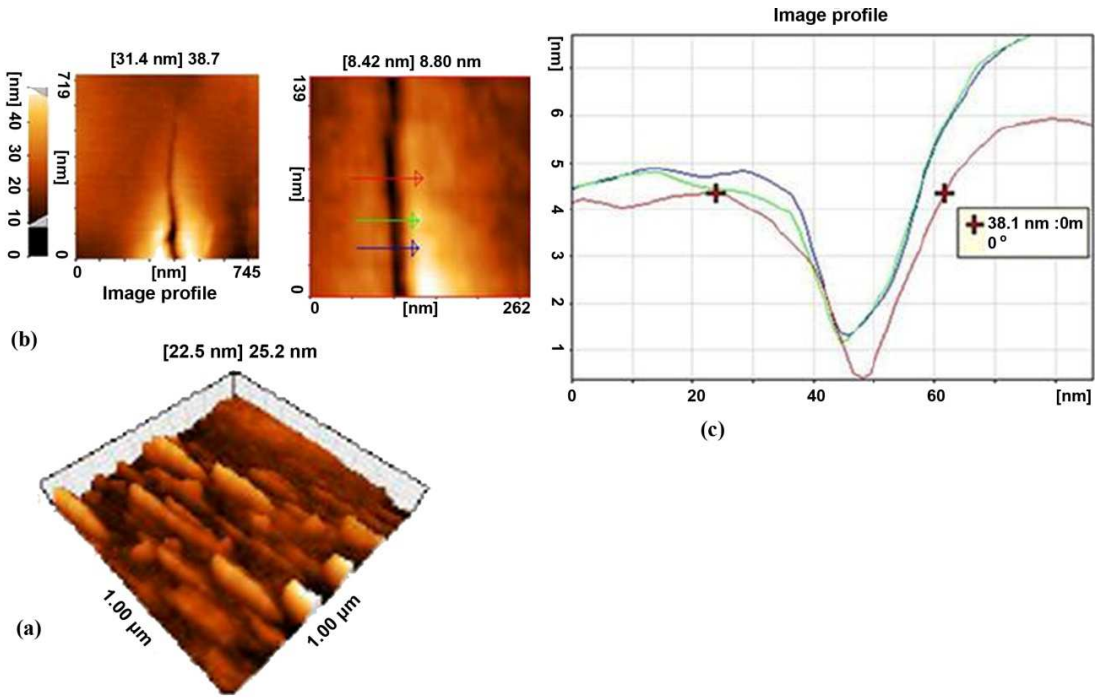

Figure 5.2: (a) The parallel arrangement of the DNA strands with applied electric field. (b) 3-dimensional view of DNA strand and (c) AFM image showing gap size of about 38 nm achieved after removing the DNA strands initially aligned using the electric field (One vector is enough. But for repeated measurements, 3 vectors were plotted to have the diameter of a recession during the time slot).

Figure 5.2(a) meanwhile shows the parallel arrangement of the DNA strands when allowed to dry under the electric field. Long successive strands are seen in the micrometer scale unlike the short and arbitrarily distributed strands shown in Figure 5.2(b). The AFM image clearly demonstrates the obvious implication of the electric

field in creating well-oriented strands due to their dipole moment. Figure 5.2(c) shows the image of the regulated impression of a DNA strand when an electric field (12 V and 200 Hz) was applied before washing away the strands on the Al surface. The dimensions created in terms of its width and depth of the NG was observed to be about 38.1 and 8.8 nm respectively. It also was found that, the DNA chain length decreases when the applied voltage increases (N. M. Khatir, S. M. Banihashemian, V. Periasamy et al., 2011). Hence, higher electric fields were found to induce dimensionally shorter strands as a result of breaking of the DNA chains. It seems that higher electric field induces straighter but shorter NG lines (Figure 5.3), highlighting possible application as nano-biowires.

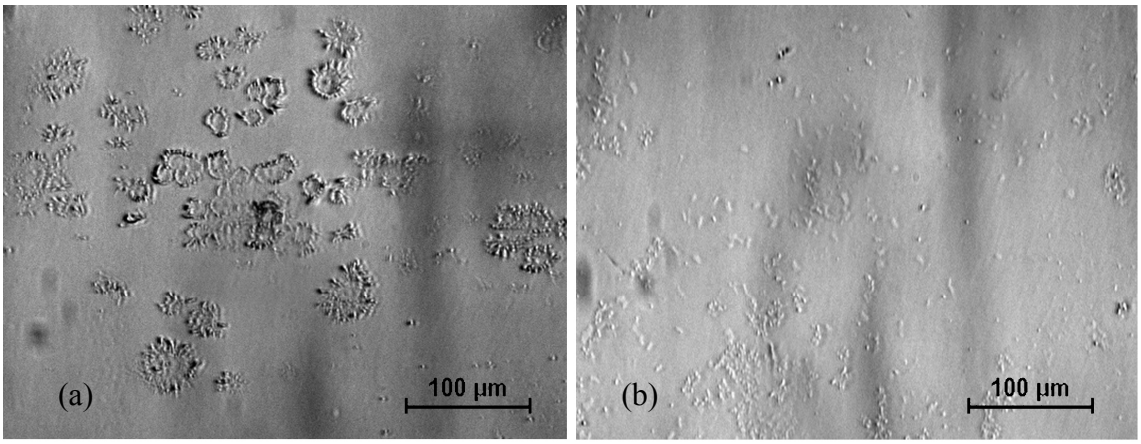

Figure 5.3: DNA strands separated at high electric field; their length will be short. Microscopic images at (a) less than 12 V and (b) more than 12 V of voltage applied.

The effect of the interaction between Al and DNA strands was investigated based on the AFM and SEM techniques. The ultra clean Al surface (100 nm thick film) undergoes erosion on direct contact with the DNA strands. Figure 5.4(a) and (b), respectively obtained from AFM and SEM imaging show the DNA on the Al-Si surface before washing. The bright lines in Figure 5.4(a) pertain to frozen DNA strands and in Figure 5.4(b) relate to unfrozen DNA strands on the Al surface. Figure 5.4(c) shows an arrow

in the depth direction view of the DNA on the Al surface. The diagram reveals a hill with a height of 8.8 nm and a width of 48.4 nm as shown in Figure 5.4(c).

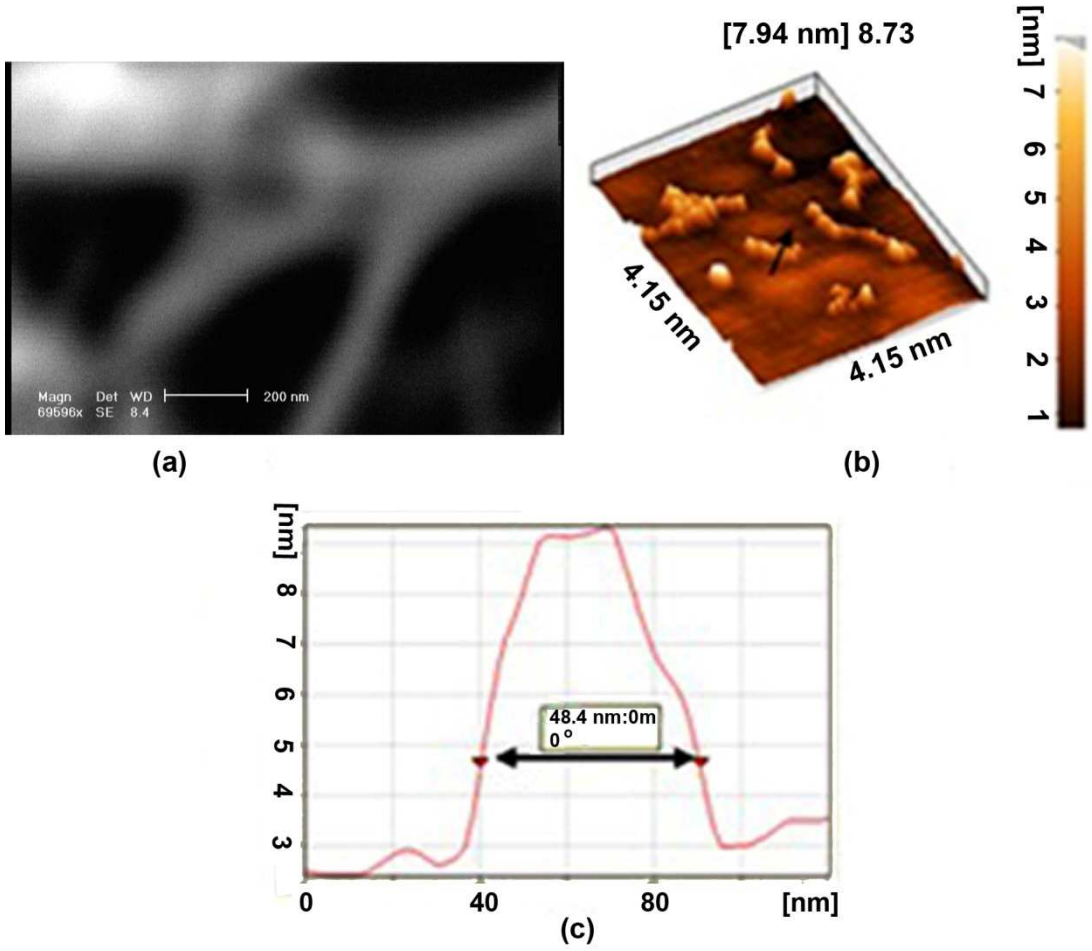

Figure 5.4: (a) A 2-dimensional view of SEM imaging of DNA on Al surface before the washing process for removing DNA strands. (b) 2-dimensional view of AFM (c) a side view of Figure 5.4(b), showing a hill with diameter around 48.4 nm and height of 8.8 nm along the black arrow.

The black arrow in Figure 5.5(a) shows the depth view of the treated surface. The picture visualizes the formed gaps well and reveals a maximum gap depth and width of 63 nm 25 nm respectively. Figure 5.5(c) gives a 3-dimensional side view of the gap, and the two back arrows point to the positions of the gaps formed along the strands. Comparison of Figure 5.4 and Figure 5.5 reveals that, in the creation of a NG, a chemical reaction between the DNA strands and Al surface occurred in such a way that the gap on the surface reveals a dimple-like footprint of DNA whose diameter

approximates that of multiple strands of DNA. This phenomenon increases the possibility that DNA strands might be useful for the design and fabrication of electronic chips for detecting the electrical behavior of DNA.

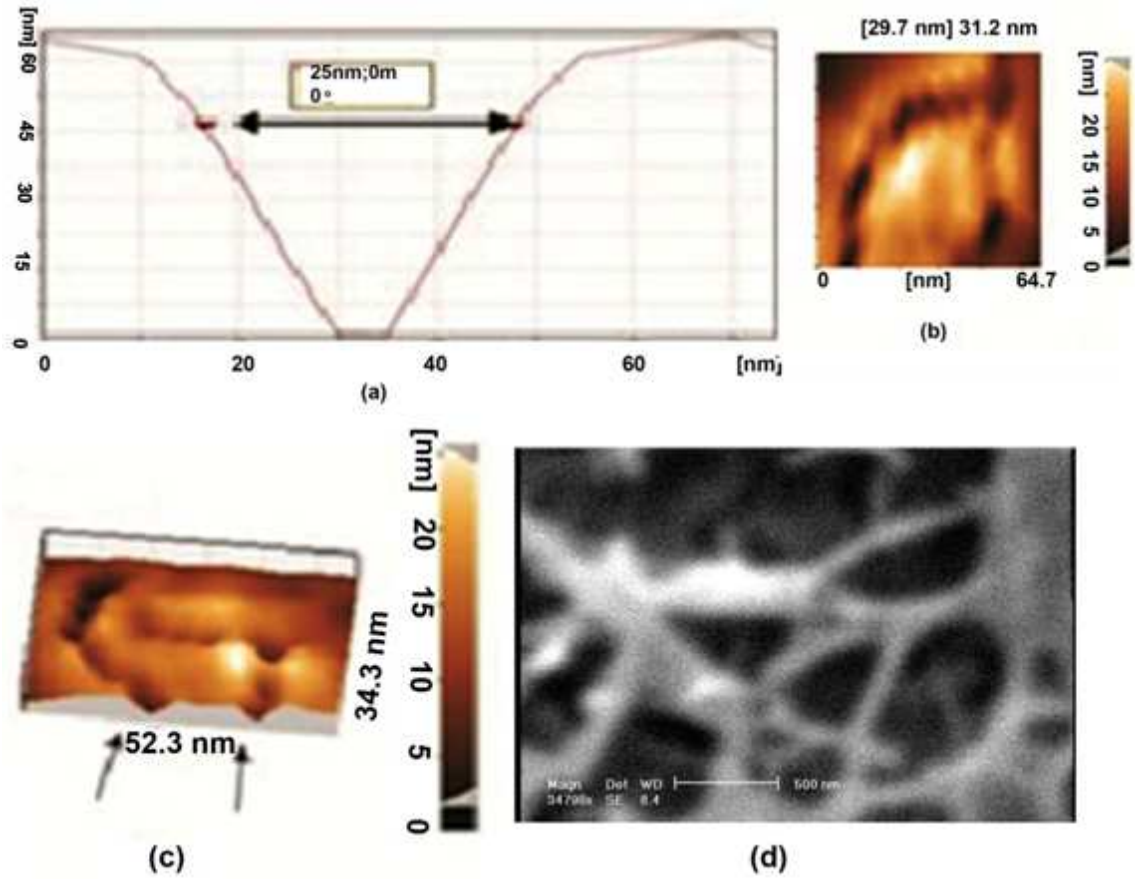

Figure 5.5: (a) Gap diameter and depth of 25 nm and 63 nm respectively. (b) View of AFM imaging of etched Al surface and (c) is a 3-dimensional view of the gap, while the two black arrows point to the positions of the gaps. (d) A 2-dimensional view of SEM imaging of DNA on Al surface.

Chemical etching, achieved by the DNA strands absorbed on the Al surface, created nanometer scaled patterns as shown in the AFM images in Figure 5.6. Figure 5.6(a) shows a 2- dimensional AFM image of the bundled DNA strands effect on the Al thin film surface, illustrating the formation of NGs corresponding to the dimensions of the strands. The curve below Figure 5.6(a) illustrates the depth profile in the direction of the arrow in Figure 5.6(a). 3-dimensional image of Figure 5.6(a) is meanwhile illustrated in Figure 5.6(b). Figure 5.6(c) shows the edge detection of bundled DNA strands effect on

the Al thin film surface and Figure 5.6(d) shows the FESEM imaging of the distance between two edges of gap (82.94 nm). As a result of the corrosion of Al thin films caused by the DNA strands, NGs were created corresponding to the dimensions of the strands.

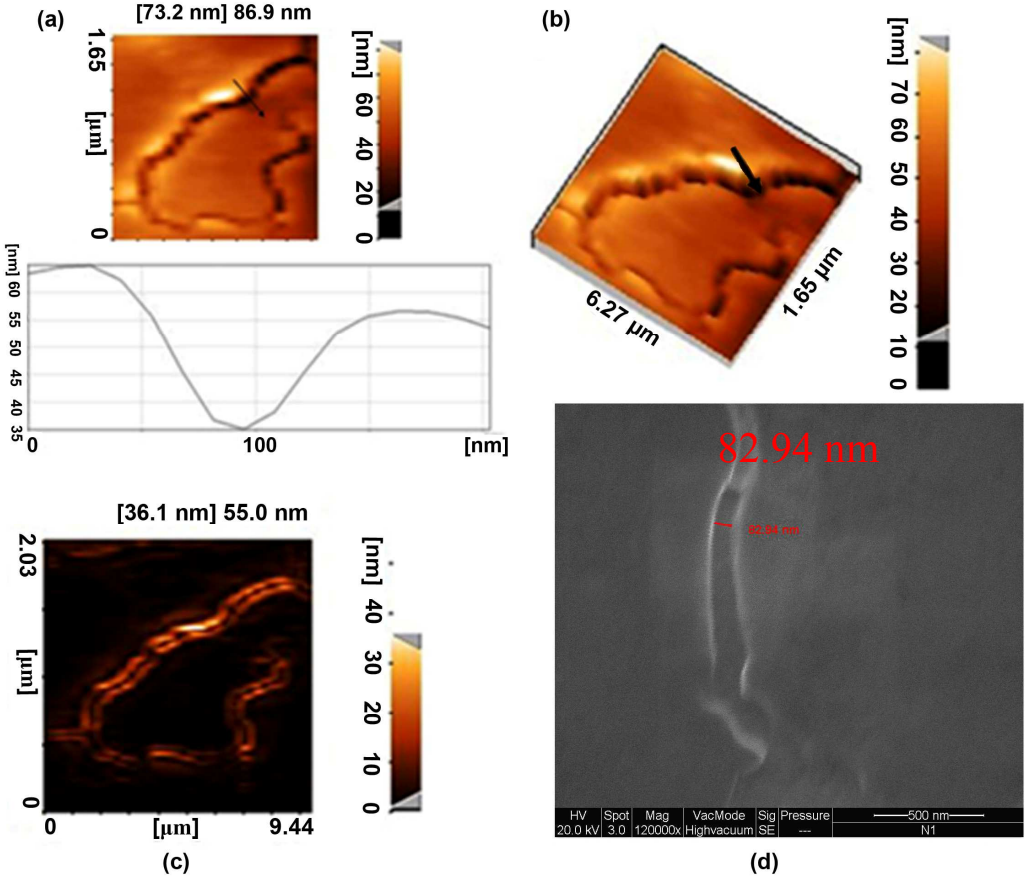

Figure 5.6: AFM imaging of bundled DNA strands effect on the Al thin film surface illustrate the formation of NGs corresponding to the dimensions of the strands used in the experiment. (a) 2-dimensional image of surface, (b) depth profile (black arrow), (c) 3-dimensional image of (a) and (d) edge detection of image in (a).

The mechanism for the interaction between Al and DNA strands is not well understood. However, it is found that in an aqueous environment the interaction is strong, while in dry conditions it is very poor. The interaction between DNA and water molecules is due to the charge exchange, which leads to changes in the charge distribution in the DNA and expulsion of charges into the solvent. Since DNA is a big molecule there are also charge exchanges between the base pairs and water molecules.

In order to investigate the moisture environment needed to create charge carriers in aqueous DNA, the effect of humidity on carrier transportation in the Au-DNA-Au structure has been studied. The concentration of DNA C (ng/nL) is inversely proportional to volume of water in solution. Therefore, the water volume is directly proportional to C^{-1} and according to Figure 5.7, an exponential increase in charge carrier in a moist environment was observed. This phenomenon is due to the increased number of carriers for transport in the environment surrounding the DNA strands that increases the number of ions. As a result of these charge carriers, the π orbital symmetry will change and the electron density of DNA will redistribute (Shannon, 1976). As a result of this, the binding type will change from covalent to ionic in aqueous situation.

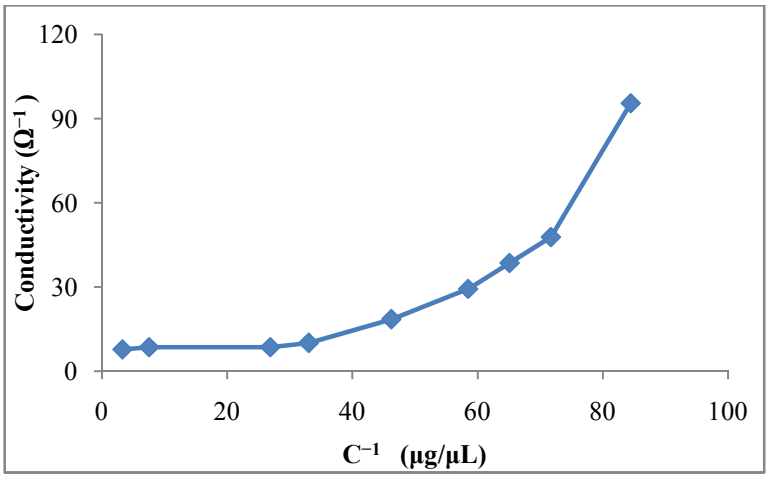

Figure 5.7: Conductivity versus reverse concentration of DNA strand (C^{-1}) in aqueous environment in Au-DNA-Au structure at room temperature.

In addition, Al is an electrochemically active material. There is very strong possibility that this interaction is caused by Al^{3+} ion binding with phosphate groups in the DNA strands (Ahmadi, Alizadeh, Shahabadi et al., 2011). The ionization potential for a phosphate group as the smallest block of the DNA is small and as such ionization of $H_2PO_4^-$ easily occurs and free charge of DNA from its sugar-phosphate backbone (Shannon, 1974). This carrier has the ability to interact with Al, at the interface of Al and the DNA strands. The surface of the Al thin film during the interaction with this

ionic buffer makes the etching process occur. Concentration of charges surrounding a DNA strand is relatively higher as compared to other areas. Thus, the depth of etching on Al thin film is larger in the vicinity of the DNA strands. Another parameter important to create this effect is the time of exposure of the DNA strands on the Al thin film. Direct observations indicate that during the first 20 minutes, no detectable effect of the etching process takes place. Interaction between the DNA strand and Al thin film should occur immediately after thermal evaporation. This was to avoid formation of oxide layer on Al surface when exposed to the environment for longer periods of time due to oxidization.

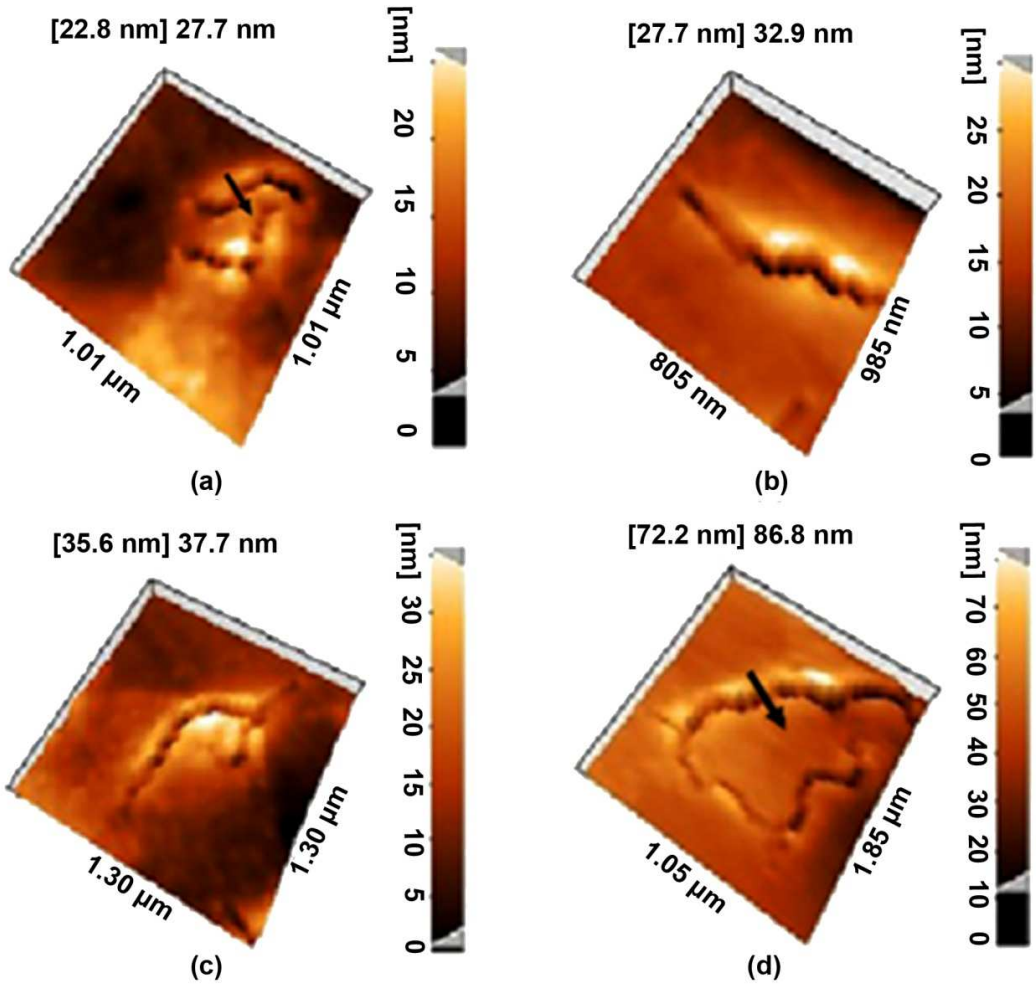

Figure 5.8: Depth profiles of DNA strands remaining on the Al surface (a) after 10 min, (b) after 20 minutes, (c) after 30 minutes and (d) after 40 minutes. The sample size was 1cm×1cm.

As a result of this chemical interaction, an etching effect occurs leaving behind DNA traces on the substrate. Accordingly, by increasing the reaction time and conducting similar experiments for 10, 20, 30 and 40 minutes of durations, images portraying different depths were achieved. As shown in Figure 5.8, after a 10 minutes period, the depth created was around 22.8 nm, which linearly increases to 72.2 nm after 40 minutes. This clearly deduces that the increase in the depth of a crack caused by DNA strands has increased with the time of interaction between DNA and the Al thin film as shown in Figure 5.9. The rate of increase in the depth of a crack is slower for interaction time between 10-30 minutes compare to that of greater than 30 minutes.

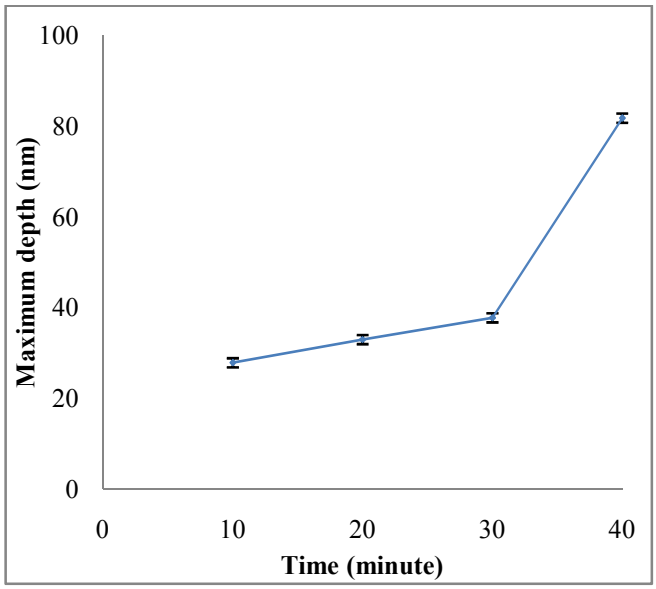

Figure 5.9: The maximum depth versus the reaction time.

Figure 5.10 presents the side views of the formed gaps to provide some supplementary information for Figure 5.8. Figures 5.10(a) and 5.10(b) differs in two aspects: gap depth and shape of the valley. As seen in Figure 5.8(a) as indicated by the arrows, the bottom of the valley is sharp and pointed while the valley shown in Figure 5.8(d) is flat-bottomed. Figure 5.8(a) corresponds to a shallower gap than the one shown in Figure 5.8(d). Actually, the related gap depths of the valleys in Figure 5.10(a) and 5.10(b) are 30 and 50 nm, respectively. The maximum depth and configuration of the gaps can be

related to the thickness of the deposited Al layers (less than 100 nm). Since DNA strands can only react with Al and are non-reactive toward Si, the Al corrosion process along the vertical direction stops as soon as the DNA strands touch the Si substrate surface. From this point on, corrosion occurs along the horizontal axis. In Figure 5.8(a), the Al-DNA interaction duration was not sufficient for DNA strands to reach the Si wafer. Consequently, the gap tips are sharp. Yet, taking advantage of longer durations of interactions, DNA strands cease their horizontal propagation upon reaching Si base.

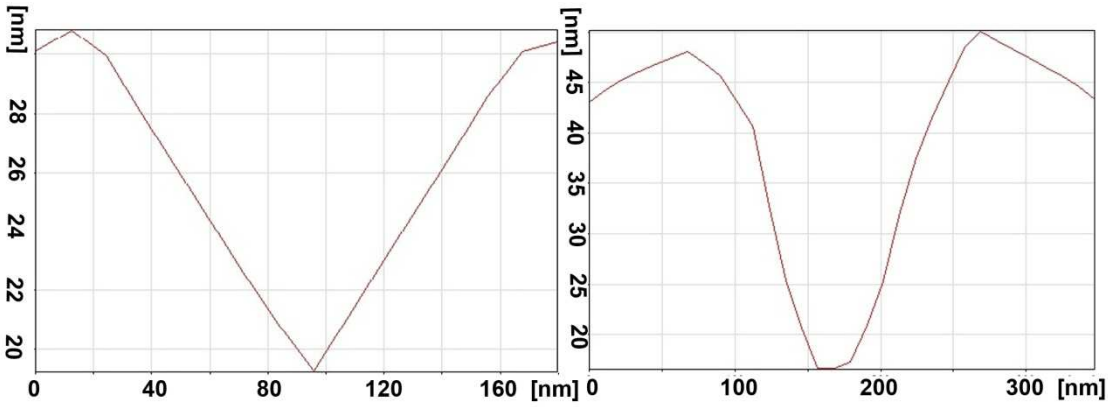

Figure 5.10**:** Side views of the gaps formed along the arrow in Figure 5.8(a, d); (a) Depth profiles of Figure 5.8(a) and (b) Figure 5.8(d) along the directions of the arrow.

Chapter VI: Electrical Device Characterization

6.0 Introduction

Electric charge and potential distribution in molecules are one of the important physical features studied. Negative clusters around these macro molecules cause repulsion and attraction forces between the DNA strands. These forces also form DNA strands so that there is a force balance between DNA strands.

6.1 Electric field effect on DNA assembly

The DNA molecules, themselves, can get along with each other due to electrostatic balance and form a consistent and harmonic structure whereas outside electric field can ease and accelerate the process.

(a) 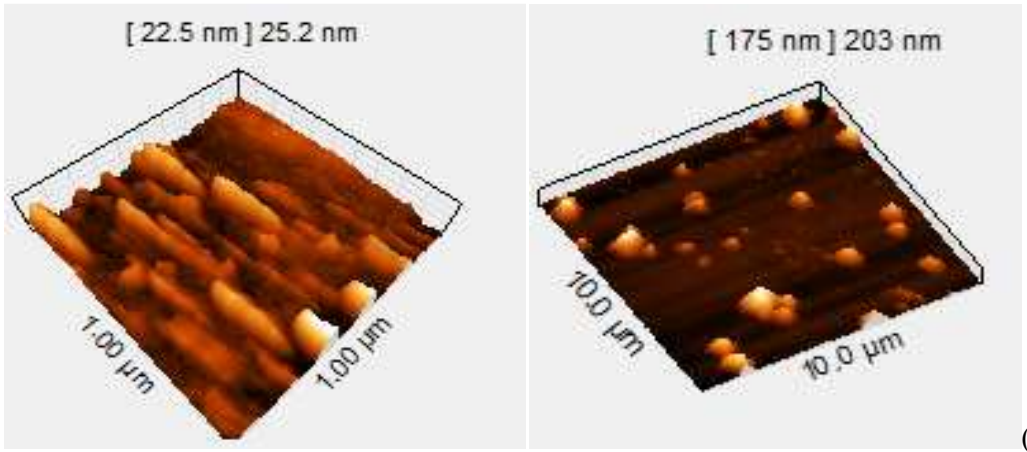

(b)

Figure 6.1: AFM imaging of bundled DNA strands (a) in the presence of external electric field and (b) without external electric field.

Figure 6.1 shows AFM image of the DNA strand with and without the application of electric field. According to Figure 6.1(b), DNA strands are “twisted” in the absence of electric field and form a bulk cluster. In Figure 6.1(a), exposed to electric field of 12 V/s applied for 30 seconds, many DNA strands are aligned to the space between the electrodes in the direction of the electric field. The thickness of the strands formed

without the electric field is 203 nm. However, thickness decreases to 25 nm in the presence of electric field. The strands were observed to not pile-up on each other and regulated in line with the electric field. This features a self-assembly of DNA strands in the presence of an external electric field (Au-DNA-Au). Response of the structure to magnetic and electric fields was investigated based on the *I-V* characteristic curve (N. M. Khatir, S. M. Banihashemian, V. Periasamy et al., 2011).

6.1.1 *I-V* Characteristics for DNA-Au Junctions without Applied Magnetic Field

A thin layer of DNA formed on a surface of glass or Si/SiO_2 with the thickness of 100 nm creates a network of molecule wires. Nano wires made from DNA, due to "energy gap" of around 3.6 to 4.5 eV in their structure, work as a semiconductor. In the presence of electric field, the nano wires become harmonic in-line with the electric field flux.

Presence of free electrons in DNA molecules introduces sensitivity to magnetic and electric fields. Therefore, a considerable response in terms of change in carrier transfer and conductivity are achieved. Since the valence band edge in DNA is below the Fermi energy level of the metal connector (Au), charge carriers overcome the potential barrier height either by thermionic emission, field emission or tunnelling field emission. Consequence of selecting thermionic method however results in nonlinear performance in *I-V* characteristics, which refers to diode performance. The following equation shows the relationship between temperature and potential barrier with current density in the junction of metal-semiconductor (Sze, Ng, 1981; R. Tung, 1992).

$$J(V,T) = AA^{*}T^{2}exp\left(-\frac{\emptyset_b}{K_BT}\right)\left[exp\left(\frac{qV^{*}}{K_BT}\right)-1\right] \qquad \text{Eq. 6.1}$$

where Φ_b is potential barrier height, A = 0.5 mm^{-2}, A^* = 134.9 ($ACm^{-2}K^{-2}$) is the Richardson constant, q is the elementary charge and K_B is Boltzmann's constants. The potential drop in the series intrinsic resistance R of MDM structure is taken into account by considering $V^* = \frac{(V-RI)}{n}$. Applying Eq. 6.1 for the MDM structure with A being average cross-section and n as diode ideal factor; the current J becomes;

$$J(V,T) = AA^*T^2 exp\left(-\frac{\emptyset_b}{K_B T}\right)\left[exp\left(\frac{q\left(\frac{V-RI}{n}\right)}{K_B T}\right) - 1\right] \qquad \text{Eq. 6.2}$$

Fitting Eq. 6.2 to the measured I-V plots, Φ_b and n parameters can be calculated (Jang, Lee, 2002). The average barrier height is $\Phi_b \approx$ 0.868 eV, which is reasonable considering a typical band gap of 3.6 to 4.2 eV for DNA, and the corresponding Schottky barrier at the interface of semiconducting and gold surface. The deduced barrier height is in good agreement with the values (0.75 eV) of measurements performed on single junctions of metallic (Au) and semiconducting (DNA). According to Eq. 6.3 (Cowley, Sze, 1965);

$$\Phi_b = w - \left(\frac{-E_g}{2} + E_I\right) \qquad \text{Eq. 6.3}$$

In equations 6.1 to 6.3, Φ_b is the potential barrier between the metal and DNA and w is the metal work function of gold. E_g is the energy gap of DNA as a semiconductor is equal to 5.1 eV (Ago, Kugler, Cacialli et al., 1999; Kim, Lägel, Moons et al., 2000; Meijer, De Leeuw, Setayesh et al., 2003). E_I meanwhile is the ionization energy of DNA, which is about 3.6 eV (Preuss, Schmidt, Seino et al., 2004). The ionization energy for each part of DNA; that is Cytosine, Thymine, Guanine and Adenine, are equal to 8.86, 9.14, 7.75 and 8.24 eV respectively (Crespo-Hernández, Arce, Ishikawa

et al., 2004; Sugiyama, Saito, 1996). If the minimum value is 7.75 eV, then the potential barrier was calculated to be 0.75 eV.

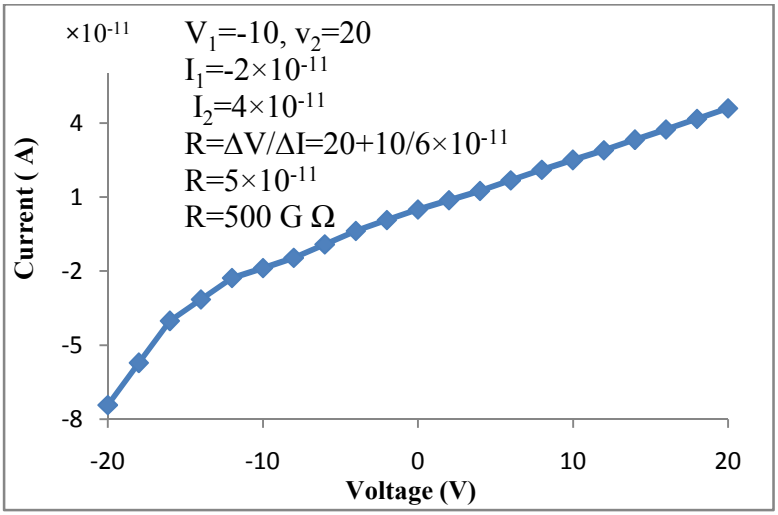

Figure 6.2: *I-V* curve of the junction between the two electrodes in the absence of DNA molecules

According to Figure 6.2, resistance between the two electrodes integrating the DNA strands was very high (approximately 500 GΩ) and their current was very low (around 10^{-11} A) at room temperature and in the absence of magnetic field. Due to conductance contributed by the DNA strands, current was increased as shown in the figure and the *I-V* characteristics changes from ohmic-linear (Figure 6.2) to exponential type (Figure 6.3) due to new Schottky junctions. According to Eq. 6.2 and Eq. 6.3, potential barrier, ideality factor, conductance, saturation current and breakdown voltage were measured for DNA-Au-Schottky junction (Table 6.1). The calculated theoretical potential barrier and experimental potential barrier were 0.75 and 0.86 eV respectively. This difference could be due to lowering of image force created at the interface of metal-semiconductor (Shannon, 1974, 1976). The parameters calculated from the DNA-Au Schottky junctions are detailed in Table 6.1.

Table 6.1: Potential barrier, ideality factor, conductance, saturation current and break down voltage for DNA-Au Schottkey barrier.

Saturation Current (*A*)	$0.00015(\pm 10^{-11})$
Current density (A/Cm^2)	$0.0003(\pm 10^{-11})$
Theoretical Potential barrier (eV)	$0.75(\pm 10^{-3})$
Experimental Potential barrier (eV)	$0.86\ (\pm 10^{-3})$
Ideal number	$30(\pm 0.1)$
Temperature ($^{\circ}C$)	$27(\pm 10^{-2})$
Magnetic field (mT)	$0(\pm 10^{-1})$

Table 6.2: Potential barriers between semiconductors and gold in units of eV.

Potential barrier (metal-semiconductor junction) (eV)	
Semiconductor	Gold
n-Silicon	0.2 (Ahmad, 1972)
p-Silicon	0.87
n-Gallium Arsenide	0.8 (Borneman, Schwarz, Stickler, 1955)
p-Gallium Arsenide	1.19 (Maksimova, Vyatkin, Pronina et al., 1968)
Germanium	0-2 (Mayer, 1959)
n-Indium Phosphide	1.01(Zhou, Langsdorf, Jones et al., 1999)
p-Indium Phosphide	0.61 (Zhou, Langsdorf, Jones et al., 1999)
DNA Theoretical	0.75
DNA-Experimental	0.86

Table 6.2 shows a comparison between semiconductors when they are connected to gold and Schottky barrier created. As seen in the table, potential barrier in Au-DNA junction was 0.86 eV, which is about the value of potential barrier in p-type Si (0.87 eV). This means that the same potential barrier can be achieved in Au-Si junctions.

However, DNA can pass larger current compared to Si and has greater sensitivity to magnetic field.

6.2 Effect of Temperature on the *I-V* Curve of Metal Structure-DNA at Zero Magnetic Fields

I-V characteristics of diode vary with temperature. Applying voltage causes a gradient in charge carrier concentration, which in turn brings about dispersive currents. Saturation current (I_s) is a function of the concentration of charge carriers, which is strongly temperature dependent. In electrical characterization for transistor and diode, thermal effects should be considered in calculating electrical parameters.

$$J(V,T) = I_s(T)\left[exp\left(\frac{q\left(\frac{V-RI}{n}\right)}{K_B T}\right) - 1\right] \qquad \text{Eq. 6.4}$$

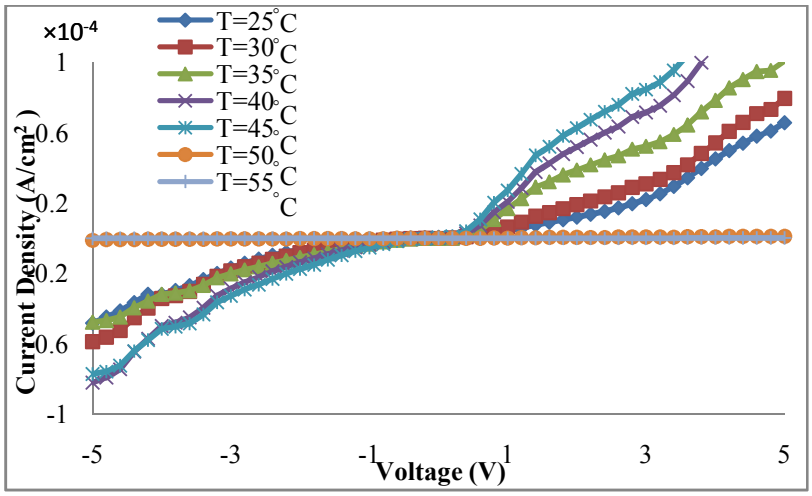

Figure 6.3: Current versus voltage for metal-DNA-metal structure in the absence of magnetic field

Since I_S and thermal voltage, V_T, (Eq. 6.4), are functions of temperature, V_T is given by KT where K is Boltzmann's constant and T is the Kelvin temperature. According to Eq. 6.1, fluctuation of I_S and V_T parameters with changes of temperature changes during

zero voltage crossing and changes in the rate of exponential graphs. Subsequently, any change in the voltage threshold will appear in the direct bias region of *I-V* curve.

Forward and reverse bias characteristic changes of temperature for the MDM are shown in Figure 6.3. For a given specified current and with increasing temperature, forward bias voltage was reduced compared to reverse bias region showing changing threshold voltage of diode. *I-V* curve illustrates that with temperature changes, current will be increased. This process increases until 50°C, after which temperature change decreases.

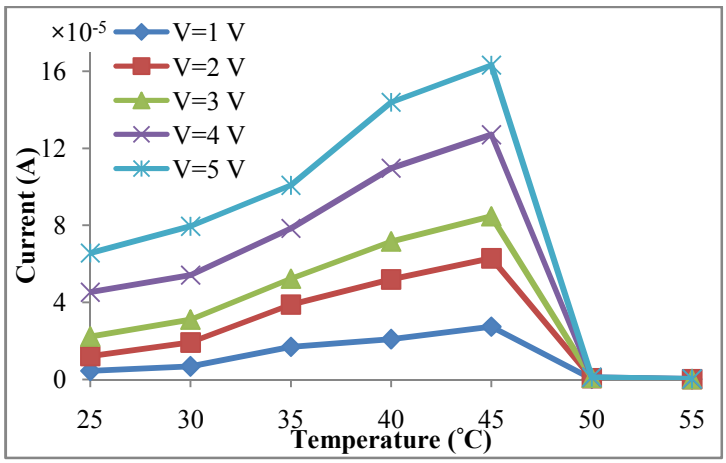

Figure 6.4: *I-V* curve for MDM structure in the absence of magnetic field under varying voltages.

As shown in Figure 6.4, at various voltages (1 to 5 V) and with increasing temperature, current increases slowly. These changes increase continuously until temperature of about 45°C. Beyond that, a sudden drop in current is seen. This indicates material changes from its original state. With increasing temperature, hydrogen bonds between the base of the macro-molecular structure of double strands of DNA would break (Crothers, 1964). By increasing the temperature, breakage of double strand to single strand results in increase of resistance represented by current decrease (Figure 6.4).

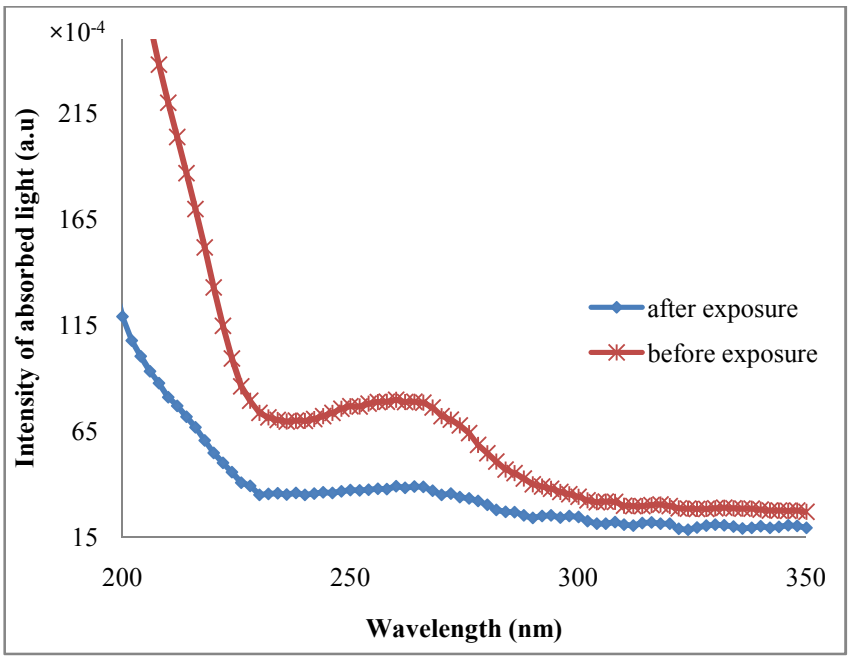

Figure 6.5: The red curve shows the DNA UV-VIS spectrum before exposure to electric and magnetic fields and the blue curve shows the DNA UV-VIS spectrum after exposure to electric and magnetic fields. As depicted in UV-VIS spectrum, the intensity of absorbed light after exposure to magnetic and electric field and increasing the temperature declined significantly. Concentrations of DNA before and after exposure are 0.3987 and 0.1947 (ng/nL), respectively.

As shown in Figure 6.5, the concentration of DNA after being influenced by magnetic and electric field declined as calculated by UV-VIS spectroscopy. Generally, by increasing the DNA temperature, the absorption of light will increase but the evidence seems to indicate decreasing absorption of light. DNA absorb UV-light due to its aromatic rings and the decrease of this rings due to the change in structure has caused the decrease in the light absorbed.

Table 6.3: Some information about DNA (Deaton, 1998).

Sample	CG (%)	Melting point	Molecular weight	Length
CCACCACCGGCGACG....GC TTCGACTGGGG A (22%), T (20%), G (35%), C (23%)	58	87.5	176975.1	567

Melting temperature of DNA used in this work was calculated based on Eq. 6.1. Table 6.3 shows the melting point, length and percentage of Guanine (G) and Cytosine (C) in DNA. DNA melting temperature with the length of 567 nm and having 58% G-C was estimated to be 87.5°C (melting point predictions performed using BioMath software).

DNA links start to break at 55°C while DNA is not melted completely. The melting point for shorter DNA strands was less than normal sized DNA strands. Addition of Guanine and Cytosine will also increase the melting point (Khandelwal, Bhyravabhotla, 2010).

T_m= 64.9°C + 41°C x (number of G's and C's – 16.4)/N Eq. 6.5

where N is the length of the primer.

Figure 6.6 shows the temperature changes depending on the saturation current. Initially, the trend increased with increasing temperature. However at 50°C, significant reduction was observed. As mentioned, this process occurs because of the change in saturation current and thermal voltage.

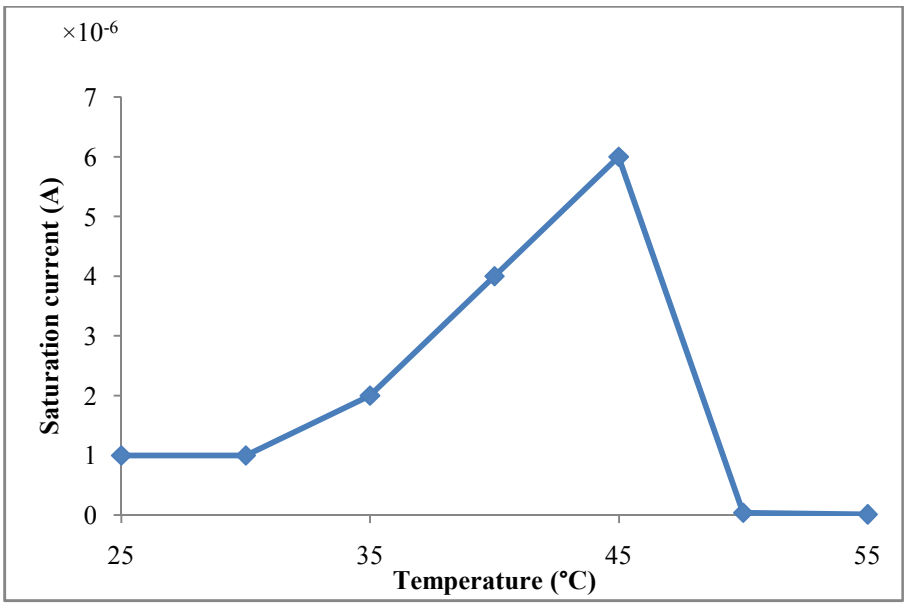

Figure 6.6: Saturation current versus temperature for MDM structure in the absence of magnetic field.

6.2.1 Calculated Values for Potential Barrier from *I-V* curve

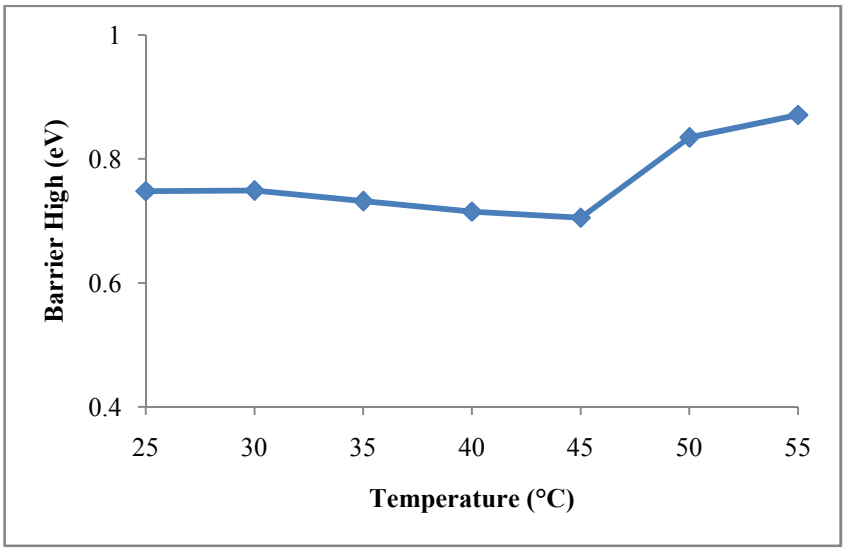

Figure 6.7: Potential barrier height versus temperature for metal-DNA-metal structure in the absence of magnetic field

Values calculated for potential barrier from the *I-V* curve shows some changes in the amount of voltage barrier. According to Figure 6.7, potential barrier decrease in a small amount at temperature variation of 45°C. Since the potential barrier was calculated from

saturated current, the decrease in potential barrier was because of increase in saturation current as a result of the temperature rise.

6.2.1.1 Potential Zero Bias

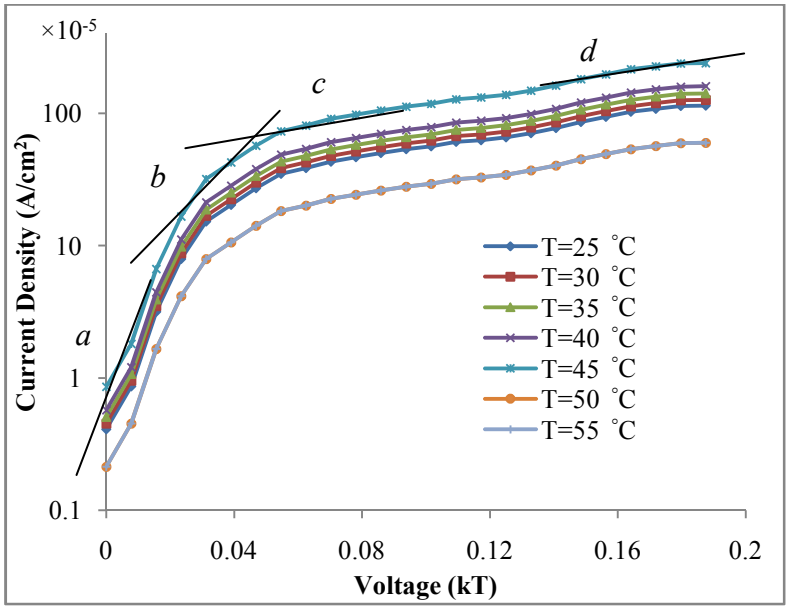

Figure 6.8: Logarithmic diagram for *I-V* in different temperatures and without exposure to magnetic field for metal-DNA-metal structure.

Calculated value for potential barrier at room temperature from Eq. 6.1 is 0.75 (eV), which is larger than the amount obtained from the *I-V* curve. Increase in temperature will increase the thermionic emission current that will increase the possibility of carriers crossing the barrier. In fact, temperature has a direct effect on the carriers' density and the current will change due to increase of carriers. However, this change in carriers will not change the actual length of the band gap but will increase the density of carriers around the band gap and bend the potential barrier in the interface junction between metal and semiconductor. However, due to the effect of temperature on saturation current, potential barrier will be lower compared to the actual value.

At 50°C, diode behaviour was not observed due to changes in the DNA structure. It exhibits a larger resistance to current. In order to investigate further, semi logarithmic *I-V* diagram was plotted as depicted in Figure 6.8. The Figure illustrates the *I-V* characterization in forward bias for Au-DNA (metal-semiconductor) junction in semi logarithmic scale. For an ideal diode in forward bias region, a line can be drawn as in Figure 6.8 to divide the diagram into several parts. If a region follows ideal diode behavior; the ideal diode emission coefficient will be equal to 1 and in other areas due to various factors, the Schottky behavior is removed from ideal diode state. In region *a*, the generated current deviates from diode performance due to recombination carriers and ideality factor becomes greater than 1.

In region *b*, the ideality factor is 1 while in region *c*, due to penetrated diffusion of carriers, the factor was increased and deviates from normal diode performance. Finally, in higher regions of *d*, ohmic effects due to ohmic resistances will lead to complete deviation from diode performance. Other results that are extracted from the *I-V* diagram are the effect of temperature increase on the current. According to Figure 6.8, a sharp change occurs in current through the MDM structure at 50 and 55°C. The changes were more visible at 55°C due to phase change in the material and new crystal structure generation as a result of the broken DNA. The concentration of DNA under the influence of magnetic and electric fields declined as calculated by UV-VIS spectroscopy.

6.2.1.2 Conductance

In order to further investigate the effects of temperature, the diagram of conductance change versus temperature was investigated in the MDM structure without the influence of magnetic field. It is obvious that, movement of carriers in a semiconductor will cause electric current. Applying an electric field will increase the overall superposition of current in one direction and the current will (flow) due to current drift. The other phenomenon that causes the carriers to move is the difference in carrier densities in two regions of material leading to migration of carriers from high-density to low density region and is called diffusion phenomenon. Applying electric field will cause the carriers to move along the electric field lines. Some factors like collision impurity and deviation from resonance network structure and increase of resistance due to collisions between carriers will reduce conductivity. Increasing temperature is a factor that will increase the resonance in network and carrier collisions. Collisions within the carriers and impurity centres will increase resistance and therefore decrease conductance.

Figure 6.9 shows the results for conductance in MDM structure due to temperature changes without application of magnetic field. Initially, it was observed that conductivity increased almost linearly with temperature, which is common in semiconductor materials. However, dramatic negative change in conductance occurs beyond 50°C due to breaking of the hydrogen bonds and altering of the double structured DNA to single structure.

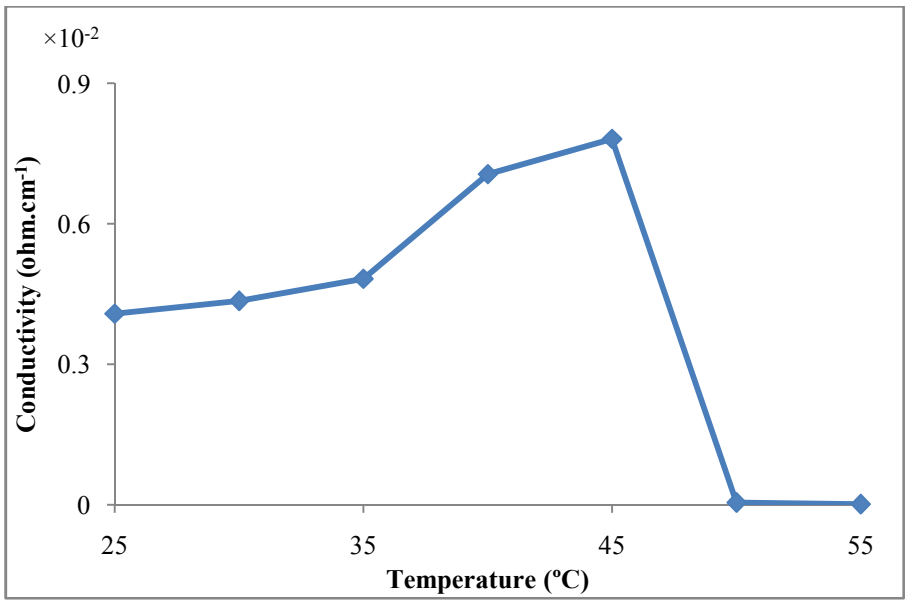

Figure 6.9: Conductance versus temperature graph in MDM structure.

Table 6.4 presents a comparison between conductance of common semiconductors such as Si, Ge, GaAs and DNA in ambient temperature. This table shows the resistivity, conductivity and temperature coefficients of various materials at 20ºC (Elliott, 1961; Madelung, 1996; Streetman, 2000; Wu, Walukiewicz, Yu et al., 2002). According to the energy band gap of the semiconductors, DNA conductance is ten times larger than the conductance of Si despite the large energy gap relative to other semiconductors (due to a Schottky barrier with Au). As such, DNA could be used as a good candidate for use in electrical circuits**.**

Table 6.4: Resistivity, conductivity and temperature coefficients of various materials at 20 °C

Material	Symbol	ρ [Ω·m] at 20°C	σ [S/m] at 20°C	Band gap (eV) at 20°C
Carbon (diamond)	C	1×10^{12}	$\sim10^{-13}$	5.5
Germanium	Ge	4.6×10^{-1}	2.17	0.67
Silicon	Si	6.40×10^{2}	1.56×10^{-3}	1.11
Gallium arsenide	GaAs	5×10^{-7}to10×10^{-3}	5×10^{-8} to 10^{3}	1.43
Deoxyribonucleic acid	DNA	$3.45\times10^{+01}$	2.89×10^{-02}	3.6-4.2

6.3 *I-V* Diagram at a Constant Temperature with Different Magnetic Fields

Organic molecules including DNA have been proposed to be used in electronic device. For most organic molecules with an unpaired spin, the coupling constants are often smaller than those in the H atom. This is because an unpaired electron in a molecule is never confined to just one nucleus and seldom to one bond, being able to move over several bonds with relative ease. In organic semiconductors (including DNA), interaction between the unpaired electrons and magnetic field cause changes to the energy gap and influence charge transfer.

Once an external magnetic field is applied to the semiconductor, the energy levels increased allowing some of them to pass above the Fermi energy. In high magnetic fields, the scattering amplitude for similar and dissimilar spins will differ (Sakurai, 2006) and the band-gap will change according to discrete energy levels. In the presence of some low magnetic fields, the band-gap does not change considerably. Also, the charge of material in a magnetic field will be subjected to Lorentz force and Drude theory. Electrons in partially filled bands and ions could be affected by the external magnetic field. A circular motion will be created by a trajectory of electrons perpendicular to the field. Additionally, in MDM structures, before the charge carriers migrate from the left electrode to the right one, they move in a disturbed and spiral fashion to left and right for many times (Kang, Jiang, Sun et al., 2011). Such disturbed movements were due to the loose coupling of electrodes and DNA. An external magnetic field alters the motion of carriers alongside the electric field and inhibits the motion of the carriers to the opposite electrode. This results in a decrease in the current in comparison to absence of a magnetic field.

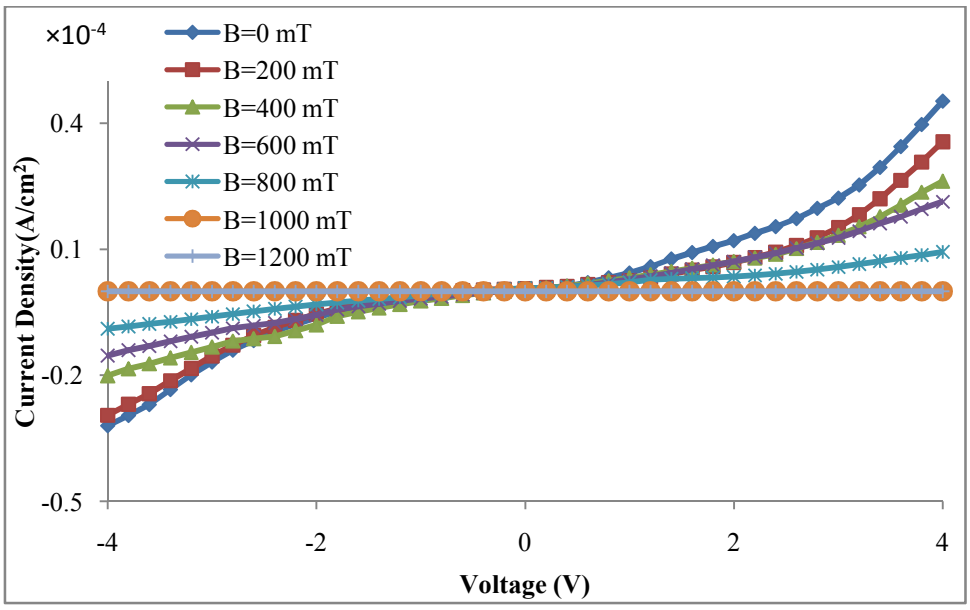

Figure 6.10: *I-V* curve generated at room temperature under the application of different magnetic fields.

It is shown here that the influence of external magnetic field on DNA molecules in Au-DNA-Au structure can efficiently change the physical features of DNA strands. The changes may involve resistivity, conductivity and band-gap. Figure 6.10 shows the *I-V* curve for Au-DNA-Au structure in the presence of various levels of magnetic fields. The transport behaviour of electrons through Au-DNA-Au structures was investigated by measuring current and conductivity/resistivity based on *I-V* curve.

$$I(V,B) = I_{S(B)}\left[exp\left(\frac{q\left(\frac{V-R(B)I}{n}\right)}{K_BT}\right) - 1\right] \qquad \text{Eq. 6.6}$$

$$I_{S(B)} = A^*(B)T^2 exp\left(-\frac{\emptyset_{b(B)}}{K_BT}\right) \qquad \text{Eq. 6.7}$$

Eq. 6.6 connects MDM structure with constant temperature and current as a function of magnetic field B, and voltage V. Related parameters used in this Eq. have been already discussed. The saturation current I_S, and resistance R, are functions of magnetic field.

Since the saturation current is related to Richardson's constant and the potential barrier, then Eq. 6.7 can be substituted in Eq. 6.6 as below;

$$I(V,B) = A^*(B)T^2 exp\left(-\frac{\emptyset_{b(B)}}{K_B T}\right)\left[exp\left(\frac{q\left(\frac{V-R(B)I}{n}\right)}{K_B T}\right) - 1\right] \quad \text{Eq. 6.8}$$

To investigate the behaviour of the diode at Au-DNA-Au interface in the presence of various magnetic fields at constant temperature, a conceptual model was designed as shown in Figure 4.10. With increasing current in the solenoid between two poles, the induced current was also linearly increased. As a result, uniform magnetic field perpendicular to the current was created between the two metal poles at the centre of the solenoid.

In order to create a stronger magnetic field, poles were brought closer and the applied magnetic field was calculated. In this case, the cryostat was taken out from the device set-up and a magnetic field (100 mT to 2000 mT) was applied to the sample. To examine the effect of connections, *I-V* characteristics were measured in presence of magnetic field. Figure 6.11 shows the *I-V* curve for connection of Au-gap-Au at the absence of DNA. Resistance (500 GΩ) between the electrodes was significant when set without DNA with current in the order of 10^{-11} A. The value obtained without the magnetic field shows no difference. It means that in this situation, magnetic field does not have any effect on the sample. Upon placing DNA in the gap between the metals and applying magnetic field, *I-V* curve was generated and investigated.

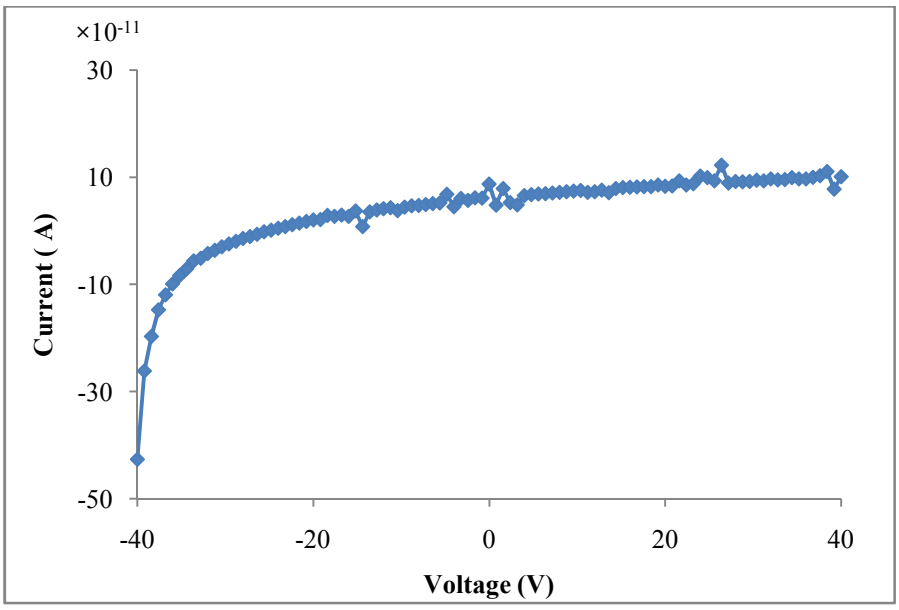

Figure 6.11: *I-V* curve of the junction between the two electrodes in the absence of DNA.

Figure 6.12 shows the saturation current with respect to magnetic field strength. The saturation current undergoes a sharp decline followed by oscillatory variations. An exponential decay in saturation current was observed with increase of field strength up to 1000 mT. Initial decline obeys a linear relation and was due to decreasing mobility of charge carriers. For a closer look at the changes, the graph in Figure 6.12 was divided into three regions. First is the line changes; reduction in more than 1000 mT (Figure 6.13). The second area involves the oscillating magnetic field changes which indicate fluctuations around a constant current in values less than 1000 mT (Figure 6.14). Figure 6.15 meanwhile shows exponential changes in magnetic fields of values less than 200 mT. Figure 6.13 generated using Eq. 6.7 indicates that the slope of the field is negative and decreasing current with the rate of 50 μA/mT. Mobility of carriers in the magnetic field was also reduced. Figure 6.14 shows that the current was reducing following an oscillatory trend with increasing magnetic field.

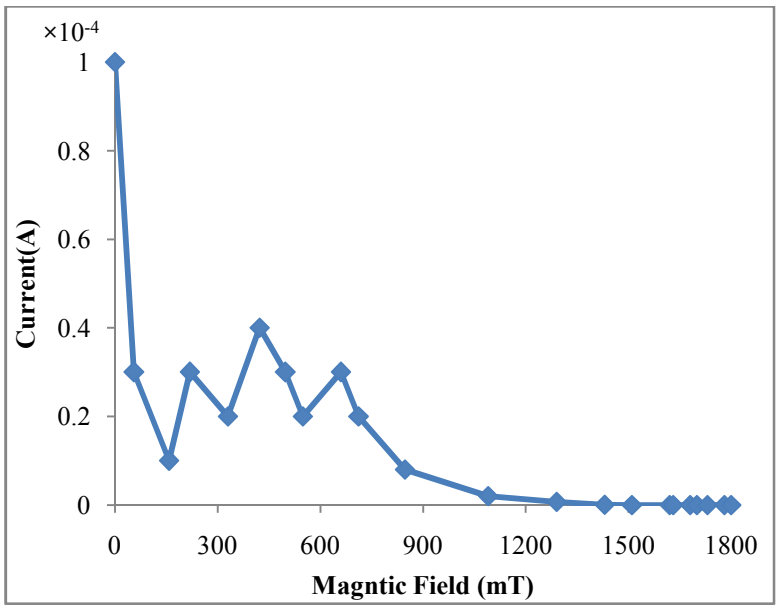

Figure 6.12: Current versus magnetic field for MDM structure.

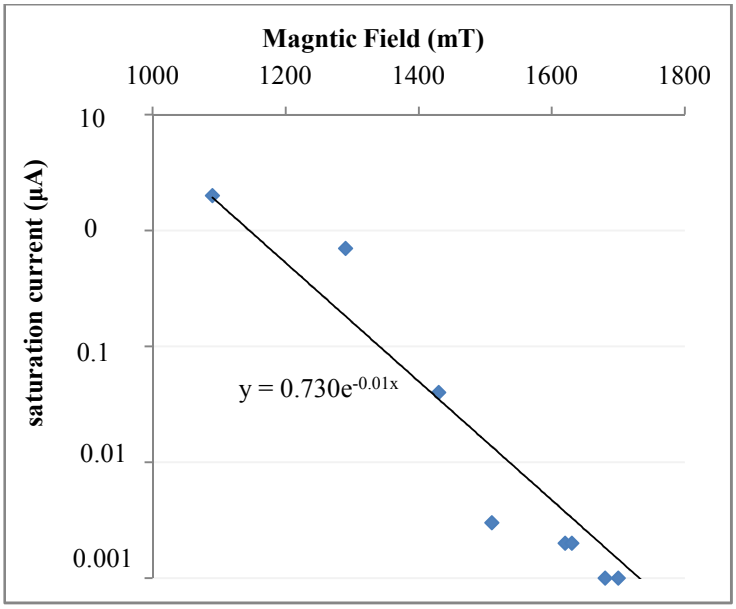

Figure 6.13: Saturation current versus magnetic field (≥ 1000 mT) for MDM structure.

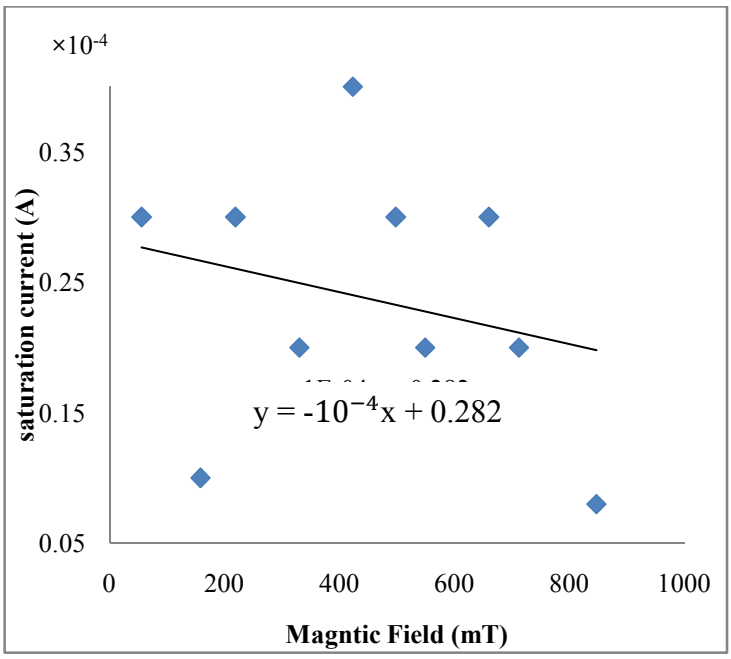

Figure 6.14: Saturation current versus magnetic field (150 mT to ≤ 1000 mT) for MDM structure.

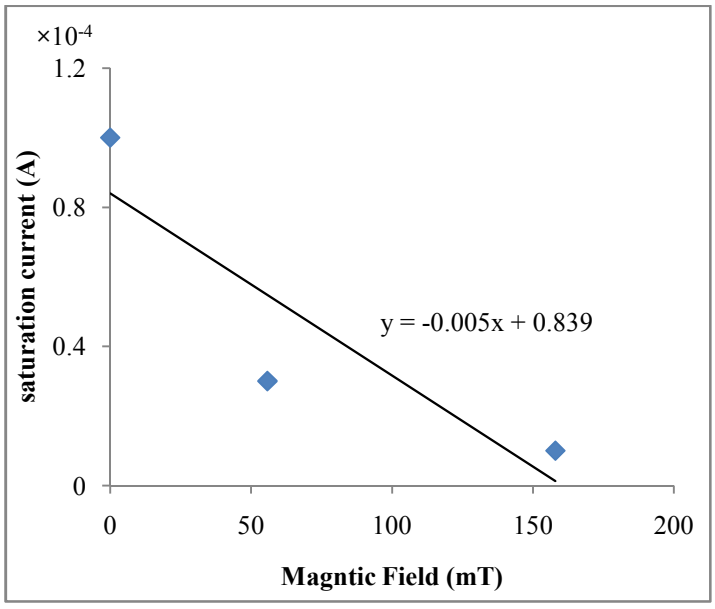

Figure 6.15: Saturation current versus magnetic field (0-200 mT) for MDM structure.

Comparing the decreasing rate in the two regions; below 150 and between 150 to 1000 mT, the reduction in Figure 6.14 was observed to be lower than Figure 6.15. Since these

changes are almost linear, it cannot be attributed to the changes in potential barrier and can only be caused by changes in carrier mobility and the Richardson constant. According to Figure 6.15 (third region), exponential decrease was observed in the current-magnetic field curve related to the potential barrier. But since this reduction shows both the exponential and linear variation, it can be concluded that the current decrease was related to the increase of potential barrier and carrier resistance (Menon, Ehsan, Shaari; Mtangi, Auret, Nyamhere et al., 2009; Tay, You, Lau et al., 2000).

6.4 Logarithmic Changes in the Ohmic Resistance in MDM Structures

Figure 6.16 shows logarithmic changes in the ohmic resistance in the structure of the MDM. Figures 6.17 and 6.18 shows resistivity versus magnetic field for less and more than 1000 mT, respectively. For area more than 1000 mT, (Figure 6.18), the resistance change was linear up to 1300 mT. The value increases sharply as increase in magnetic field due to cyclotron effects in charge carriers under electric and magnetic fields. In Eq.s 6.6 and 6.7, R (B) shows the relationship between resistances and magnetic field.

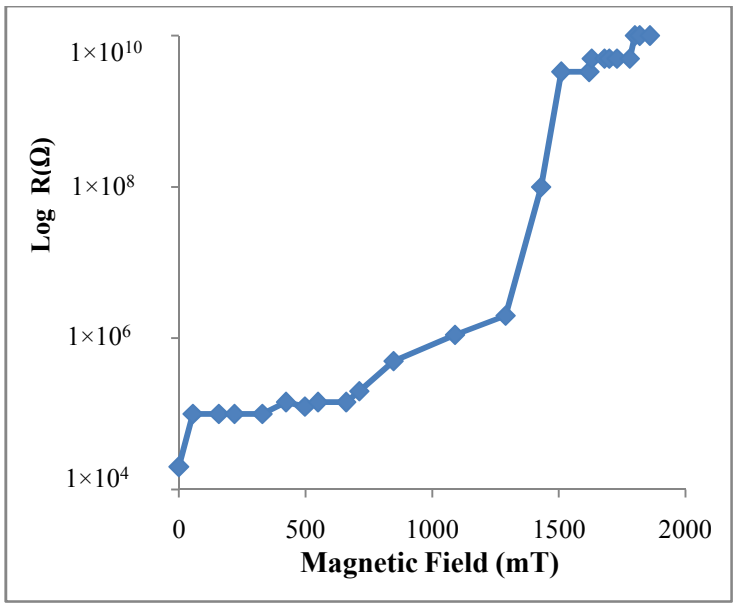

Figure 6.16: Logarithmic resistivity versus magnetic field for MDM structure.

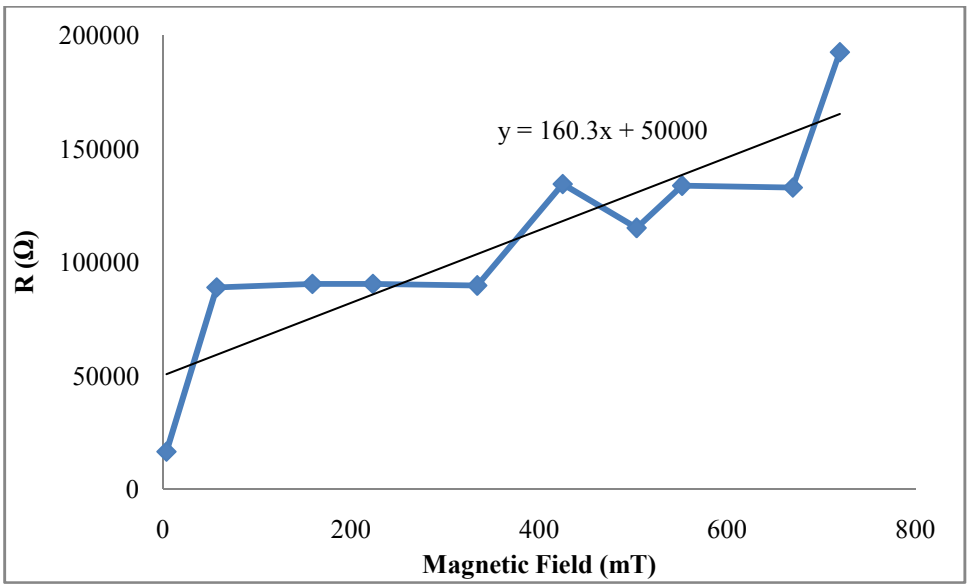

Figure 6.17: Resistivity versus magnetic field (≤ 1000mT) for MDM structure.

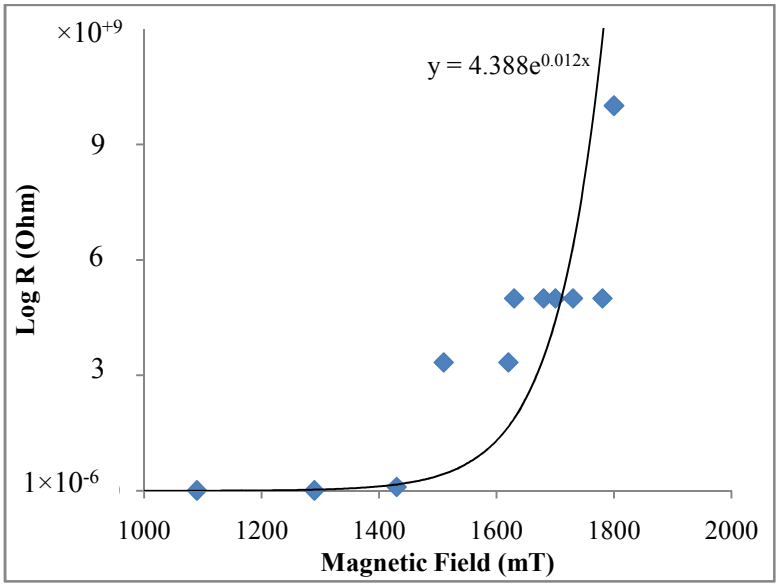

Figure 6.18: Resistivity versus magnetic field (≥ 1000mT) for MDM structure.

According to trend-line of the curve in Figure 6.17, this increase was obtained from;

$$y = 160.37x + 50000 \qquad \text{Eq. 6.9}$$

For high magnetic fields, the increase is exponential and the equation is;

$$y = 500e^{0.0092x}$$ Eq. 6.10

In general, Eq 6.9 is for less than 1000 mT (Figure 6.17) and Eq. 6.10 is for more than 1000 mT (Figure 6.18). Both of these equations, therefore illustrates the mechanisms governing the motion of carriers in the MDM structure in a magnetic field of less and more than 1000 mT. Increased resistance of the carrier motion was related to several other phenomena that can be derived from the energy level of the applied external field. This property makes it possible to use this structure as magnetic field sensors. In the next section, the relationship governing saturated current (Eq. 6.6) and *I-V* curve in the presence of magnetic field and temperature changes were investigated.

6.5 *I-V* curve at variable temperature and magnetic field

To evaluate effect of external magnetic field on potential barrier and Richardson constant changes, *I-V* curve at various temperatures and magnetic fields were investigated. Figure 6.19 shows *I-V* curves at variable temperature/magnetic fields.

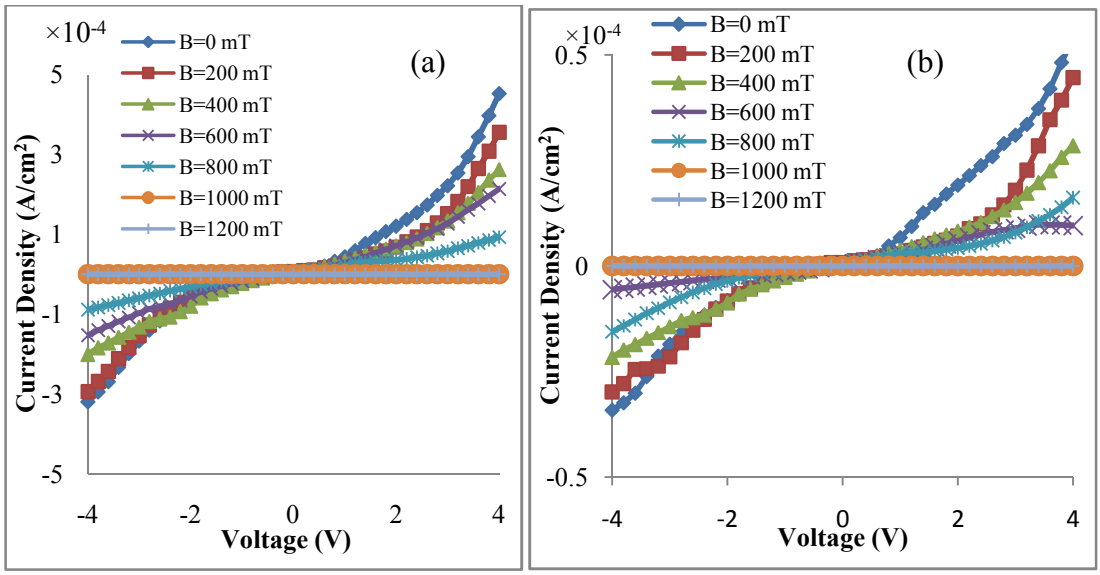

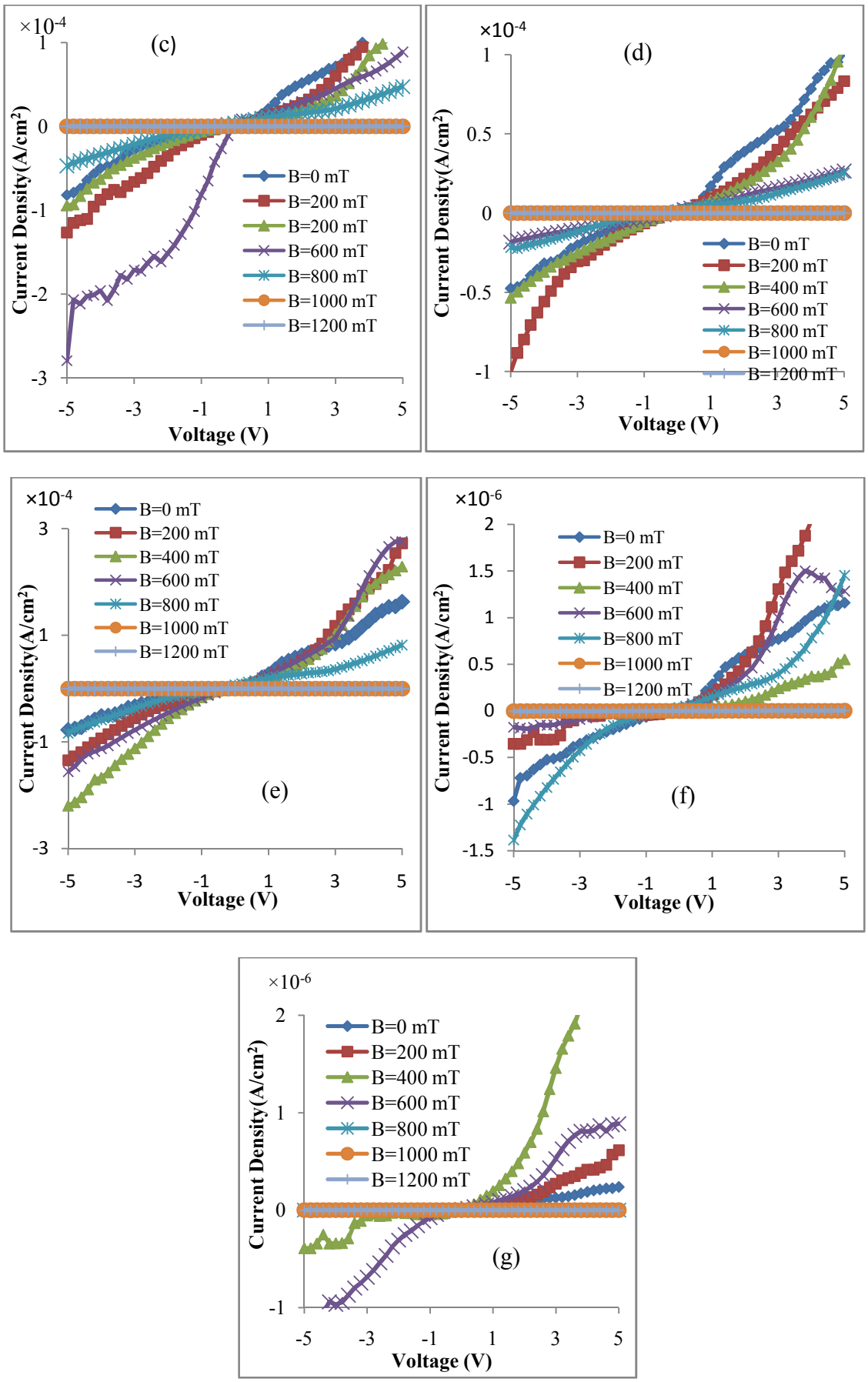

Figure 6.19: *I-V* curves at generated constant temperatures ((a) 25°C, (b) 30°C, (c) 35°C, (d) 40°C, (e) 45°C, (f) 50°C and (g) 55°C) using different magnetic fields.

The second column in Table 6.5 shows that the Richardson constant changes due to temperature changes and current intensity was calculated. Together with Figure 6.19 the Richardson constant was shown to vary due to the magnetic field fluctuation. Based on these observations, relationship can be obtained for the magnetic field and Richardson constant. From Eq. 6.13 and 6.14, Richardson constant was calculated at 1.58×10^{-1} Acm^2/KmT. With increasing magnetic field, the Richardson constant increases (Figure 6.20). Richardson constant has direct relationship with effective mass of the carrier when passing through the electric field. In this case, when the effective mass increases, the mobility reduces. This results in a lower rate of carrier penetration through the potential barrier.

As such, collision and resistance were increased and the number of electrons decreased from the left electrode to the right one. Finally, decrease in current and increase in the potential barrier were observed. Calculated potential barrier (Table 6.5), according to Figure 6.19 and Eq. 6.8, indicates that the potential barrier in magnetic fields less than 1000 mT did not change much. But at higher magnetic fields, the potential barrier increased significantly. Potential barrier changes in magnetic fields less than 1000 mT (Figure 6.21), is almost linear and very slow at a rate of 1×10^{-5}eV/mT.

However, for magnetic fields higher than 1000 mT (Figure 6.22), the changes are rapid and the rate is 2×10^{-3}eV/mT. The physical reasons for this phenomenon can be caused by cleavage of energy levels, increase in the height of potential barrier between metal and DNA and increased resistance in the structure of DNA.

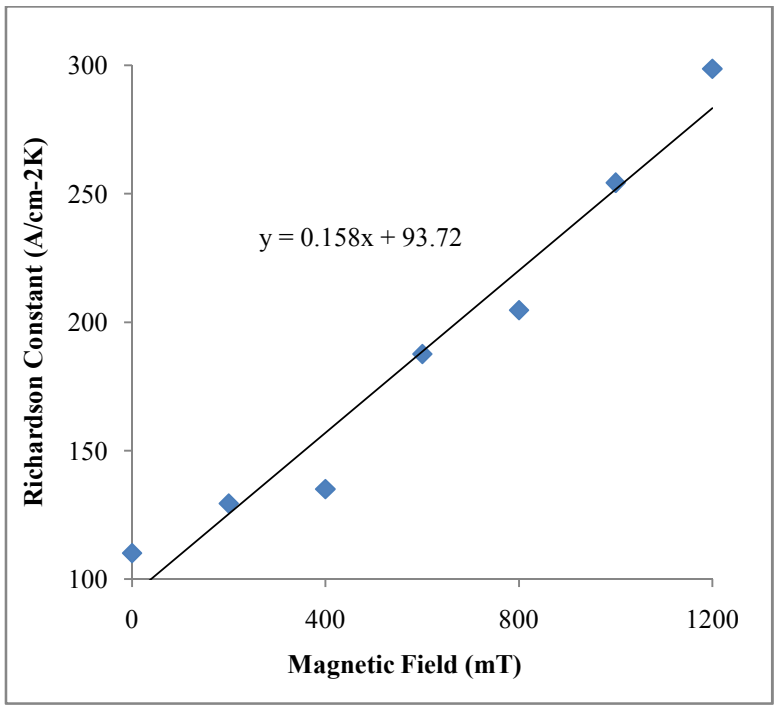

Figure 6.20: Richardson constant versus magnetic field for MDM structure.

In magnetic fields larger than 800 mT, resistance suddenly increases. This resistance was due to changes in DNA resistance and in macromolecules of DNA. In summary, it could be concluded that with increasing magnetic field, the current rate through the sample decreases and the potential barrier and the resistance increases. Sample in high magnetic fields show significant changes in behaviour and diode characteristic is removed; ohmic behaviour and resistance meanwhile are observed to increase. These changes were caused by the Lorentz force and increase of the rotational magnetic field and external electric field. It is also related to changes in the DNA structure as a result of external radiation field, opening up the vibrations of double bonds and hydrogen bonds between base pairs.

Finally, if the magnetic field changes are less than 800 mT, DNA structure will change linearly according to the changes. However, if the magnetic field exceeds 800 mT, DNA structure cannot follow the changes and will be disturbed and damaged. Although this

feature may be used to fabricate magnetic field sensors, the time factor must be considered since long-term fluctuations of hydrogen bonds and dipoles at strong external magnetic field many cause breaking of molecular links. This may make it difficult to recover the changes to the primary position (N. M. Khatir, S. M. Banihashemian, V. Periasamy et al., 2012).

Table 6.5: Potential barrier via magnetic field in Au-DNA-Au (V_b) and Richardson constant (A^*) via magnetic field in Au-DNA-Au structure.

B (mT)	A^* ($ACm^{-2}K^{-2}$)	V_b (eV)
0.00	134.925	0.883
200.00	129.454	0.880
400.00	135.014	0.882
600.00	187.596	0.890
800.00	204.640	0.886
1000.00	254.186	1.156
1200.00	298.586	1.175

$$I(V,T) = I_s(B,T)\left[exp\left(\frac{q\left(\frac{V-RI}{n}\right)}{K_B T}\right) - 1\right] \quad \text{Eq. 6.11}$$

$$0<B<1000\ mT \Rightarrow I(B) = -1 \times 10^{-2} B + 3 \times 10^{-5} \quad \text{Eq. 6.12}$$

$$B>>1000\ mT \Rightarrow I(B) = 0.7303\ e^{-0.012B} \quad \text{Eq. 6.13}$$

$$0<B<1000\ mT \Rightarrow V(B) = 1 \times 10^{-5} B + 0.8778 \quad \text{Eq. 6.14}$$

$$B>>1000\ mT \Rightarrow V(B) = 2 \times 10^{-3} B + 0.88 \quad \text{Eq. 6.15}$$

$$0<B<1000\ mT \Rightarrow A^*(B) = 0.158B + 93.728 \quad \text{Eq. 6.16}$$

$$B>>1000\ mT \Rightarrow A^*(B) = 0.158B + 93.728 \quad \text{Eq. 6.17}$$

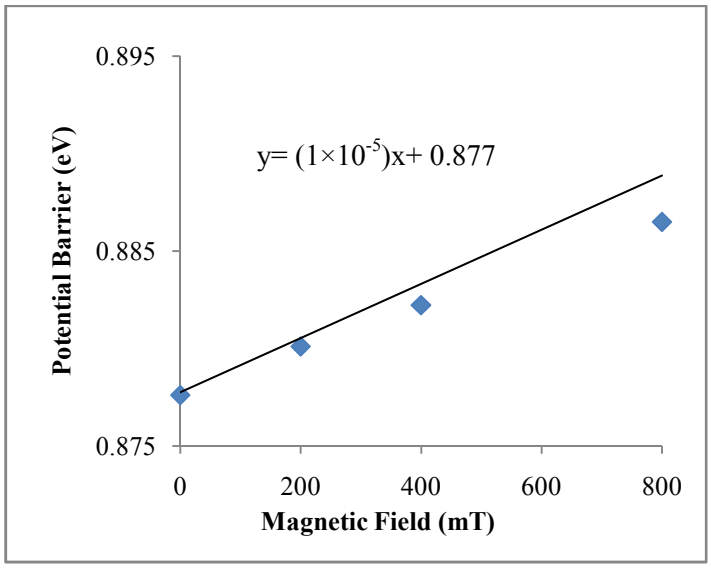

Figure 6.21: Potential barrier versus magnetic field (≤ 800 mT) for MDM structure.

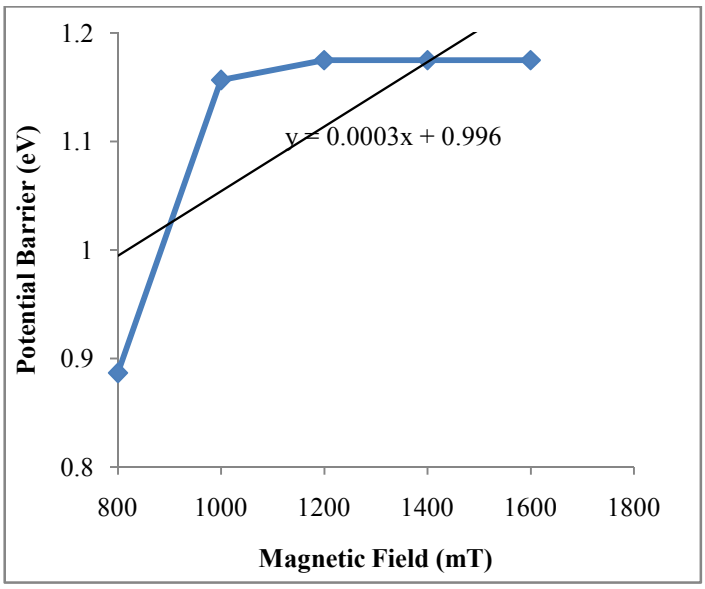

Figure 6.22: Potential barrier versus magnetic field (≥ 800 mT) for MDM structure.

6.6 Evaluation of MDM structure in the Presence of Magnetic Field

In order to thoroughly investigate closely of variations of current in the presence of magnetic field, differences between values of current in presence and absence of magnetic field *(I(B=0)-I(B=b))* versus voltage is illustrated in Figure 6.23. As seen, a gradual decline in current occurs with increase of field strength. It is known from this figure that in the absence of magnetic field, the current exceeds that of in its presence, which results in a positive differential current in forward bias and negative in reverse.

$$I(B=0) > I(B) \Longrightarrow I(B=0)-I(B)>0 \ \text{for } v>0 \quad \text{and } I(B=0)-I(B)<0 \ \text{for } v<0 \qquad \text{Eq. 6.18}$$

Therefore, the difference between the current in the presence and absence of a magnetic field for higher magnetic fields increases. Magnetic resistance also rises linearly with the field strength.

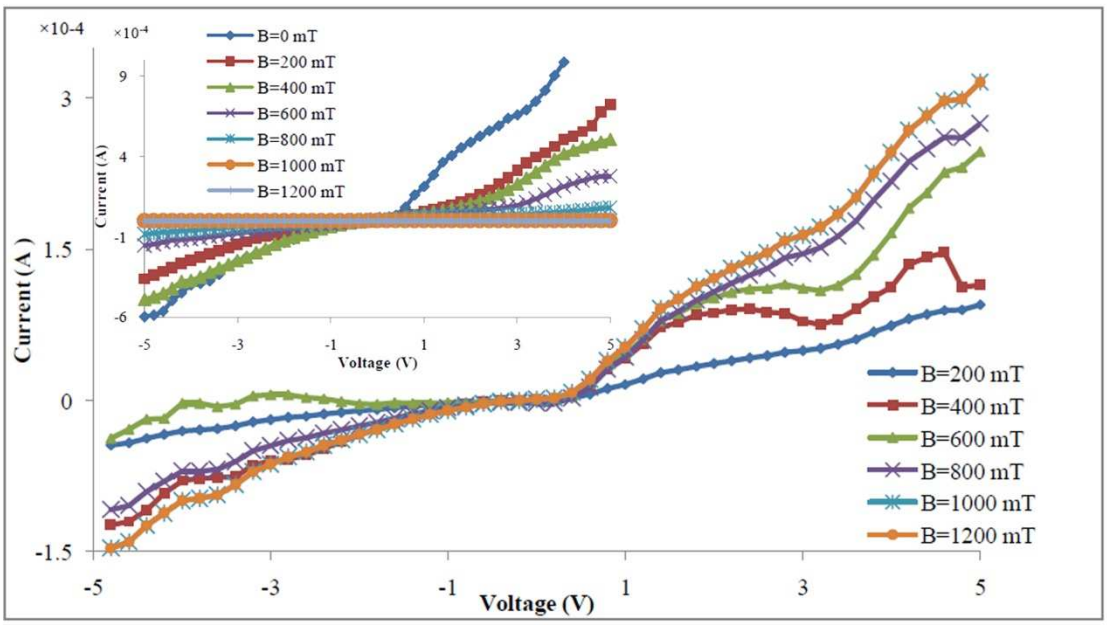

Figure 6.23: *I(B=0)-I(B)* via voltage in the presence and absence of various magnetic fields for Au-DNA-Au structure.The inset figure shows the total curve including zero magnetic fields but the main figure indicates the current without the zero magnetic fields current.

S is a parameter to investigate increase or decrease of the current rate due to external factors which is defined using the following equation;

$$S = \frac{I(B=0) - I(B)}{I(B=0)} \qquad \text{Eq. 6.19}$$

In this relation, *I(B)* is the current rate in the presence of magnetic field and *I(B=0)* is in the absence of magnetic field. According to Eq. 6.19, relative changes in the current makes a good option in fabrication of magnetic field sensors. Figure 6.24 shows the sensitivity rate in the case of direct bias in magnetic fields of less than 1200 mT. Since reverse bias changes are minor, it was ignored in the calculations.

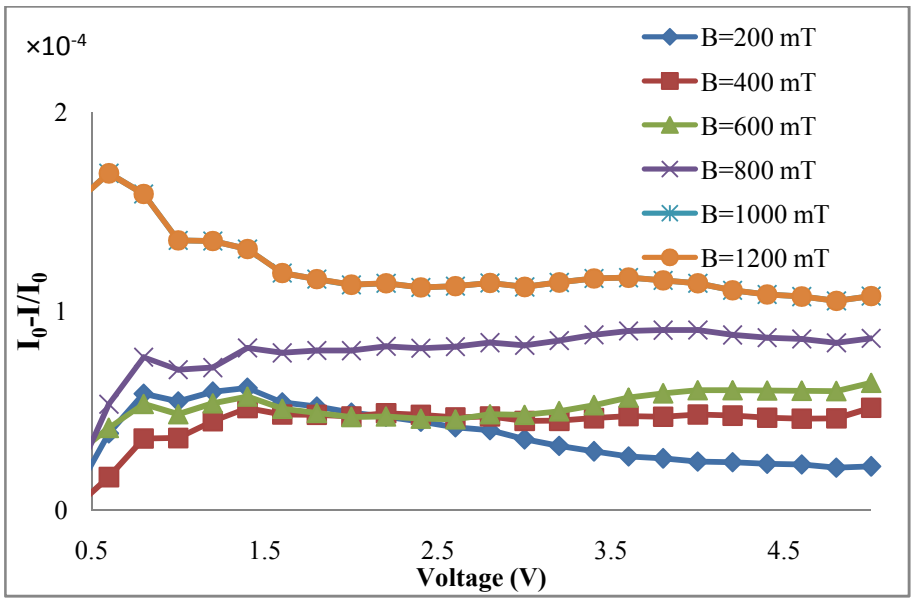

Figure 6.24: *S* parameters at different magnetic fields.

The results of Figure 6.24 can be divided into several categories. First, the effect of low-voltage field was explained. As it can be seen from the figure, sensitivity rate at low voltages was higher than at high voltages since at low voltage, the current rate is lower. Although the effect of the magnetic field is small, the difference is significant. Current was reduced at high voltages, but not eliminated due to different mechanisms for detecting magnetic field.

The second category involves result obtained from the graph, which is the sensitivity-voltage curve located in the positive sector of the *I-V* curve. This means that current change due to magnetic field is positive according to the numerator in Eq. 6.19. This fact illustrates that the current without any magnetic field is positive. This shows that current at the presence of a magnetic field is always positive. Magnetic field reduces current and increases resistance. This is also mentioned in the previous section as a result of increased resistance due to increased collision and Lorentz force.

The third issue is how current changes according to voltage in the presence of magnetic field. It is observed from Figure 6.24 that the changes are fast in the beginning but become slower and linear towards the end.

$$Ratio = \frac{I(B = 0)}{I(B)} \qquad \text{Eq. 6.20}$$

Fourth, in this chart the changes in magnetic fields higher than 800 mT were considered. The current in such fields is so insignificant that it is almost negligible. So, in this part changes cannot be seen in the large fields, while these changes are available. It should be investigated in a separate curve that shows relative effects of current at the absence and presence of magnetic field. It is defined as in Eq. 6.20.

Figure 6.25 show graphs of relative *I-V* curves at room temperature in magnetic fields from 200 to 1200 mT. The vertical axis is plotted logarithmically, while the axis represents the relative current rate smaller than 1. As a result, in an external magnetic field, the current is reduced. The current reduction in magnetic fields less than 800 mT was close to 1 and in fields greater than 800 mT was in the order of 10^{-5}. Since this change in voltage higher than 1 and less than -1 is almost constant, the current does not change much with increasing voltage. It can be concluded that the change in high voltage was because of increase in magnetic resistance and carrier scattering and collisions in magnetic field.

According to cyclotron motion of carriers in magnetic field, before carriers reach the electrodes from left to right, they undergo collisions. As such, the speed will decrease towards the electric field and mobility reduced. At lower voltage of 1 V, the rate of change of current was not linear but approximately exponential. This was as a result of

distribution effects at the interface of Au-DNA. There are two factors that reduce the carrier rate in the potential barrier. First is the charges created around the potential barrier at the interface between the metal-semiconductor. Since these charges are very close together, they contribute greatly to the scattering of the charge carriers. The second factor is related to the free carriers that pass through the potential barrier. These two factors will reduce the current of carriers and causes penetration to increase exponentially.

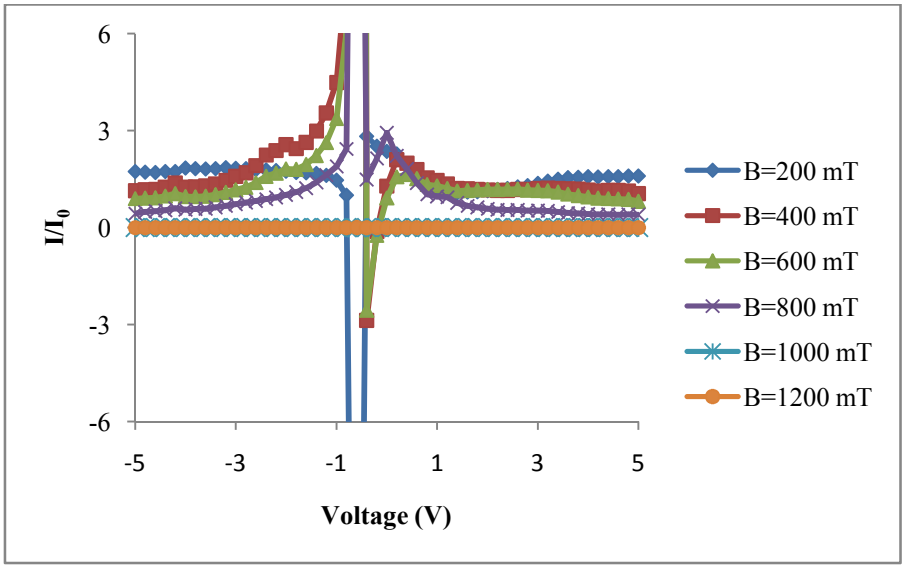

Figure 6.25: I/I_0 curve of voltage at different magnetic fields.

6.7 Effect of Magnetic Field on the Breakdown Voltage of Au-DNA-Au

When a reverse bias voltage is connected to a metal-semiconductor, the electric field is increased. This field can be so high as to break covalent bonds and create pairs of electrons-holes. The motion of electrons and holes are created in a reverse bias current. In *I-V* curve for ideal diode at reverse bias region, the current does not change before breakdown voltage and is equal to saturated current. The phenomenon that causes deviations from this ideal diode conduction is due to current generated because of recombination carrier.

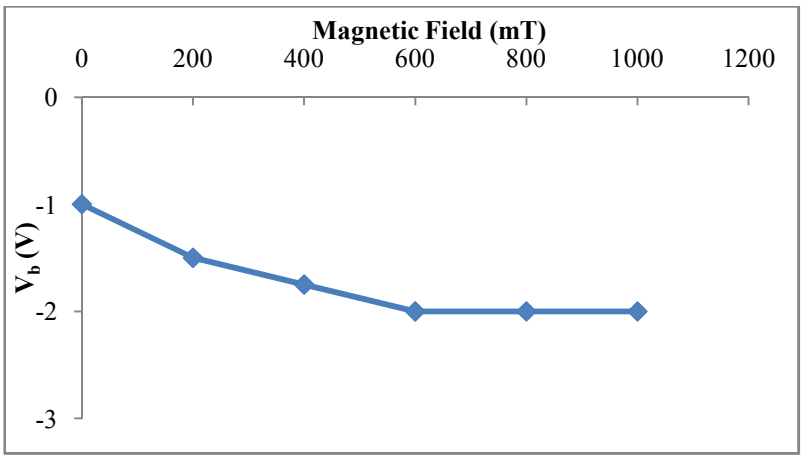

Figure 6.26: Changes in the breakdown voltage under application of different magnetic fields.

Figure 6.26 shows the magnetic field changes in the breakdown voltage region. Here, breakdown voltage increases with increasing magnetic field. Electron and hole pairs are generated with applying voltage. In the presence of magnetic field before electron and hole pairs reach from left to right electrodes, they are trapped by the magnetic field. These factors cause cyclotron motion and increase collision, which in turn increases the resistance. In this case, the breakdown voltage decreases. Repeated collisions cause resistance to increase and thus contribute to a smaller increment of current.

Chapter VII: Conclusions

7.0 Introduction

The aims of these studies were based on electrical characterization of Au-DNA-Au and Al-DNA-Al structures in the presence and absence of external magnetic fields. When the DNA strands were applied direct transfer in buffer solutions onto thin films of Al on Si substrate, chemical interactions between the strands and Al creates nanometer scale arbitrary patterning. This interesting observation does not allow using Al as a MDM structure because of unstable contact. However, a new patterning method using the DNA strands were found capable of producing NGs of less than 100 nm. Therefore, the present work was investigated in two parts; the fabrication of metal-DNA-metal device and the effect of magnetic field to the electrical characteristics of the device. As a result of this research, it was found that NGs could be created when DNA was deposited on Al metal surface. The device was also found to be very sensitive to the effect of magnetic field above certain magnetic field strength. Therefore it can be suggested that there is a possibility of using this device as a magnetic sensor.

7.1 Summary of Findings

7.1.1 DNA as a Material to Create Nano Pattern

DNA strands can be used for creating nano scale patterning on Al thin film. The DNA strands were applied in buffer solutions onto thin films of Al over Si substrate. Chemical interactions between the DNA strands and Al create nanometer scale arbitrary patterns. The average size for this pattern was measured using SEM technique to be less than 100 nm. This simple and cost-effective method can be utilized in the fabrication of various components in electronic chips for microelectronics and nano electro-mechanical system (NEMS) applications in general.

7.1.2 DNA as Magnetic Field Sensor in MDM Structure

Gold thin film evaporated with thermal evaporation technique used a MDM structure (Au-DNA- Au). In the presence and absence of external magnetic fields with strengths less than 1200 mT, the electric behavior of DNA strands was investigated through its *I-V* curve. Acquisition of the *I-V* graph demonstrated that DNA as a semiconductor exhibits diode behavior in the MDM structure. The results are as below;

The current versus magnetic field strength followed a decreasing trend because of a diminished mobility in the presence of a low magnetic field. This made clear that an externally imposed magnetic field would boost resistance of the MDM structure. The DNA-Au interface potential barrier did not show significant variation in the magnetic field below 800 mT. However, an increase was observed above 800 mT. In summary, it could be concluded that with increasing magnetic field, the current rate through the sample decreases and the potential barrier and the resistance increases.

Observation show that an externally imposed magnetic field increases resistance and decreases current in all range of magnetic fields applied. As such, sample in high magnetic fields show significant changes in electrical behavior. Diode behavior was removed and the ohmic behavior and the resistance increase. These changes may be caused by Lorentz force when rotational magnetic field and external electric field are increased. It can also relate to changes in the DNA structure by external radiation field, as it opens up the vibrations of double bonds and hydrogen bonds between base pairs.

Richardson constant varies in the presence of magnetic field, increasing linearly with increasing strength of magnetic fields. It has direct relationship with the carrier effective mass while passing through the electric field. Carrier effective mass increases and

therefore results in the reduction of mobility. This only allows the charge carriers to penetrate through the potential barrier at a lower rate. Increase of temperature will lead to exponential increase in conductance and are common in semiconductor materials. At 50°C, conductance changes dramatically due to breaking of the hydrogen bonds, altering the double structured DNA to single structured strands.

The amount of breakdown bias was decreased with the increase of magnetic field strength. When a reverse bias voltage was connected to a metal-semiconductor junction, the electric field was increased. This field can be high enough to break covalent bonds and create pairs of electrons-holes. The motion of electrons and holes are created in a reverse bias current. In *I-V* curve for ideal diode at reverse bias region, the current does not change before breakdown voltage and is equal to saturated current. The phenomenon that causes deviations from this ideal diode conduction is due to current generated because of recombination carriers.

7.2 Future Works

The utilization of DNA in electronic device such as micro and nano sensors in recent years has increased. High throughput micro array sensors in biotechnology applications and medical diagnosis, MEMS and NEMS opens up new windows for utilization of DNA based sensors. Microarray and nano array of DNA strands are cutting edge research for the present and future. Humidity sensors, temperature sensors, magnetic field sensors and medical pre-test chips are important research pertaining to DNA based sensors. These new potentials and applications will result in interesting studies in the field of physics and electronics. The figure below summarizes the potential applications of M-DNA-M device that will be in the mainstream research in future.

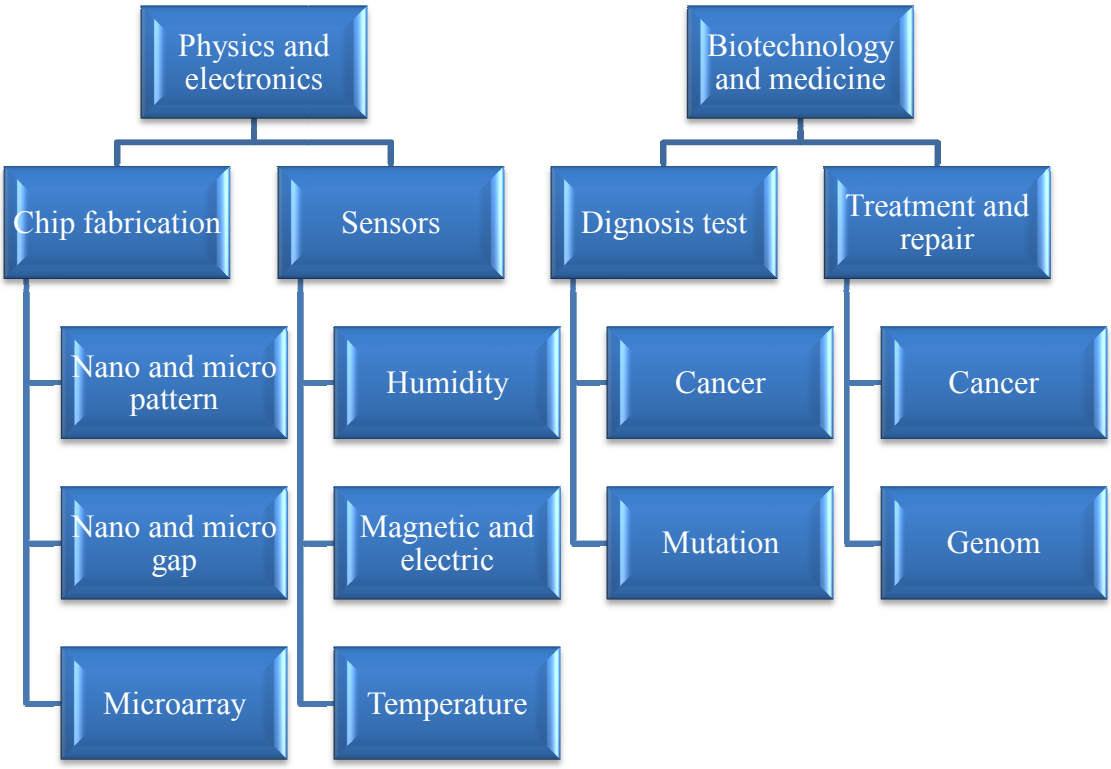

Figure 7.1: Summary of the potential applications of M-DNA-M device that can be explored in the future.

Appendix A

Category	$\rho(\Omega cm)$	DNA sequence	Buffer	References
Insulator	$10^{13}\Omega$	λ-DNA	Na^{+}	(E. Braun, Eichen, Sivan et al., 1998)
		30 bp Poly(dG). poly(dC)	Na citrate+ EDTA (Na^{+})	(Porath, Bezryadin, De Vries et al., 2000b)
	$>10^{6}$	λ-DNA	—	(De Pablo, Moreno-Herrero, Colchero et al., 2000)
	$10^{13}\Omega$	Poly(dG). poly(dC)	HEPES (Mg^{2+})	(Storm, Van Noort, De Vries et al., 2001)
	$>10^{6}$	Thiol-modified λ-DNA	No buffer Mg^{2+}	(Zhang, Austin, Kraeft et al., 2002)
		Thiolated 12 bp Poly(GC). poly(CG)	TE buffer (K^{+})	(M. Xu, Tsukamoto, Ishida et al., 2005)
	($>10^{11}\Omega$)	1.7-2.9μm Poly(dG). poly(dC)	No buffer (Na+)	(Lee, Tanaka, Otsuka et al., 2002)
	($>10^{13}\Omega$)	1.7-2.9μm Poly(dG). poly(dC) 0.5-1.5μm Poly(dA). poly(dT)	No buffer (Na+)	(Taniguchi, 2006)
Semiconductor (ion conduction)	10^{5}	2000 bp Salmon testes	TTA[e]	(Okahata, Kobayashi, Tanaka et al., 1998)
(contamination)	($\sim 10^{6}\Omega$)	λ-DNA	Tris–HCl + EDTA	(Fink, Schönenberger, 1999)
(insulator)	1.2×10^{3} 1.9×10^{2}	λ-DNA	Tris–HCl + EDTA + NaCl	(Tran, Alavi, Gruner, 2000)
(ion conduction)	1	Poly(dG). poly(dC)	Tris–HCl	(Cai, Tabata, Kawai, 2000)
	10^{3}	Thiol-modified λ-DNA	—	(Hartzell, McCord, Asare et al., 2003)
	($1.3\times10^{6}\Omega$) ($10^{8}\Omega$)	Poly(dG). poly(dC) p-type Poly(dA).	Tris–HCl	(Yoo, Ha, Lee et al., 2001)

		poly(dT) n-type		
		λ-DNA	Tris–HCl (Na+)	(Rakitin, Aich, Papadopoulos et al., 2001)
Conductor	Super-conductor (<1K)	λ-DNA	Mg^{2+}	(Kasumov, Kociak, Gueron et al., 2001)

Appendix B

I-V characteristics

The current density contributed is

$$J_z = -ev_z \frac{dN}{L^3}$$

We assume that $-\begin{cases} k_z > 0 \\ E_z > eV_{bi} \end{cases}$. Note that all values of E_x and E_y are permitted as they represent motion in the x − y plane which is not constrained by the barrier in the +z direction. Note that (Mishra, Singh, 2008)

$$(E_x - E_C) = \frac{\hbar^2 k_x^2}{2m^*}$$

With related relationships for $(E_y - E_C)$ and $(E_z - E_C)$ and applying the condition $(E_z - E_C) > eV_{bi}$ gives a minimum value of

$$k_{min} = \sqrt{eV_{bi}\left(\frac{2m^*}{\hbar^2}\right)}$$

Also

$$v_z = \frac{\hbar k_z}{m^*}$$

Therefore

$$J_z = \frac{-e}{(2\pi)^3}\int_{-\infty}^{+\infty} dk_x \int_{-\infty}^{+\infty} dk_y \int_{k_{min}}^{+\infty} \frac{dk_x}{m^*} dk_z.$$

$$2\exp\left[-(E_x + E_y + E_z)/k_B T\right].\exp[-(E_C - E_F)/k_B T]\exp\left(\frac{E_C}{k_B T}\right) =$$

$$-\frac{2e}{(2\pi)^3}\int_x.\int_y.\int_z \exp\left(-\frac{E_C - E_F}{k_B T}\right)$$

Where

$$\int_x \int_y = \int_{-\infty}^{\infty} \exp\left(\frac{\hbar^2 k_x^2}{2m^* k_B T}\right) dk_x = \frac{\sqrt{2\pi m^* k_B T}}{\hbar}$$

And

$$\int_z = \int_{k_{min}}^{+\infty} \exp\left(-\frac{\hbar^2 k_z^2}{k_B T}\right).\frac{\hbar\, k_z}{m^*}.dk_z$$

$$= \frac{k_B T}{\hbar}\exp\left(-\hbar^2 k_{min}^2 \Big/ k_B T\right) = \frac{k_B T}{\hbar}\exp\left(\frac{-eV_{bi}}{k_B T}\right)$$

Therefore

$$J_z = \frac{4\pi}{(2\pi\hbar)^3}.em^* k_B^2 T^2 \exp\left(-\frac{(eV_{bi}(E_C - E_F))}{k_B T}\right)$$

Or

$$J_z = A^*.T^2 \exp\left(\frac{-e\emptyset_B}{k_B T}\right) = j_{s\to m}(V = 0)$$

Where

$$A^* = \frac{4\pi e m^* k_B^2}{2\pi\hbar^3} = 120 A\, cm^{-2} K^{-2} \times \frac{m^*}{m_0}$$

A^* is the Richardson constant and $\emptyset_B = eV_{bi}(E_C - E_F)$, the barrier seen by electrons in the metal of the Schottky barrier height at $V = 0$. We have calculated $J_{s\to m}$. The study can be simply extended to a forward bias of V_F , the only change being replacing the barrier, V_{bi} by the new barrier $V_{bi} - V_F$. These changes I_z to

$$I_z = \frac{k_B T}{\hbar}\exp\left(-\frac{eV_{bi}}{k_B T}\right).\exp\left(\frac{eV_F}{k_B T}\right)$$

Or

$$j_{s\to m}(V = V_F) = j_{s\to m}(V = 0).\exp\left(\frac{eV_F}{k_B T}\right)$$

Since the current flow from the metal to the semiconductor is unchanged:

$$J(V = V_F) = j_{s\to m}(V = V_F) - j_{m\to s}(V = V_F)$$
$$= A^{*}T^{2}\exp\left(\frac{-q\emptyset_B}{k_B T}\right)\left[\exp\left(\frac{eV_F}{k_B T}\right) - 1\right]$$

References

Ago, H., Kugler, T., Cacialli, F., Salaneck, W.R., Shaffer, M.S.P., Windle, A.H. and Friend, R.H. (1999). Work functions and surface functional groups of multiwall carbon nanotubes. *The Journal of Physical Chemistry B, 103*(38), 8116-8121.

Ahmad, K. (1972). Contact potentials and barrier heights in gold-silicon and aluminum-silicon contacts. *Journal of Applied Physics, 43*(11), 4706-4713.

Ahmadi, F, Alizadeh, AA, Shahabadi, N and Rahimi-Nasrabadi, M. (2011). Study binding of Al–curcumin complex to ds-DNA, monitoring by multispectroscopic and voltammetric techniques. *Spectrochimica Acta Part A: Molecular and Biomolecular Spectroscopy, 79*(5), 1466-1474.

Alivisatos, A.P., Johnsson, K.P., Peng, X., Wilson, T.E., Loweth, C.J., Bruchez, M.P. and Schultz, P.G. (1996). Organization of'nanocrystal molecules' using DNA. *Nature, 382*, 609-611.

Anastassopoulou, J. (2003). Metal-DNA interactions. *Journal of Molecular Structure, 651*, 19-26.

Anguelouch, A., Reich, DH, Chien, CL and Tondra, M. (2004). Detection of ferromagnetic nanowires using GMR sensors. *Magnetics, IEEE Transactions on, 40*(4), 2997-2999.

Aziz, M., Golovchenko, J., Branton, D., McMullan, C., Stein, D. and Li, J. (2001). Ion-beam sculpting at nanometre length scales. *Nature, 412*(6843), 166-169.

Bain, C.D., Troughton, E.B., Tao, Y.T., Evall, J., Whitesides, G.M. and Nuzzo, R.G. (1989). Formation of monolayer films by the spontaneous assembly of organic thiols from solution onto gold. *Journal of the American Chemical Society, 111*(1), 321-335.

Banks, D. (2006). *Microengineering, MEMS, and interfacing: a practical guide* (Vol. 199): CRC.

Bardeen, J. (1947). Surface states and rectification at a metal semi-conductor contact. *Physical Review, 71*(10), 717-727.

Berlin, Y.A., Burin, A.L. and Ratner, M.A. (2001). Charge hopping in DNA. *Journal of the American Chemical Society, 123*(2), 260–268.

Berlin, Y.A., Burin, A.L. and Ratner, M.A. (2002). Elementary steps for charge transport in DNA: thermal activation vs. tunneling. *Chemical physics, 275*(1-3), 61-74.

Bethe, H.A. and Laboratory, Massachusetts Institute of Technology. Radiation. (1942). *Theory of the boundary layer of crystal rectifiers*: Radiation Laboratory, Massachusetts Institute of Technology.

Bezryadin, A and Dekker, C. (1997). Nanofabrication of electrodes with sub-5 nm spacing for transport experiments on single molecules and metal clusters. *Journal of Vacuum Science & Technology B: Microelectronics and Nanometer Structures, 15*, 793-799.

Bezryadin, A, Dekker, C and Schmid, G. (1997). Electrostatic trapping of single conducting nanoparticles between nanoelectrodes. *Applied Physics Letters, 71*(9), 1273-1275.

BioMath. (2011). http://www.promega.com/techserv/tools/biomath/calc11.htm.

Black, A. J., Nealey, P. F., Thywissen, J. H., Deshpande, M., El-Zein, N., Maracas, G. N., Prentiss, M. and Whitesides, G. M. (2000). Microfabrication of two layer structures of electrically isolated wires using self-assembly to guide the deposition of insulating organic polymer. *Sensors and Actuators A: Physical, 86*(1-2), 96-102.

Blank, M. and Goodman, R. (1997). Do electromagnetic fields interact directly with DNA? *Bioelectromagnetics, 18*(2), 111-115.

Blank, M., Soo, L., Lin, H., Henderson, AS and Goodman, R. (1992). Changes in transcription in HL-60 cells following exposure to alternating currents from electric fields. *Bioelectrochemistry and Bioenergetics, 28*(1-2), 301-309.

Boon, E.M. and Barton, J.K. (2002). Charge transport in DNA. *Current Opinion in Structural Biology, 12*(3), 320-329.

Boon, E.M., Barton, J.K., Pradeepkumar, P.I., Isaksson, J., Petit, C. and Chattopadhyaya, J. (2002). An Electrochemical Probe of DNA Stacking in an Antisense Oligonucleotide Containing a C3 endo Locked Sugar. *Angewandte Chemie, 114*(18), 3552-3555.

Borneman, EH, Schwarz, RF and Stickler, JJ. (1955). Rectification Properties of Metal Semiconductor Contacts. *Journal of Applied Physics, 26*(8), 1021-1028.

Böttger, H. and Bryksin, V.V. (1985). Hopping conduction in solids. *VCH, Deerfield Beach, Florida*.

Braun, E., Eichen, Y., Sivan, U. and Ben-Yoseph, G. (1998). DNA-templated assembly and electrode attachment of a conducting silver wire. *Nature, 391*(6669), 775-778.

Braun, E. and Keren, K. (2004). From DNA to transistors. *Advances in Physics, 53*(4), 441-496.

Braun, F. (1874). On the Current Transport in Metal Sulfides (in German). *Annal. Phys. Chem, 153*, 556–563.

Brauns, E.B., Madaras, M.L., Coleman, R.S., Murphy, C.J. and Berg, M.A. (1999). Measurement of local DNA reorganization on the picosecond and nanosecond time scales. *Journal of the American Chemical Society, 121*(50), 11644-11649.

Breslin, D.T., Coury, J.E., Anderson, J.R., McFail-Isom, L., Kan, Y., Williams, L.D., Bottomley, L.A. and Schuster, G.B. (1997). Anthraquinone photonuclease structure determines its mode of binding to DNA and the cleavage chemistry observed. *Journal of the American Chemical Society, 119*(21), 5043-5044.

Brun, A.M. and Harriman, A. (1992). Dynamics of electron transfer between intercalated polycyclic molecules: effect of interspersed bases. *Journal of the American Chemical Society, 114*(10), 3656-3660.

Brun, A.M. and Harriman, A. (1994). Energy-and electron-transfer processes involving palladium porphyrins bound to DNA. *Journal of the American Chemical Society, 116*(23), 10383-10393.

Brust, M., Bethell, D., Kiely, C.J. and Schiffrin, D.J. (1998). Self-assembled gold nanoparticle thin films with nonmetallic optical and electronic properties. *Langmuir, 14*(19), 5425-5429.

Bustamante, C., Smith, S.B., Liphardt, J. and Smith, D. (2000). Single-molecule studies of DNA mechanics. *Current Opinion in Structural Biology, 10*(3), 279-285.

Cai, L., Tabata, H. and Kawai, T. (2000). Self-assembled DNA networks and their electrical conductivity. *Applied Physics Letters, 77*, 3105-3106.

Chen, J. and Seeman, N.C. (1991). Synthesis from DNA of a molecule with the connectivity of a cube. *Nature, 350*(6319), 631-633.

Chen, W., Turro, C., Friedman, L.A., Barton, J.K. and Turro, N.J. (1997). Resonance raman investigation of Ru (phen) 2 (dppz) 2+ and related complexes in water and in the presence of DNA. *The Journal of Physical Chemistry B, 101*(35), 6995-7000.

Chhabra, Rahul. (2009). *Structural and functional perspectives of DNA directed self-assembly.* (PhD), Arizona State University, ProQuest.

Choo, Y.H. and Devereux, O.F. (1975). Barrier-Type Aluminum Oxide Films Formed under Prolonged Anodizing. *Journal of The Electrochemical Society, 122*, 1645-1653.

Chow, K.C. and Tung, W.L. (2000). Magnetic field exposure enhances DNA repair through the induction of DnaK/J synthesis. *FEBS letters, 478*(1-2), 133-136.

Chu, SZ, Wada, K., Inoue, S., Isogai, M., Katsuta, Y. and Yasumori, A. (2006). Large-scale fabrication of ordered nanoporous alumina films with arbitrary pore intervals by critical-potential anodization. *Journal of the Electrochemical Society, 153*, B384.

Cingolani, Roberto, Rinaldi, Ross, Maruccio, Giuseppe and Biasco, Adriana. (2002). Nanotechnology approaches to self-organized bio-molecular devices. *Physica E: Low-dimensional Systems and Nanostructures, 13*(2–4), 1229-1235.

Cohen, H., Nogues, C., Ullien, D., Daube, S., Naaman, R. and Porath, D. (2006). Electrical characterization of self-assembled single- and double-stranded DNA monolayers using conductive AFM. *Faraday Discussions, 131*, 367-376.

Cowley, AM and Sze, SM. (1965). Surface States and Barrier Height of Metal-Semiconductor Systems. *Journal of Applied Physics, 36*(10), 3212-3220.

Crespo-Hernández, C.E., Arce, R., Ishikawa, Y., Gorb, L., Leszczynski, J. and Close, D.M. (2004). Ab initio ionization energy thresholds of DNA and RNA bases in gas phase and in aqueous solution. *The Journal of Physical Chemistry A, 108*(30), 6373-6377.

Crothers, D.M. (1964). The kinetics of DNA denaturation. *Journal of Molecular Biology, 9*(3), 712-733.

Crowell, CR and Sze, SM. (1966). Current transport in metal-semiconductor barriers. *Solid-State Electronics, 9*(11-12), 1035-1048.

Dahm, R. (2005). Friedrich Miescher and the discovery of DNA. *Developmental Biology, 278*(2), 274-288.

Damghanian, M. and Majlis, BY. (2008). *A modified lift-off technique to prevent pattern following effect in microfabrication.* Paper presented at the International Conference on Semiconductor Electronics (ICSE) 2008, Johor Bahru, Malaysia

Daniel, B. and Barton, J.K. (1997). Sensitivity of DNA-mediated electron transfer to the intervening -stack: a probe for the integrity of the DNA base stack. *Journal of the American Chemical Society, 119*(21), 5045-5046.

De Pablo, PJ, Moreno-Herrero, F., Colchero, J., Gómez Herrero, J., Herrero, P., Baro, AM, Ordejón, P., Soler, J.M. and Artacho, E. (2000). Absence of dc-Conductivity in -DNA. *Physical Review Letters, 85*(23), 4992-4995.

De Yu, Z. and Grote, J.G. (2007). *Photoelectrical effect and current-voltage characteristics in DNA-metal Schottky barriers.* Paper presented at the Organic Photonic Materials and Devices IX, San Jose, California.

Dewarrat, F. (2002). *Electric characterization of DNA.* (PhD Thesis), University of Basel.

Di Ventra M., Zwolak, M. (2004). DNA electronics. *DNA, 36*, 67-100.

Djalali, R., Chen, Y. and Matsui, H. (2003). Au nanocrystal growth on nanotubes controlled by conformations and charges of sequenced peptide templates. *Journal of the American Chemical Society, 125*(19), 5873-5879.

Dubois, L.H. and Nuzzo, R.G. (1992). Synthesis, structure, and properties of model organic surfaces. *Annual Review of Physical Chemistry, 43*(1), 437-463.

Dunlap, D.D., García, R., Schabtach, E. and Bustamante, C. (1993). Masking generates contiguous segments of metal-coated and bare DNA for scanning tunneling

microscope imaging. *Proceedings of the National Academy of Sciences of the United States of America, 90*(16), 7652-7655.

Ejsing, L., Hansen, M.F., Menon, A.K., Ferreira, HA, Graham, DL and Freitas, PP. (2004). Planar Hall effect sensor for magnetic micro-and nanobead detection. *Applied Physics Letters, 84*, 4729-4731.

Eley, DD and Spivey, DI. (1962). Semiconductivity of organic substances. Part 9. Nucleic acid in the dry state. *Transactions of Faraday Society, 58*, 411-415.

Elliott, R. J. (1961). Symmetry of Excitons in Cu2O. *Physical Review, 124*, 340-345.

Endres, RG, Cox, DL and Singh, RRP. (2004). Colloquium: The quest for high-conductance DNA. *Reviews of Modern Physics, 76*(1), 195-214.

Erdem, A. and Ozsoz, M. (2002). Electrochemical DNA Biosensors Based on DNA Drug Interactions. *Electroanalysis, 14*(14), 965-974.

Estrela, P., Migliorato, P., Takiguchi, H., Fukushima, H. and Nebashi, S. (2005). Electrical detection of biomolecular interactions with metal–insulator–semiconductor diodes. *Biosensors and Bioelectronics, 20*(8), 1580-1586.

Estrela, P., Stewart, A. G., Yan, F. and Migliorato, P. (2005). Field effect detection of biomolecular interactions. *Electrochimica Acta, 50*(25–26), 4995-5000.

Fahlman, R.P. and Sen, D. (2002). DNA conformational switches as sensitive electronic sensors of analytes. *Journal of the American Chemical Society, 124*(17), 4610-4616.

Felice, R. and Porath, D. (2008). DNA-based Nanoelectronics *NanoBioTechnology* (pp. 141-185).

Felice, Rosa Di. (2009). *DNA-Based Nanoelectronics*: Springer.

Fendler, J.H. (1996). Self-assembled nanostructured materials. *Chemistry of Materials, 8*(8), 1616-1624.

Ferreira, H.A., Graham, D.L., Feliciano, N., Clarke, L.A., Amaral, M.D. and Freitas, P.P. (2005). Detection of cystic fibrosis related DNA targets using AC field focusing of magnetic labels and spin-valve sensors. *IEEE Transactions on Magnetics, 41*(10), 4140-4142.

Ferreira, HA, Cardoso, FA, Ferreira, R., Cardoso, S. and Freitas, PP. (2006). Magnetoresistive DNA chips based on ac field focusing of magnetic labels. *Journal of Applied Physics, 99*, 105-107.

Ferreira, HA, Feliciano, N., Graham, DL, Clarke, LA, Amaral, MD and Freitas, PP. (2005). Rapid DNA hybridization based on ac field focusing of magnetically labeled target DNA. *Applied Physics Letters, 87*(1), 013901-013903.

Fink, H.W. and Schönenberger, C. (1999). Electrical conduction through DNA molecules. *Nature, 398*(6726), 407-410.

Ford, W.E., Harnack, O., Yasuda, A. and Wessels, J.M. (2001). Platinated DNA as precursors to templated chains of metal nanoparticles. *Advanced Materials, 13*(23), 1793-1797.

Freitas, PP, Ferreira, HA, Graham, DL, Clarke, LA, Amaral, MD, Martins, V., Fonseca, L. and Cabral, JS. (2004). *Magnetoresistive DNA chips*: Academic Press, New York.

Fritz, J., Baller, MK, Lang, HP, Rothuizen, H., Vettiger, P. and Meyer, E. (2000). Translating biomolecular recognition into nanomechanics. *Science, 288*(5464), 316-318.

Gasper, S.M. and Schuster, G.B. (1997). Intramolecular photoinduced electron transfer to anthraquinones linked to duplex DNA: The effect of gaps and traps on long-

range radical cation migration. *Journal of the American Chemical Society, 119*(52), 12762-12771.

Giese, B. (2002). Long-distance electron transfer through DNA. *Annual Review of Biochemistry, 71*(1), 51-70.

Gooding, J.J. (2002). Electrochemical DNA hybridization biosensors. *Electroanalysis, 14*(17), 1149-1156.

Grozema, F.C., Siebbeles, L.D.A., Berlin, Y.A. and Ratner, M.A. (2002). Hole mobility in DNA: Effects of static and dynamic structural fluctuations. *ChemPhysChem, 3*(6), 536-539.

Guallar, V., Douhal, A., Moreno, M. and Lluch, J.M. (1999). DNA mutations induced by proton and charge transfer in the low-lying excited singlet electronic states of the DNA base pairs: A theoretical insight. *The Journal of Physical Chemistry A, 103*(31), 6251-6256.

Güllü, Ö, Çankaya, M., Barış, Ö, Biber, M., Özdemir, H., Güllüce, M. and Türüt, A. (2008). DNA-based organic-on-inorganic semiconductor Schottky structures. *Applied Surface Science, 254*(16), 5175-5180.

Güllü, Ö and Türüt, A. (2011). Electronic properties of Al/DNA/p-Si MIS diode: Application as temperature sensor. *Journal of Alloys and Compounds, 509*(3), 571-577.

Güllü, Ömer. (2010). Ultrahigh (100%) barrier modification of n-InP Schottky diode by DNA biopolymer nanofilms. *Microelectronic Engineering, 87*(4), 648-651.

Harnack, O., Ford, W.E., Yasuda, A. and Wessels, J.M. (2002). Tris (hydroxymethyl) phosphine-capped gold particles templated by DNA as nanowire precursors. *Nano Letters, 2*(9), 919-923.

Harriman, A. (1999). Electron tunneling in DNA. *Angewandte Chemie International Edition, 38*(7), 945-949.

Hartzell, B., McCord, B., Asare, D., Chen, H., Heremans, JJ and Soghomonian, V. (2003). Comparative current–voltage characteristics of nicked and repaired - DNA. *Applied Physics Letters, 82*, 4800-4802.

Heller, A. (2000). Spiers memorial lecture. On the hypothesis of cathodic protection of genes. *Faraday Discussion, 116*, 1-13.

Henbest, K.B., Maeda, K., Hore, PJ, Joshi, M., Bacher, A., Bittl, R., Weber, S., Timmel, C.R. and Schleicher, E. (2008). Magnetic-field effect on the photoactivation reaction of Escherichia coli DNA photolyase. *Proceedings of the National Academy of Sciences, 105*(38), 14395-14399.

Henderson, P.T., Jones, D., Hampikian, G., Kan, Y. and Schuster, G.B. (1999). Long-distance charge transport in duplex DNA: the phonon-assisted polaron-like hopping mechanism. *Proceedings of the National Academy of Sciences, 96*(15), 8353-8358.

Henisch, H.K. (1957). Rectifying Semi-conductor Contacts: Clarendon Press, Oxford.

Henrichs, S., Collier, CP, Saykally, RJ, Shen, YR and Heath, JR. (2000). The dielectric function of silver nanoparticle langmuir monolayers compressed through the metal insulator transition. *Journal of the American Chemical Society, 122*(17), 4077-4083.

Hermon, Z., Caspi, S. and Ben-Jacob, E. (1998). Prediction of charge and dipole solitons in DNA molecules based on the behaviour of phosphate bridges as tunnel elements. *Europhysics Letters, 43*, 482-487.

Herne, T.M. and Tarlov, M.J. (1997). Characterization of DNA probes immobilized on gold surfaces. *Journal of the American Chemical Society, 119*(38), 8916-8920.

Hickman, J.J., Laibinis, P.E., Auerbach, D.I., Zou, C., Gardner, T.J., Whitesides, G.M. and Wrighton, M.S. (1992). Toward orthogonal self-assembly of redox active molecules on platinum and gold: selective reaction of disulfide with gold and isocyanide with platinum. *Langmuir, 8*(2), 357-359.

Hihath, J., Guo, S., Zhang, P. and Tao, N. (2012). Effects of cytosine methylation on DNA charge transport. *Journal of Physics Condensed Matter, 24*(16).

Hodzic, V., Hodzic, V. and Newcomb, R. W. (2007). Modeling of the electrical conductivity of DNA. *IEEE Transactions on Circuits and Systems I: Regular Papers, 54*(11 SPEC. ISS.), 2360-2364.

Jang, Moongyu and Lee, Junghwan. (2002). Analysis of Schottky barrier height in small contacts using a thermionic-field emission model. *ETRI Journal, 24*(6), 455-461.

Ju, H. and Zhao, H. (2005). Electrochemical biosensors for DNA analysis. *Frontiers in Bioscience, 10*(1), 37–46.

Kalofonou, Melpomeni and Toumazou, Chris. (2013). Semiconductor technology for early detection of DNA methylation for cancer: From concept to practice. *Sensors and Actuators B: Chemical, 178*(0), 572-580.

Kamioka, H., Suzuki, M., Tamiya, E. and Karube, I. (1989). DNA cleavage using semiconductor-photocatalysts. *Journal of Molecular Catalysis, 54*(1), 1-8.

Kang, D., Jiang, H., Sun, Z., Qu, Z. and Xie, S. (2011). Magnetic field tuned charge transport in a G4-DNA molecular device. *Journal of Physics Condensed Matter, 23*, 055302-055306.

Kanno, T., Tanaka, H., Miyoshi, N., Fukuda, M. and Kawai, T. (2000). Base sequence dependence of deoxyribonucleic acid studied by scanning tunneling microscopy. *Japanese Journal of Applied Physics, Part 1 Letters, 1*(39), 1892-1893.

Kanno, T., Tanaka, H., Miyoshi, N. and Kawai, T. (2000a). Formation and control of two-dimensional deoxyribonucleic acid network. *Applied Physics Letters, 77*(23), 3848-3850.

Kanno, T., Tanaka, H., Miyoshi, N. and Kawai, T. (2000b). A new self-fabrication of large-scale deoxyribonucleic acid network on mica surfaces. *Japanese Journal of Applied Physics, Part 2 Letters, 39*(4A), 269-270.

Kasianowicz, J.J., Brandin, E., Branton, D. and Deamer, D.W. (1996). Characterization of individual polynucleotide molecules using a membrane channel. *Proceedings of the National Academy of Sciences, 93*(24), 13770-13773

Kasumov, A.Y., Kociak, M., Gueron, S., Reulet, B., Volkov, VT, Klinov, DV and Bouchiat, H. (2001). Proximity-induced superconductivity in DNA. *Science, 291*(5502), 280-282.

Kelley, S.O., Boon, E.M., Barton, J.K., Jackson, N.M. and Hill, M.G. (1999). Single-base mismatch detection based on charge transduction through DNA. *Nucleic Acids Research, 27*(24), 4830-4837.

Keren, Kinneret, Berman, Rotem S, Buchstab, Evgeny, Sivan, Uri and Braun, Erez. (2003). DNA-templated carbon nanotube field-effect transistor. *Science, 302*(5649), 1380-1382.

Khandelwal, G. and Bhyravabhotla, J. (2010). A phenomenological model for predicting melting temperatures of DNA Sequences. *PloS one, 5*(8), e12433.

Kim, JS, Lägel, B., Moons, E., Johansson, N., Baikie, ID, Salaneck, W.R., Friend, RH and Cacialli, F. (2000). Kelvin probe and ultraviolet photoemission measurements of indium tin oxide work function: a comparison. *Synthetic Metals, 111*, 311-314.

Krider, E.S. and Meade, T.J. (1998). Electron transfer in DNA: covalent attachment of spectroscopically unique donor and acceptor complexes. *Journal of Biological Inorganic Chemistry, 3*(2), 222-225.

Kumar, Ashish and Prakash, Rajiv. (2011). Synthesis of nano ground nutshell-like polyindole by supramolecular assembled salts of ss-DNA assisted chloroauric acid. *Chemical Physics Letters, 511*(1–3), 77-81.

Kumar, C.V., Punzalan, E.H.A. and Tan, W.B. (2000). Adenine-thymine base pair recognition by an anthryl probe from the DNA minor groove. *Tetrahedron, 56*(36), 7027-7040.

Lakhno, VD. (2000). Soliton-like solutions and electron transfer in DNA. *Journal of Biological Physics, 26*(2), 133-147.

Lee, H.Y., Tanaka, H., Otsuka, Y., Yoo, K.H., Lee, J.O. and Kawai, T. (2002). Control of electrical conduction in DNA using oxygen hole doping. *Applied Physics Letters, 80*, 1670-1672.

Lehn, J.M. (1990). Perspectives in Supramolecular Chemistry—From Molecular Recognition towards Molecular Information Processing and Self-Organization. *Angewandte Chemie International Edition in English, 29*(11), 1304-1319.

Leondes, C.T. (2006). *MEMS/NEMS: Handbook techniques and applications*: Springer.

Lepselter, MP and Sze, SM. (1968). Silicon Schottky Barrier diode with near-ideal IV characteristics. *Bell System Technical Journal 47*(2), 195-208.

Lewis, F.D. and Letsinger, R.L. (1998). Distance-dependent photoinduced electron transfer in synthetic single-strand and hairpin DNA. *Journal of Biological Inorganic Chemistry, 3*(2), 215-221.

Li, S.H. and Chow, K.C. (2001). Magnetic field exposure induces DNA degradation. *Biochemical and Biophysical Research Communications, 280*(5), 1385-1388.

Li, X. and Bhushan, B. (2003). Fatigue studies of nanoscale structures for MEMS/NEMS applications using nanoindentation techniques. *Surface and Coatings Technology, 163*, 521-526.

Li, X., Bhushan, B., Takashima, K., Baek, C.W. and Kim, Y.K. (2003). Mechanical characterization of micro/nanoscale structures for MEMS/NEMS applications using nanoindentation techniques. *Ultramicroscopy, 97*(1-4), 481-494.

Li, X.Q. and Yan, Y.J. (2001). Electrical transport through individual DNA molecules. *Applied Physics Letters, 79*(14), 2190-2192.

Liang, Z., Freed, J.H., Keyes, R.S. and Bobst, A.M. (2000). An electron spin resonance study of DNA dynamics using the slowly relaxing local structure model. *The Journal of Physical Chemistry B, 104*(22), 5372-5381.

Lincoln, P., Tuite, E. and Nordén, B. (1997). Short-Circuiting the Molecular Wire: Cooperative Binding of -[Ru (phen) 2dppz] 2+ and -[Rh (phi) 2bipy] 3+ to DNA. *Journal of the American Chemical Society, 119*(6), 1454-1455.

Lisdat, F., Ge, B., Krause, B., Ehrlich, A., Bienert, H. and Scheller, FW. (2001). Nucleic Acid–Promoted Electron Transfer to Cytochrome c. *Electroanalysis, 13*(15), 1225-1230.

Liu, F., Sha, R. and Seeman, N.C. (1999). Modifying the surface features of two-dimensional DNA crystals. *Journal of the American Chemical Society, 121*(5), 917-922.

Lo, P.K., Karam, P., Aldaye, F.A., McLaughlin, C.K., Hamblin, G.D., Cosa, G. and Sleiman, H.F. (2010). Loading and selective release of cargo in DNA nanotubes with longitudinal variation. *Nature Chemistry, 2*(4), 319-328.

Loft, S. and Poulsen, HE. (1996). Cancer risk and oxidative DNA damage in man. *Journal of Molecular Medicine, 74*(6), 297-312.

Lukatsky, DB and Frenkel, D. (2005). Surface and bulk dissolution properties, and selectivity of DNA-linked nanoparticle assemblies. *The Journal of Chemical Physics, 122*, 214904-214915.

Madelung, O. (1996). *Semiconductors-basic data*: Springer Berlin.

Madou, MJ and Kellogg, GJ. (1998). The LabCDTM: a centrifuge-based microfluidic platform for diagnostics. *Systems and Technologies for Clinical Diagnostics and Drug Discovery, 3259*, 80-93.

Maksimova, NK, Vyatkin, AP, Pronina, IT and Zharov, AA. (1968). Gold-gallium arsenide surface-barrier junctions. *Russian Physics Journal, 11*(7), 58-59.

Malaquin, L, Vieu, C, Genevieve, M, Tauran, Y, Carcenac, F, Pourciel, ML, Leberre, V and Trévisiol, E. (2004). Nanoelectrode-based devices for electrical biodetection in liquid solution. *Microelectronic Engineering, 73*, 887-892.

Manohar, S. (2010). *DNA-carbon nanotube interactions*. (PhD Thesis), Lehigh University.

Manual book for photoresist. Universiti Kebangsaan Malaysia.

Mao, C., LaBean, T.H., Reif, J.H. and Seeman, N.C. (2000). Logical computation using algorithmic self-assembly of DNA triple-crossover molecules. *Nature, 407*(6803), 493-496.

Mao, C., Sun, W. and Seeman, N.C. (1999). Designed two-dimensional DNA Holliday junction arrays visualized by atomic force microscopy. *Journal of the American Chemical Society, 121*(23), 5437-5443.

Marshall, A. and Hodgson, J. (1998). DNA chips: an array of possibilities. *DNA, 16*(1), 27-28.

Martin, B.R., Dermody, D.J., Reiss, B.D., Fang, M., Lyon, L.A., Natan, M.J. and Mallouk, T.E. (1999). Orthogonal self assembly on colloidal gold platinum nanorods. *Advanced Materials, 11*(12), 1021-1025.

Marziali, A. and Akeson, M. (2001). New DNA sequencing methods. *Annual Review of Biomedical Engineering, 3*(1), 195-223.

Mayer, J.W. (1959). Performance of Germanium and Silicon Surface Barrier Diodes as Alpha-Particle Spectrometers. *Journal of Applied Physics, 30*(12), 1937-1944.

McCarty, M. (1986). *The transforming principle: Discovering that genes are made of DNA*. New York: Norton & Co Inc.

Meijer, EJ, De Leeuw, DM, Setayesh, S., Van Veenendaal, E., Huisman, BH, Blom, PWM, Hummelen, JC, Scherf, U. and Klapwijk, TM. (2003). Solution-processed ambipolar organic field-effect transistors and inverters. *Nature Materials, 2*(10), 678-682.

Meldrum, D.R. and Holl, M.R. (2002). Microscale bioanalytical systems. *Science, 297*(5584), 1197-1198

Meller, A., Nivon, L. and Branton, D. (2001). Voltage-driven DNA translocations through a nanopore. *Physical Review Letters, 86*(15), 3435-3438.

Menon, P.S., Ehsan, A.A. and Shaari, S. Modeling and Optimization of Three-Dimensional Interdigitated Lateral pin Photodiodes Based on In0. 53Ga0. 47As Absorbers for Optical Communications *Advances in Photodiods*.

Mertig, M., Ciacchi, L.C., Seidel, R., Pompe, W. and De Vita, A. (2002). DNA as a selective metallization template. *Nano Letters, 2*(8), 841-844.

Mishra, Umesh K. and Singh, Jasprit. (2008). *Semiconductor Device Physics and Design*: Springer.

Mott, NF. (1938). *Note on the contact between a metal and an insulator or semiconductor.* Paper presented at the Mathematical Proceedings of the Cambridge Philosophical Society.

Mtangi, W., Auret, FD, Nyamhere, C., Janse van Rensburg, PJ and Chawanda, M.D. (2009). Analysis of temperature dependent I–V measurements on Pd/ZnO Schottky barrier diodes and the determination of the Richardson constant. *Physica B: Condensed Matter, 404*(8), 1092-1096.

Murphy, CJ, Arkin, MR, Jenkins, Y., Ghatlia, ND, Bossmann, SH, Turro, NJ and Barton, JK. (1993). Long-range photoinduced electron transfer through a DNA helix. *Science, 262*(5136), 1025-1029.

N. M. Khatir , S. M. Banihashemian , V. Periasamy and Majid, W. H. Abd. (2010). A New Method of Fabricating Nano-Gaps on Aluminium/ Silicon Structures Using DNA Strands. Malaysian Patent Number 2010700067.

N. M. Khatir, S. M. Banihashemian, V. Periasamy, R. Ritikos, W. H. Abd Majid and S.A Rahman. (2012). Electrical Characterization of Gold-DNA-Gold Structures in Presence of an External Magnetic Field by Means of IV Curve Analysis. *Sensors, 12*(3), 3578-3586.

N. M. Khatir, S. M. Banihashemian, V. Periasamy, W. H. Abd Majid, S.A Rahman and F. Shahhosseini. (2011). DNA Strand Patterns on Aluminium Thin Films. *Sensors, 11*(7), 6719-6727.

Nalwa, H.S. (2005). *Handbook of nanostructured biomaterials and their applications in nanobiotechnology* (Vol. 2): American Scientific Publishers.

Netzel, T.L. (1998). Present status and future directions of research in electron-transfer mediated by DNA. *Journal of Biological Inorganic Chemistry, 3*(2), 210-214.

Niemeyer, C.M. (2010). Semisynthetic DNA–protein conjugates for biosensing and nanofabrication. *Angewandte Chemie International Edition, 49*(7), 1200-1216.

Niemeyer, C.M. and Adler, M. (2002). Nanomechanical devices based on DNA. *Angewandte Chemie International Edition, 41*(20), 3779-3783.

Niemeyer, C.M., Bürger, W. and Peplies, J. (1998). Covalent DNA–streptavidin conjugates as building blocks for novel biometallic nanostructures. *Angewandte Chemie International Edition, 37*(16), 2265-2268.

Nulf, C.J. and Corey, D.R. (2002). DNA assembly using bis-peptide nucleic acids (bisPNAs). *Nucleic Acids Research, 30*(13), 2782–2789.

Nuzzo, R.G. and Allara, D.L. (1983). Adsorption of bifunctional organic disulfides on gold surfaces. *Journal of the American Chemical Society, 105*(13), 4481-4483.

Ohayon, Yoel. (2011). *Topological Bonding of DNA Nanostructures*
(PhD Thesis), New York University.

Okahata, Y., Kobayashi, T., Tanaka, K. and Shimomura, M. (1998). Anisotropic electric conductivity in an aligned DNA cast film. *Journal of the American Chemical Society, 120*(24), 6165-6166.

Olson, EJC, Hu, D., Hörmann, A., Jonkman, AM, Arkin, MR, Stemp, EDA, Barton, JK and Barbara, PF. (1997). First Observation of the Key Intermediate in the "Light-Switch" Mechanism of [Ru (phen) 2dppz] 2+. *Journal of the American Chemical Society, 119*(47), 11458-11467.

Park, S, Kim, G, Choi, K and Lee, J. (2010). Fabrication of a 3D stamp with the micro- and nano-scale patterns through combined NIL and optical lithography processes. *Microelectronic Engineering, 87*(5-8), 968-971.

Pathak, S., Choi, S.K., Arnheim, N. and Thompson, M.E. (2001). Hydroxylated quantum dots as luminescent probes for in situ hybridization. *Journal of the American Chemical Society, 123*(17), 4103-4104.

Patolsky, F., Weizmann, Y., Lioubashevski, O. and Willner, I. (2002). Au Nanoparticle Nanowires Based on DNA and Polylysine Templates. *Angewandte Chemie, 114*(13), 2429-2433.

Petrov, EG, Tolokh, IS and May, V. (1998). Magnetic field control of an electron tunnel current through a molecular wire. *The Journal of Chemical Physics, 108*, 4386-4396.

Petty, M.C. (2007). *Molecular electronics: from principles to practice* (Vol. 22). United States of America: Wiley-Interscience.

Polcari, A., Romano, P., Sabatino, L., Vecchio, E. D., Consales, M., Cusano, A., Cutolo, A. and Colantuoni, V. (2011). Electrical and optical characterization of DNA molecules as a function of concentration in aqueous solution. *Journal of Applied Physics, 109*(7).

Porath, D., Bezryadin, A., De Vries, S. and Dekker, C. (2000a). Direct measurement of electrical transport through DNA molecules. *Nature, 403*(6770), 635-637.

Porath, D., Bezryadin, A., De Vries, S. and Dekker, C. (2000b). Direct measurement of electrical transport through DNA molecules. *Nature, 403*(6770), 635-638.

Porath, D., Cuniberti, G. and Di Felice, R. (2004). Charge transport in DNA-based devices. *Long-Range Charge Transfer in DNA II*, 183-228.

Preuss, M, Schmidt, WG, Seino, K, Furthmüller, J and Bechstedt, F. (2004). Ground-and excited-state properties of DNA base molecules from plane-wave calculations using ultrasoft pseudopotentials. *Journal of Computational Chemistry, 25*(1), 112-122.

Priyadarshy, S., Risser, S.M. and Beratan, D.N. (1998). DNA-mediated electron transfer. *Journal of Biological Inorganic Chemistry, 3*(2), 196-200.

Rakitin, A, Aich, P, Papadopoulos, C, Kobzar, Y, Vedeneev, AS, Lee, JS and Xu, JM. (2001). Metallic conduction through engineered DNA: DNA nanoelectronic building blocks. *Physical ReviewLetters, 86*(16), 3670-3673.

Reichert, J, Ochs, R, Beckmann, D, Weber, HB, Mayor, M and Löhneysen, H. (2002). Driving current through single organic molecules. *Physical Review Letters, 88*(17), 176804.

Reisner, W., Larsen, N.B., Flyvbjerg, H., Tegenfeldt, J.O. and Kristensen, A. (2009). Directed self-organization of single DNA molecules in a nanoslit via embedded nanopit arrays. *Proceedings of the National Academy of Sciences, 106*(1), 79-84.

Richter, J., Mertig, M., Pompe, W., Mönch, I. and Schackert, H.K. (2001). Construction of highly conductive nanowires on a DNA template. *Applied Physics Letters, 78*, 536-538.

Rife, JC, Miller, MM, Sheehan, PE, Tamanaha, CR, Tondra, M. and Whitman, LJ. (2003). Design and performance of GMR sensors for the detection of magnetic microbeads in biosensors. *Sensors and Actuators A: Physical, 107*(3), 209-218.

Roche, S. (2003). Sequence dependent DNA-mediated conduction. *Physical Review Letters, 91*(10), 108101-108104.

Saenger, W. (1984). *Principles of nucleic acid structure*: Springer-Verlag New York.

Sakurai, J.J. (2006). *Advanced quantum mechanics*: Pearson Education India.

Sartor, V., Boone, E. and Schuster, G.B. (2001). Long-distance radical cation migration through A/T base pairs in DNA: An experimental test of theory. *The Journal of Physical Chemistry B, 105*(45), 11057-11059.

Sastry, M. (2000). Nanostructured thin films by self-assembly of surface modified colloidal particles. *Current Science, 78*(9), 1089-1097.

Schmid, Günter and Hornyak, Gabor L. (1997). Metal clusters - new perspectives in future nanoelectronics. *Current Opinion in Solid State and Materials Science, 2*(2), 204-212.

Schuster, G.B. (2000). Long-range charge transfer in DNA: transient structural distortions control the distance dependence. *Accounts of chemical research, 33*(4), 253-260.

Schwartz, David Eric, Gong, Ping and Shepard, Kenneth L. (2008). Time-resolved Förster-resonance-energy-transfer DNA assay on an active CMOS microarray. *Biosensors and Bioelectronics, 24*(3), 383-390.

Seeman, N.C. (1982). Nucleic acid junctions and lattices* 1. *Journal of Theoretical Biology, 99*(2), 237-247.

Seeman, N.C. (1998). DNA nanotechnology: novel DNA constructions. *Annual Review of Biophysics and Biomolecular Structure, 27*(1), 225-248.

Seeman, N.C. (1999). DNA engineering and its application to nanotechnology. *Trends Biotechnology, 17*(11), 437-443.

Seeman, N.C. and Kallenbach, N.R. (1983). Design of immobile nucleic acid junctions. *Biophysical Journal, 44*(2), 201-209.

Shannon, JM. (1974). Reducing the effective height of a Schottky barrier using low-energy ion implantation. *Applied Physics Letters, 24*(8), 369-371.

Shannon, JM. (1976). Control of Schottky barrier height using highly doped surface layers. *Solid-State Electronics, 19*(6), 537-543.

Shen, W., Liu, X., Mazumdar, D. and Xiao, G. (2005). In situ detection of single micron-sized magnetic beads using magnetic tunnel junction sensors. *Applied Physics Letters, 86*, 253901-253903.

Shi, J. and Bergstrom, D.E. (1997). Assembly of novel DNA cycles with rigid tetrahedral linkers. *Angewandte Chemie International Edition in English, 36*(1 2), 111-113.

Steenken, S. (1989). Purine bases, nucleosides, and nucleotides: aqueous solution redox chemistry and transformation reactions of their radical cations and e-and OH adducts. *Chemical Reviews, 89*(3), 503-520.

Steenken, S. (1997). Electron transfer in DNA? Competition by ultra-fast proton transfer? *Biological Chemistry, 378*(11), 1293-1297.

Storm, AJ, Van Noort, J, De Vries, S and Dekker, C. (2001). Insulating behavior for DNA molecules between nanoelectrodes at the 100 nm length scale. *Applied Physics Letters, 79*, 3881-3883.

Streetman, Ben G.; Sanjay Banerjee (2000). *Solid State electronic devices* New Jersey.

Sugiyama, H. and Saito, I. (1996). Theoretical studies of GG-specific photocleavage of DNA via electron transfer: significant lowering of ionization potential and 5'-localization of HOMO of stacked GG bases in B-form DNA. *Journal of the American Chemical Society, 118*(30), 7063-7068.

Sze, SM and Ng, K.K. (1981). Metal-Semiconductor Contacts. *Physics of Semiconductor Devices, 2*, 245-311.

T. S. Mayer, T. N. Jackson, M. J. Natan, and T. E. Mallouk. (1999). *Self-Assembly Nanoscale Components for Molecular Electronics* Paper presented at the Materials Research Conference, Boston.

Taniguchi, M., Kawai, T. (2006). DNA electronics. *Physica E: Low-dimensional Systems and Nanostructures, 33*(1), 1-12.

Taton, T.A., Mirkin, C.A. and Letsinger, R.L. (2000). Scanometric DNA array detection with nanoparticle probes. *Science, 289*(5485), 1757-1760.

Tay, BK, You, GF, Lau, SP and Shi, X. (2000). Plasma flow simulation in an off-plane double bend magnetic filter. *Surface and Coatings Technology, 133*, 593-597.

Terbrueggen, R.H., Johann, T.W. and Barton, J.K. (1998). Functionalized rhodium intercalators for DNA recognition. *Inorganic Chemistry, 37*(26), 6874-6883.

Tran, P., Alavi, B. and Gruner, G. (2000). Charge transport along the -DNA double helix. *Physical Review Letters, 85*(7), 1564-1567.

Trimbach, D., Feldman, K., Spencer, N. D., Broer, D. J. and Bastiaansen, C. W. M. (2003). Block copolymer thermoplastic elastomers for microcontact printing. *Langmuir, 19*(26), 10957-10961.

Tsvetkova, T., Takahashi, S., Zayats, A., Dawson, P., Turner, R., Bischoff, L., Angelov, O. and Dimova-Malinovska, D. (2005). Fabrication of nano-scale optical patterns in amorphous silicon carbide with focused ion beam writing. *Vacuum, 79*(1-2), 100-105.

Tung, R.T. (2001). Recent advances in Schottky barrier concepts. *Materials Science and Engineering R: Reports, 35*(1-3), 1-138.

Tung, RT. (1992). Electron transport at metal-semiconductor interfaces: General theory. *Physical Review B, 45*(23), 13509–13523.

Turro, N.J. and Barton, J.K. (1998). Paradigms, supermolecules, electron transfer and chemistry at a distance. What's the problem? The science or the paradigm? *Journal of Biological Inorganic Chemistry, 3*(2), 201-209.

van der Wijst, Tushar, Guerra, Célia Fonseca, Swart, Marcel and Bickelhaupt, F Matthias. (2006). Performance of various density functionals for the hydrogen bonds in DNA base pairs. *Chemical Physics Letters, 426*(4), 415-421.

Vercoutere, W., Winters-Hilt, S., Olsen, H., Deamer, D., Haussler, D. and Akeson, M. (2001). Rapid discrimination among individual DNA hairpin molecules at single-nucleotide resolution using an ion channel. *Nature Biotechnology, 19*(3), 248-252.

Wacaser, B. A., Maughan, M. J., Mowat, I. A., Niederhauser, T. L., Linford, M. R. and Davis, R. C. (2003). Chemomechanical surface patterning and functionalization of silicon surfaces using an atomic force microscope. *Applied Physics Letters, 82*, 808-810.

Wan, C., Fiebig, T., Kelley, S.O., Treadway, C.R., Barton, J.K. and Zewail, A.H. (1999). Femtosecond dynamics of DNA-mediated electron transfer. *Proceedings of the National Academy of Sciences, 96*(11), 6014-6019

Wang, J. and Kawde, A.N. (2002). Magnetic-field stimulated DNA oxidation. *Electrochemistry Communications, 4*(4), 349-352.

Watanabe, H., Manabe, C., Shigematsu, T., Shimotani, K. and Shimizu, M. (2001). Single molecule DNA device measured with triple-probe atomic force microscope. *Applied Physics Letters, 79*(15), 2462-2464.

Watson, J.D and Crick F, H.C. (1953). Molecular structure of nucleic acids. *Nature, 171*(4356), 737-738.

Wemmer, D. (1998). Reading DNA. *Nature Structural Biology, 5*(3), 169-171.

Wemmer, D.E. (2000). Designed sequence-specific minor groove ligands. *Annual Review of Biophysics and Biomolecular Structure, 29*(1), 439-461.

Whetten, R.L., Khoury, J.T., Alvarez, M.M., Murthy, S., Vezmar, I., Wang, ZL, Stephens, P.W., Cleveland, C.L., Luedtke, WD and Landman, U. (1996). Nanocrystal gold molecules. *Advanced Materials, 8*(5), 428-433.

William Jr, D. (2007). *Materials Science and Engineering an Introduction*. United States of America: John Wiley and Sons.

Williams, T.T., Odom, D.T. and Barton, J.K. (2000). Variations in DNA charge transport with nucleotide composition and sequence. *Journal of the American Chemical Society, 122*(37), 9048-9049.

Winfree, E., Liu, F., Wenzler, L.A. and Seeman, N.C. (1998). Design and self-assembly of two-dimensional DNA crystals. *Nature, 394*(6693), 539-544.

Wu, J., Du, F., Zhang, P., Khan, I.A., Chen, J. and Liang, Y. (2005). Thermodynamics of the interaction of aluminum ions with DNA: implications for the biological function of aluminum. *Journal of Inorganic Biochemistry, 99*(5), 1145-1154.

Wu, J., Walukiewicz, W., Yu, KM, Ager III, JW, Haller, EE, Lu, H., Schaff, W.J., Saito, Y. and Nanishi, Y. (2002). Unusual properties of the fundamental band gap of InN. *Applied Physics Letters, 80*, 3967-3971.

Xu, B., Zhang, P., Li, X. and Tao, N. (2004). Direct conductance measurement of single DNA molecules in aqueous solution. *Nano Letters, 4*(6), 1105-1108.

Xu, MS, Tsukamoto, S., Ishida, S., Kitamura, M., Arakawa, Y., Endres, RG and Shimoda, M. (2005). Conductance of single thiolated poly (GC)-poly (GC) DNA molecules. *Applied Physics Letters, 87*(8), 083902-083903.

Yan, H., Park, S.H., Finkelstein, G., Reif, J.H. and LaBean, T.H. (2003). DNA-templated self-assembly of protein arrays and highly conductive nanowires. *Science, 301*(5641), 1882-1884.

Yan, YJ and Zhang, H. (2002). Toward the Mechanism of Long-Range Charge Transfer in DNA: Theories and Models. *Journal of Theoretical and Computational Chemistry, 1*(1), 225-244.

Yang, M., Yau, H.C.M. and Chan, H.L. (1998). Adsorption kinetics and ligand-binding properties of thiol-modified double-stranded DNA on a gold surface. *Langmuir, 14*(21), 6121-6129.

Yoo, K.H., Ha, DH, Lee, J.O., Park, JW, Kim, J., Kim, JJ, Lee, H.Y., Kawai, T. and Choi, H.Y. (2001). Electrical conduction through poly (dA)-poly (dT) and poly (dG)-poly (dC) DNA molecules. *Physical Review Letters, 87*(19), 198102-198104.

Yurke, B., Turberfield, A.J., Mills Jr, A.P., Simmel, F.C. and Neumann, J.L. (2000). A DNA-fuelled molecular machine made of DNA. *Nature, 406*(6796), 605-608.

Zaouk, Rabih, Park, Benjamin Y and Madou, Marc J. (2006). Introduction to microfabrication techniques *Microfluidic Techniques* (pp. 5-15): Springer.

Zhang, Y., Austin, RH, Kraeft, J., Cox, EC and Ong, NP. (2002). Insulating behavior of DNA on the micron scale. *Physical Review Letters, 89*(19), 198102-198105.

Zhou, X., Langsdorf, B.L., Jones, F.E. and Lonergan, M.C. (1999). Electrochemical tuning of indium phosphide| poly (acetylene) interfaces. *Inorganica Chimica Acta, 294*(2), 207-213.